UNIVERSITY OF CALIFORNIA
SANTA CRUZ

A GENETIC SCREEN IN C. ELEGANS TO IDENTIFY ALLELES THAT BLOCK NONSTOP mRNA DECAY

A dissertation submitted in partial satisfaction
of the requirements for the degree of

DOCTOR OF PHILOSOPHY

in

MOLECULAR, CELL, AND DEVELOPMENTAL BIOLOGY

by

Marissa L. Glover

June 2021

The Dissertation of Marissa L. Glover
is approved by:

_____
Professor Joshua Arribere, Chair

_____
Professor Manuel Ares

_____
Professor Susan Strome

_____
Professor Alan Zahler

_____
Quentin Williams
Acting Vice Provost and Dean of Graduate Students

Table of Contents

FIGURE LIST

ABSTRACT

A GENETIC SCREEN IN C. ELEGANS TO IDENTIFY ALLELES THAT BLOCK NONSTOP mRNA DECAY

Marissa L. Glover

Life relies on accurate protein synthesis and the fidelity of mRNA translation is crucial to maintain cellular homeostasis. Subtle errors in mRNAs are often not detected before translation initiation and can result in production of toxic proteins if left unchecked. These mRNAs are regulated by translation surveillance pathways, including mRNAs lacking stop codons (nonstop decay) and mRNAs that block translation elongation (no-go decay). Central to nonstop and no-go decay is the process of ribosome stalling, where trailing ribosomes collide behind the first stalled ribosome, generating a "traffic jam" of ribosomes. Ribosome collisions on an erroneous mRNA trigger decay of both the offending mRNA and the nascent peptide chain to prevent deleterious outcomes, such as ribosome sequestration and production of dominant negative proteins. However, the mechanisms by which decay machinery recognizes aberrant mRNAs are not well understood. Therefore, I performed a genetic screen to identify factors required for nonstop mRNA decay in *C. elegans*.

Here I report the mutants isolated from the genetic screen. We discovered a novel endonuclease, NONU-1, that is required for both nonstop and no-go mRNA decay. The domain architecture of NONU-1 is conserved throughout metazoans and homologs in *S. cerevisiae* have a conserved function in nonstop decay. NONU-1 contains an Smr RNase domain that is required for the formation of mRNA cleavage fragments in the vicinity of stalled ribosomes, though a subset of cleavages persist in

nonu-1 mutants. Therefore, we propose that another functionally redundant nuclease exists to suppress nonstop and no-go mRNAs.

We also identified the homolog of the ribosome rescue factor Hbs1, K07A12.4. K07A12.4 contains a conserved GTPase domain that is required to repress nonstop mRNAs. Most eukaryotes also express Ski7, a paralog of Hbs1 that is required to facilitate interactions between the SKI helicase complex and the RNA exosome to degrade nonstop mRNAs. Depending on the organism, Ski7 is either an alternative splice isoform of the *HBS1* gene or a separate paralogous gene. However, *k07a12.4* does not encode a Ski7-like protein and a candidate Ski7 gene has not been identified in *C. elegans*. New alleles of genes encoding components of the SKI complex, *skih-2* and *ttc-37*, were also isolated from the genetic screen. The collection of mutants will be useful to understand SKI's role in nonstop and no-go mRNA repression.

DEDICATION

To my beloved saplings, Sequoia and Willow. You bring me so much happiness and have made me more fulfilled than I could have ever imagined. Thank you for understanding when I had to work instead of playing with you. I promise that the sacrifices I made to pursue this dream will be repaid to you. I love you and I will always support you in following your dreams.

ACKNOWLEDGEMENTS

First and foremost, I would like to thank my advisor, Joshua Arribere. He has been a supportive and inspirational mentor throughout this journey. I learned more than I ever expected to and truly grew as a scientist. He went above and beyond in many regards and though I was his first grad student, it did not show in his advising abilities. I will definitely miss the mentorship and the hilarious Josh-isms like “I’m not smart. They just gave me a lab.” and “Just doing anything is not easy in lab.”

My thesis committee Manny Ares, Susan Strome, and Al Zahler. I was so lucky to have such supportive mentors on my team. They are brilliant scientists that I continue to look up to. Each one of them thought about my project carefully and provided invaluable feedback. I truly missed seeing them around Sinsheimer during the pandemic.

All of the wonderful lab mates I had the pleasure of working with over the years: Makena, Thea, Radha, Dori, Heddy, Parissa, Matt, Nitin, Swathi, John, Annie, Marcus, Audrey, and Enisha. Everyone created a positive lab environment with their support, which made grad school much more bearable.

My friends and family that have supported me throughout my education. They were so encouraging and always told me how proud they are of me. I enjoyed the much needed get togethers to take my mind off of grad school. I cannot thank them enough for all of the love and support.

Everyone that supported and donated to my family and I when we lost our house in the CZU fire. We would not have recovered if it weren’t for the kind

donations. It was truly humbling to see the MCD community support us so much. I am forever grateful and cannot thank this wonderful community enough.

Cory, Sequoia, Willow, and Gibbs. I am so lucky to have such a wonderful family. When Cory and I got together 10 years ago, we both had no idea where life would take us. He was always supportive of my dream of going into research and he agreed to move with me wherever I chose for grad school. I cannot thank him enough for that. He worked so hard to help support our family while I made pennies in grad school. He took care of our children when I was too busy with work. I am so happy that it's finally over and I can enjoy life with my family more. Sequoia and Willow have been a breath of fresh air during this roller coaster. I loved every much needed break that I got to spend with them. They kept me sane and always made me see the bigger picture when I was stressed out. And Mr. Gibbs, the best boy ever. I always love coming home to his excited howls and tail wags. He is the best work-from-home pal and snuggle buddy.

CHAPTER 1: INTRODUCTION

Canonical mRNA translation in eukaryotes

All domains of life rely on rapid and accurate protein synthesis to maintain healthy cellular fitness. Protein synthesis is a highly regulated process in which ribosomes decode mRNA molecules to their cognate polypeptide. The number of proteins that are created from each transcript is dependent on mRNA half-life and translational efficiency, which are both driven by features of the mRNA itself. Cells must rigorously regulate each stage of translation to produce the correct number of proteins at the right time and place to maintain a healthy proteome.

The process of mRNA translation is composed of four stages: initiation, elongation, termination, and recycling. For a detailed overview of translation initiation (Merrick and Pavitt, 2018), elongation (Dever et al., 2018), termination (Hellen, 2018), and recycling (Hellen, 2018) see the referenced reviews. During initiation, a ribosome is recruited to the start codon on the transcript to begin protein synthesis (reviewed in Hinnebusch and Lorsch, 2012). Eukaryotic initiation factor (eIF) 2 binds to the initiator methionyl-transfer RNA (Met-tRNA$_i$) and GTP to form the ternary complex (Kapp and Lorsch, 2004). The ternary complex along with additional eIFs then join the 40S ribosomal subunit to form the 43S preinitiation complex (PIC), which attaches to the 5' UTR of a capped mRNA bound by the eIF4 complex (Gingras et al., 1999; Dever, 2002; Kolupaeva et al., 2005). A structural rearrangement in the PIC induces hydrolysis of GTP bound to eIF2, and release of inorganic phosphate is controlled by start codon recognition (Algire et al., 2005). The

PIC scans the 5' UTR until the start codon is located and base pairs to the anticodon of the Met-tRNA$_i$ in the peptidyl (P) site of the ribosome (Kozak, 1978; Cigan et al., 1988; Pestova et al., 1998). Release of eIF2-GDP and some of the other eIFs allows the 60S ribosomal subunit to bind and form an elongation-competent 80S ribosome (Pestova et al., 2000; Kapp and Lorsch, 2004; Pisarev et al., 2006).

Elongation is an iterative process by which the ribosome faithfully synthesizes the protein encoded by the transcript undergoing translation (reviewed in Dever and Green, 2012). The first step of elongation requires GTP-bound eukaryotic elongation factor (eEF) 1A to bind aminoacyl-tRNA and deliver the tRNA to the aminoacyl (A) site of the ribosome (Gromadski et al., 2007; Voorhees and Ramakrishnan, 2013). The tRNA has an anticodon loop that interacts with the cognate codon of the mRNA, which forms a codon:anticodon helix, stabilizing the tRNA:eEF1A:GTP complex in the A site (Rodnina et al., 2005; Voorhees and Ramakrishnan, 2013; Shao et al., 2016; Choi et al., 2018). When correct codon:anticodon pairing occurs, eEF1A hydrolyzes GTP, accommodating the aminoacyl-tRNA in the A site (Loveland et al., 2017). Peptide bond formation then rapidly ensues with the P site peptidyl-tRNA, elongating the nascent chain by one amino acid (Schmeing et al., 2005; Beringer and Rodnina, 2007). Ribosomal ratcheting prompts the tRNAs to move into hybrid P/E and A/P states, while GTP-bound eEF2 enters the A site and promotes GTP hydrolysis (Taylor et al., 2007; Budkevich et al., 2011; Behrmann et al., 2015). Upon GTP hydrolysis, the ribosome translocates to the adjacent downstream codon to start

a new round of elongation (Behrmann et al., 2015; Flis et al., 2018). This process repeats until a termination codon is reached, unless elongation is inhibited.

Translation termination occurs when a stop codon enters the A site of the ribosome and is facilitated by eukaryotic release factor (eRF) 1 and eRF3 (Stansfield et al., 1995; Zhouravleva et al., 1995; Alkalaeva et al., 2006). eRF3 is a GTPase that delivers the tRNA-shaped protein eRF1 to the A site (Cheng et al., 2009; des Georges et al., 2014; Preis et al., 2014). eRF1 contains a NIKS motif that interprets stop codons via codon:anticodon-like interactions (Chavatte et al., 2002; Bulygin et al., 2010; Brown et al., 2015). Upon stop codon recognition, eRF3 hydrolyzes GTP, causing eRF1 to adopt a conformation that exposes the peptidyl-tRNA ester bond and allows the catalytic GGQ motif of eRF1 to induce peptide release (Frolova et al., 1999; Alkalaeva et al., 2006; Cheng et al., 2009; Loh and Song, 2010). eRF1 is capable of inducing peptide release alone, but eRF3 strongly increases this activity and enhances the rate of termination (Alkalaeva et al., 2006; Eyler and Green, 2011).

Ribosome recycling is initiated by the highly conserved ATPase ABCE1, which also acts on vacant 80S ribosomes and stalled elongating ribosomes (Pisarev et al., 2010; Pisareva et al., 2011). ABCE1 binds eRF1, inducing conformational shifts in eRF1 that cause subsequent conformational changes in ABCE1 (Pisarev et al., 2010). The changes in ABCE1 destabilize bridges between the 40S and 60S ribosomal subunits, triggering ribosomal splitting (Heuer et al., 2017). ATP hydrolysis by ABCE1 increases the rate of this reaction and is required to split eRF1 from post-termination complexes (Pisarev et al., 2010; Pisareva et al., 2011;

Shoemaker and Green, 2011). After subunit splitting, the 40S subunit remains bound to deacylated tRNA and mRNA until initiation factors eIF1, eIF1A, and eIF3 release them (Pisarev et al., 2010). Recycling is then complete, and the separated subunits are poised for subsequent rounds of translation.

Translation surveillance

Gene expression is comprised of many complex molecular mechanisms that must ensure faithful decoding of genetic information. Although these mechanisms have high fidelity, errors are made during transcription, pre-mRNA processing, and translation, potentially resulting in deleterious protein products (Graber et al., 1999; Zaher and Green, 2009; Skandalis, 2016; Gout et al., 2017). Deleterious proteins can also arise from damage, stress, and mutations, therefore organisms evolved quality control mechanisms to prevent aberrant proteins from being synthesized (LaRiviere et al., 2006; Guydosh and Green, 2014; Simms et al., 2014). Failure to induce quality control pathways can result in misfolded or dominant-negative proteins, which are responsible for numerous diseases (reviewed in Balchin et al., 2016). Contrarily, hyperactive quality control can hinder normal gene expression, thus cells must maintain a healthy balance of these mechanisms.

Translation surveillance encompasses highly conserved quality control mechanisms that buffer cells from deleterious errors during mRNA translation, where the ribosome acts as a sensor to detect some aberrant mRNAs (reviewed in Simms et al., 2017). At least three major pathways contribute to translation surveillance:

nonsense-mediated decay, nonstop decay, and no-go decay. Each of these pathways functions to prevent the expression of aberrant proteins, though each pathway recognizes distinct defects within the transcript (Losson and Lacroute, 1979; Hodgkin et al., 1989; Frischmeyer et al., 2002; van Hoof et al., 2002; Doma and Parker, 2006). NMD was the first translation surveillance pathway to be discovered and has been the most heavily studied, though the work presented here focuses on nonstop and no-go decay.

Nonstop decay

Two decades ago, the Dietz and Parker labs noticed that mRNAs lacking stop codons are unstable in eukaryotes and the instability is not dependent on canonical mRNA turnover pathways (Frischmeyer et al., 2002; van Hoof et al., 2002). They discovered a pathway that prevents the production of aberrant nonstop proteins from stop codon-less mRNAs and named the pathway nonstop decay. Transcripts lacking an in-frame stop codon are substrates for nonstop decay. Nonstop mRNAs can arise from premature polyadenylation, cryptic polyadenylation, stop codon readthrough, a stop codon mutation, or mRNA cleavage (Graber et al., 1999; Inada and Aiba, 2005; Meaux et al., 2006; Wilson et al., 2007). When no in-frame stop codons are present, the ribosome translates into the poly-A tail and either stalls within the poly-A tail or on the 3' edge of the mRNA (Guydosh and Green, 2017). Ribosomal stalling elicits rapid degradation of the offending transcript and the nascent peptide to prevent the accumulation of potentially toxic proteins (Frischmeyer et al., 2002; van Hoof et al.,

2002; Bengtson and Joazeiro, 2010; Shao et al., 2013; Shen et al., 2015). There is strong evidence of multiple pathways being utilized to alleviate ribosomal stalling and prevent pathological issues, including endonucleolytic cleavage, exonucleolytic digestion, ubiquitination, and ribosome rescue (see Ribosome collisions below).

No-go decay

A few years after the discovery of nonstop decay, the Parker lab discovered that mRNAs with features that block translation elongation are considerably unstable due to endonucleolytic cleavage of the mRNA (Doma and Parker, 2006). This mechanism to clear stalled translation elongation complexes is called no-go decay. Transcripts that inhibit translation elongation and induce ribosomal stalling within the open reading frame are substrates for no-go decay (Doma and Parker, 2006). Certain secondary structures such as hairpins and pseudoknots, stretches of rare codons, stretches of codons that encode polybasic amino acids, and damaged mRNAs are some features that cause ribosomal stalling (Doma and Parker, 2006; Kuroha et al., 2010; Letzring et al., 2013; Simms et al., 2014). Similar to nonstop decay, ribosomal stalling during no-go gives rise to mRNA decay and nascent peptide degradation, though some of the factors involved differ.

Ribosome collisions

For over a decade it was believed that a single ribosome stalling event is sufficient to initiate mRNA decay. However, recent evidence suggests that

subsequent to a single ribosome stalling during translation elongation, another trailing ribosome collides with the stalled ribosome and the collision is required to initiate mRNA decay (Simms et al., 2017) (Figure 1.1A). Since the discovery of ribosome collisions, multiple cryo-EM structures have been resolved that show the di-ribosome (disome) architecture in high resolution (Juszkiewicz et al., 2018; Ikeuchi et al., 2019). The disome structure consists of the leading ribosome in the post-translocation state with an empty A site and the second ribosome in a hybrid state with A/P and P/E tRNAs. A distinct 40S-40S interface is created by the disome, exposing specific sites on the 40S subunits that are ubiquitinated by the E3 ubiquitin ligase Hel2/ZNF598 (yeast/mammals) (Juszkiewicz et al., 2018; Ikeuchi et al., 2019) (Figure 1.1A). In yeast, Hel2 mediates ubiquitination on the 40S protein uS10 and uS3, while in mammals ZNF598 ubiquitinates eS10 and uS10 (Saito et al., 2015; Garzia et al., 2017; Sundaramoorthy et al., 2017; Juszkiewicz et al., 2018; Ikeuchi et al., 2019). However, the "readers" of the ubiquitination marks remain elusive.

Hel2/ZNF598 acts early during ribosome-associated quality control, selectively targeting disomes as the minimal structure to permit ribosome rescue and prevent further accumulation of collided ribosomes (Juszkiewicz and Hegde, 2017; Sundaramoorthy et al., 2017; Juszkiewicz et al., 2018; Ikeuchi et al., 2019). Interestingly, an *in vitro* system showed that the proportion of ubiquitination by ZNF598 increases for complexes containing more ribosomes (Juszkiewicz et al., 2018). These results support a model where each trailing ribosome in a stall-inducing collision can be ubiquitinated by ZNF598. Without ribosomal ubiquitination by

Hel2/ZNF598, ribosomes resume elongation and readthrough the stall site, often frameshifting in multiple frames (Letzring et al., 2013; Matsuo et al., 2017;

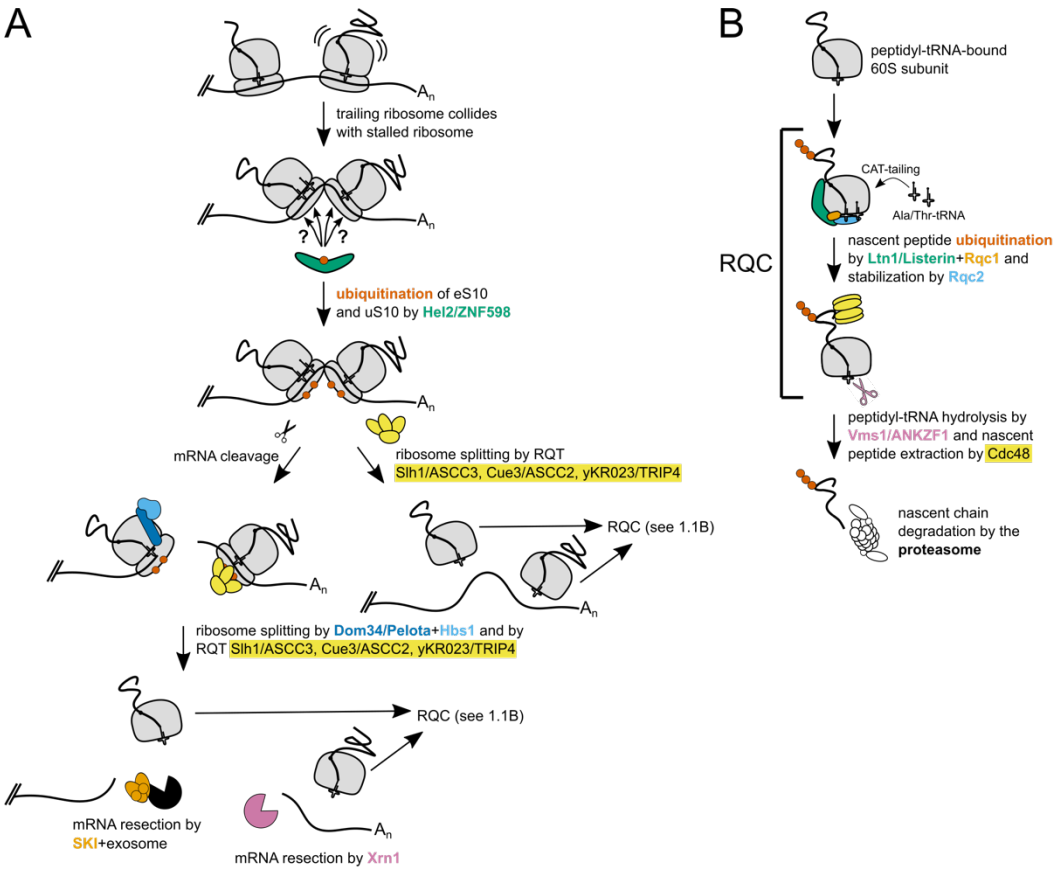

Figure 1.1: Mechanisms involved in nonstop and no-go decay
A. Model of ribosome collisions, the endonucleolytic cleavage pathway, and the Ribosome Quality Control Trigger (RQT) pathway. Hel2/ZNF598 (green) recognizes collided ribosomes and ubiquitinates (red) ribosomal proteins, though it is unclear if eS10 and uS10 are ubiquitinated on both ribosomes. Ubiquitination triggers endonucleolytic cleavage or ribosome splitting by the RQT complex (Slh1/ASCC3, Cue3/ASCC2, and yKR023/TRIP4 (yellow)). Dom34/Pelota (light blue) and Hbs1 (dark blue) splits ribosomes with an empty A site. The upstream cleavage fragment is degraded by the SKI complex (orange) and the exosome, and the downstream cleavage fragment is degraded by Xrn1 (pink). Peptidyl-tRNA-bound 60S subunits are then targeted by RQC as shown in (B).
B. Model of Ribosome Quality Control (RQC) mechanisms. The peptidyl-tRNA-bound 60S subunit is recognized by Ltn1/Listerin (green), Rqc1 (orange), and Rqc2 (light blue). CAT-tailing occurs if Ltn1 is unable to reach lysine residues on the nascent peptide and Ltn1/Listerin ubiquitinates (red) the nascent peptide chain. The peptidyl-tRNA is hydrolyzed by Vms1/ANKZF1 (pink) and the nascent peptide is extracted by Cdc48 (yellow). The ubiquinated nascent chain is degraded by the proteasome.

Juszkiewicz et al., 2020). Therefore, Hel2/ZNF598 prevents stalled ribosomes from further elongating, potentially in the wrong frame, and promotes downstream pathways of ribosome quality control.

ZNF598 also forms a complex with the alternative cap-binding protein, 4EHP, and a bridging factor, GIGYF2, to initiate a negative feedback loop and repress translation initiation of transcripts containing ribosome collisions (Morita et al., 2012; Hickey et al. 2020; Juszkiewicz et al., 2020). By repressing initiation of problematic mRNAs, cells avoid expending energy on translation of aberrant mRNAs and ribosome-associated quality control. It is hypothesized that ZNF598 acts as a scaffold for recruitment of 4EHP and GIGYF2, which sequester the mRNA cap and block translation initiation (Hickey et al. 2020). However, 4EHP and GIGYF2 are able to repress initiation of problematic mRNAs in the absence of ZNF598, suggesting ZNF598-independent recruitment mechanisms (Hickey et al. 2020).

Another highly conserved eukaryotic-specific protein that is also a component of the ribosome, Asc1/RACK1, has been implicated in recognizing collided ribosomes and is necessary for ribosomal ubiquitination by Hel2/ZNF598 (Kuroha et al., 2010; Ikeuchi and Inada, 2016; Sundaramoorthy et al., 2017). Asc1/RACK1 exhibits pleiotropy and is involved in multiple different signal transduction pathways, complicating studies on the role of Asc1/RACK1 in ribosome collisions (McLeod et al., 2000; Chong et al., 2005; Kadrmas et al., 2007; Guo et al., 2009). Nevertheless, findings show that Asc1/RACK1 regulates 40S ubiquitination on the ribosomal proteins uS3, uS5, and uS10 independent of Hel2/ZNF598 and is necessary for translation arrest after collisions to inhibit frameshifting and readthrough of the stall site (Letzring et al., 2013; Wolf and Grayhack, 2015; Sitron et al., 2017; Sundaramoorthy et al., 2017). However, the ubiquitination is likely not carried out by

Asc1/RACK1 itself as Asc1/RACK1 lacks an E3 ligase domain (Deshaies and Joazeiro, 2009). Asc1/RACK1 functions before the downstream steps of nonstop and no-go decay including mRNA endonucleolytic cleavage and Ribosome Quality Control (RQC) (Ikeuchi and Inada, 2016; Sundaramoorthy et al., 2017). In yeast, mRNA cleavage was shown to be dependent on Asc1 in cells lacking the ribosome rescue factor Dom34 (Ikeuchi and Inada, 2016). However, Asc1 is not required for degradation of nonstop proteins (Dimitrova et al., 2009; Kuroha et al., 2010). Notably, the cryo-EM structure of collided ribosomes revealed that both Asc1/RACK1 molecules directly interact and this interface includes the Hel2/ZNF598 targets uS3, uS10, and eS10 (Juszkiewicz et al., 2018; Ikeuchi et al., 2019). Therefore, the Asc1/RACK1 molecules may serve as a platform for Hel2/ZNF598 to recognize collided ribosomes, though this remains to be explored.

Endonucleolytic cleavage and mRNA decay

There are many steps that occur downstream of Hel2/ZNF598 that are dependent on 40S ubiquitination, though the order of events and the role of each step are still only partially resolved. The factors involved in downstream events include an endonuclease, a helicase-containing ribosome quality control complex, and ribosome rescue factors (Doma and Parker, 2006; Pisareva et al., 2011; Tsuboi et al., 2012; Matsuo et al., 2017; Sitron et al., 2017; Hashimoto et al., 2020) (Figure 1.1A). Ribosome collisions have been shown to induce endonucleolytic cleavages of problematic mRNAs and Hel2 is crucial to generate the cleavage fragments,

suggesting that either Hel2 or the resulting ubiquitination recruits an endonuclease (Ikeuchi et al., 2019).

mRNA cleavage is an early irreversible step to ensure mRNA degradation and until recently, the endonuclease implicated in nonstop and no-go decay was unknown (see Chapter 2) (Figure 1.1A). Based on ribosome profiling data and cleavage fragment analysis, it was hypothesized that subsequent to ribosome collisions, a ribosome associated endonuclease cleaves mRNA between the tightly packed ribosomes (Guydosh and Green, 2017; Simms et al., 2017; Ibrahim et al., 2018). mRNA cleavage greatly reduces the half-life of nonstop and no-go targets by exposing cleavage fragments to exonucleases and also causes nonstop/no-go decay to be self-perpetuating as it creates a nonstop substrate, causing further targeting by nonstop decay machinery (Frischmeyer et al., 2002; van Hoof et al., 2002; Doma and Parker, 2006; Passos et al., 2009; Guydosh and Green, 2017). Cleavages in the vicinity of collided ribosomes have been shown to create a 3' fragment with a 5' hydroxyl, which must get phosphorylated to be degraded by the 5'>3' exonuclease Xrn1(Navickas et al., 2020) (Figure 1.1A). In yeast, the tRNA ligase Rlg1/Trl1 is responsible for phosphorylating 3' cleavage fragments, though Rlg1/Trl1 is absent in animals and raises the question of what protein carries out this function (Navickas et al., 2020).

The prevailing model is that the 5' cleavage fragment is rapidly degraded by the SKI complex along with the cytoplasmic RNA exosome (van Hoof et al., 2002; Doma and Parker, 2006; Hashimoto et al., 2017; Arribere and Fire, 2018) (Figure

1.1A). Proteins of the SKI complex were originally discovered due to their involvement in an antiviral mechanism in *S. cerevisiae* and were later found to be required for both nonstop and no-go decay (Toh-E et al., 1978; van Hoof et al., 2002; Doma and Parker, 2006). The SKI complex is comprised of the RNA helicase Ski2, the tetratricopeptide repeat protein Ski3, and the WD repeat protein Ski8 (Anderson and Parker, 1998; Brown et al., 2000; Halbach et al., 2013; Schmidt et al., 2016). In yeast, Ski7 is required to associate the SKI complex with the exosome. However, in other organisms this function is completed by an alternatively spliced isoform of the ribosome rescue factor Hbs1 (Araki et al., 2001; Wang et al., 2005; Kowalinski et al., 2016; Kalisiak et al., 2017; Marshall et al., 2018). Recent structural studies indicate that the SKI complex binds to ribosomes near the mRNA entrance tunnel and the mRNA is threaded from the ribosome through the helicase Ski2 and into the exosome (Schmidt et al., 2016). The SKI complex is also capable of extracting mRNA from ribosomes in an *in vitro* reconstituted mammalian translation system and could conceivably function to remove mRNA from stalled ribosomes, though mechanism this has not been analyzed *in vivo* (Zinoviev et al., 2020).

Dom34/Pelota and Hbs1 are factors that have a crucial role to rescue stalled ribosomes in both nonstop and no-go decay and are structural homologs of the canonical termination factors eRF1 and eRF3, respectively (Atkinson et al., 2008; Passos et al., 2009; Saito et al., 2013). Similar to the mechanism of eRF1 delivery to the A site of terminating ribosomes by eRF3, GTP-bound Hbs1 delivers Dom34/Pelota to the A site of stalled ribosomes (Passos et al., 2009; Becker et al.,

2011; Pisareva et al., 2011) (Figure 1.1A). For years it was thought that Dom34/Pelota needs the A site to be devoid of mRNA, but studies have shown that the mRNA can be locally displaced in the A site, allowing Dom34/Pelota to occupy the A site (Shao and Hegde, 2014; Shao et al., 2016). However, it is proposed that Dom34/Pelota preferentially dissociates ribosomes stalled on the 3' edge of an mRNA with an empty A site, whereas internally stalled ribosomes may be regulated by another set of proteins (see Ribosome quality control trigger pathway) (Pisareva et al., 2011; Shoemaker and Green, 2011; Juszkiewicz et al., 2020). This suggests Dom34/Pelota only functions in no-go decay after endonucleolytic cleavage occurs between a disome, causing the trailing ribosome to have an empty A site. Upon GTP hydrolysis, Hbs1 dissociates and the ribosome recycling factor ABCE1 is recruited to work in concert with Dom34/Pelota to split the ribosome into subunits (Pisareva et al., 2011; Shoemaker and Green, 2011; Becker et al., 2012; Shao et al., 2016). Unlike eRF1, Dom34/Pelota lacks the conserved catalytic GGQ motif that is essential to facilitate peptide hydrolysis, thus a peptidyl-tRNA-bound 60S subunit remains after splitting (Lee et al., 2007; Atkinson et al., 2008; Shoemaker and Green, 2011).

Ribosome quality control trigger (RQT) pathway

Several studies have insinuated that there are multiple pathways to alleviate ribosome collisions with distinct mechanisms and specificities to ensure potency and avoid ribosome accumulation on mRNAs. Additional factors have recently been implicated in stalled ribosome dissociation independent of endonucleolytic cleavage.

However, the mechanism is poorly understood. The RNA helicase Slh1/ASCC3, ubiquitin-binding protein Cue3/ASCC2, and zinc finger-type protein yKR023/TRIP4 form the RQC trigger (RQT) complex, which may recognize ubiquitinated collided ribosomes via Cue3/ASCC2 (Matsuo et al., 2017; Sitron et al., 2017; Ikeuchi et al., 2019; Hashimoto et al., 2020; Matsuo et al., 2020) (Figure 1.1A). These factors were found to associate with Hel2 by affinity purification of Hel2-bound ribosomes and were also independently identified by genetic screens for ribosome readthrough (Matsuo et al., 2017; Sitron et al., 2017). Slh1/ASCC3's helicase activity and the ubiquitin-binding activity of Cue3/ASCC2 are required for RQT function of dissociating stalled ribosomes, though it remains enigmatic how the RQT complex induces ribosome splitting (Matsuo et al., 2017). However, similar to a Hel2/ZNF598 deletion, knockout of Slh1/ASCC3 results in a readthrough of stalling sequences, thus part of its function is to prevent generation of potentially toxic proteins (Matsuo et al., 2017; Sitron et al., 2017).

Despite the unknown aspects of the RQT complex functions, studies are consistent with the requirement of the RQT complex in dissociating and recycling ribosomes that are stalled internally, opposed to those stalled on the 3' edge of the mRNA (Juszkiewicz et al., 2020; Matsuo et al., 2020). Interestingly, knockout of Slh1/ASCC3 enhances the levels of endonucleolytic cleavage, implying that the two pathways work together to ensure a robust response to relieve ribosome stalling and collisions (D'Orazio et al., 2019; Ikeuchi et al., 2019). Both pathways rely on 40S ubiquitination by Hel2/ZNF598 and feed into the downstream steps of RQC, though

the interdependence between pathways remains curious and certain conditions may favor a specific pathway.

Ribosome quality control (RQC)

The potentially toxic proteins generated during translation of stall-inducing mRNAs are degraded in a process called Ribosome Quality Control (RQC). After ribosome splitting, the peptidyl-tRNA-bound 60S subunit is subjected to RQC (Bengtson and Joazeiro, 2010; Brandman et al., 2012; Defenouillere et al., 2013; Verma et al., 2013) (Figure 1.1B). The E3 ubiquitin ligase Ltn1/Listerin selectively recognizes dissociated 60S subunits containing a peptidyl-tRNA and forms a complex with the factors Rqc1 and Rqc2 (Shao et al., 2013; Shao and Hegde, 2014). With Rqc1, Ltn1/Listerin ubiquitinates lysine residues within the nascent chain and recruits the ATPase Cdc48, which enables extraction of the nascent chain for proteasomal degradation (Bengtson and Joazeiro, 2010; Brandman et al., 2012; Defenouillere et al., 2013). Rqc2 stabilizes Ltn1/Listerin binding to the 60S subunit, prevents the 40S subunit from reassociating, and if necessary, Rqc2 modifies nascent peptides with C-terminal alanine- and threonine-containing tails (CAT tails) (Lyumkis et al., 2014; Shao et al., 2015; Shen et al., 2015; Yonashiro et al., 2016; Kostova et al., 2017).

CAT tailing is a fail-safe mechanism to resolve situations in which ubiquitination or extraction of the nascent chain is inhibited (Shen et al., 2015; Yonashiro et al., 2016; Kostova et al., 2017). Rqc2 promotes alanyl- and threonyl-tRNAs to bind the A site and extend the nascent peptide chain to expose lysine

residues for ubiquitination by Ltn1/Listerin (Shen et al., 2015; Yonashiro et al., 2016; Kostova et al., 2017). CAT tails also function as a degron that target nascent chains for degradation by the proteasome, therefore aberrant nascent chains lacking ubiquitin will still be destroyed if they escape the Ltn1/Listerin-mediated pathway (Choe et al., 2016; Defenouillere et al., 2016; Sitron and Brandman, 2019). Upon nascent chain ubiquitination, the peptidyl-tRNA is hydrolyzed by Vms1/ANKZF1 to release the nascent chain, which is extracted by Cdc48 and degraded by the proteasome (Brandman et al., 2012; Defenouillere et al., 2013; Verma et al., 2013; Verma et al., 2018). RQC is then complete and the 60S subunit is free to participate in a new round of translation.

C. elegans as a model to study translation surveillance

Historically, the majority of research on nonstop and no-go decay has been exclusively carried out in *S. cerevisiae* and mammalian cells. However, the large evolutionary distance between *S. cerevisiae* and mammals makes it difficult to directly transfer models between the systems. For example, while Hel2 and ZNF598 are conserved between yeast and mammals, respectively, their ubiquitination targets differ and may have different consequences for downstream factors (Saito et al., 2015; Garzia et al., 2017; Sundaramoorthy et al., 2017; Juszkiewicz et al., 2018; Ikeuchi et al., 2019). Therefore, studies on nonstop and no-go decay would benefit from a genetically tractable metazoan that yields results transferable to mammalian

models. *C. elegans* provides these benefits and is an ideal model to study translation surveillance.

Despite hundreds of millions of years of divergence between *C. elegans* and humans, comparative proteomics has shown that ~80% of the worm proteome has homologs in humans, enabling studies on basic molecular mechanisms that also operate in humans (Kaletta and Hengartner, 2006). *C. elegans* is amenable to high throughput genetic experiments that are extremely time-consuming or costly in mice and other vertebrates. Genetic screens are powerful tools widely used in *C. elegans* to identify functional genes and assign them to a pathway (reviewed in Jorgensen and Mango, 2002). Thousands of worm genomes can effortlessly be mutagenized, and homozygous mutations are easily maintained due to the hermaphroditic nature of *C. elegans* (Brenner, 1974; reviewed in Jorgensen and Mango, 2002). *C. elegans* can also exist as males, allowing for sexual crosses to obtain specific strains (Brenner, 1974; reviewed in Corsi et al., 2015). Additionally, there are a variety of visible phenotypes and genetic chromosomal balancers to ease the process of strain construction and maintenance (reviewed in Corsi et al., 2015).

C. elegans has an exceptionally fast reproductive cycle and short lifespan, which are beneficial to generating strains and obtaining experimental results. Reaching adulthood from a fertilized egg only takes about three days and each hermaphroditic adult can produce up to 300 progenies, enabling large-scale manufacturing of animals with simplicity (Brenner, 1974; reviewed in Corsi et al., 2015). Furthermore, *C elegans* has the benefits of a well-annotated genome and

transcriptomic technologies, in addition to the wide swath of molecular tools that have been applied in *C. elegans* including RNAi, CRISPR/Cas9, and microscopy (*C. elegans* Sequencing Consortium, 1998; Fire et al., 1998; Wang et al., 2009; Shakes et al., 2012; Friedland et al., 2013; Arribere et al., 2014; Ortiz et al., 2014). Overall, *C. elegans* is a tremendously valuable model organism that can yield novel information on the mechanisms of nonstop and no-go decay that has been lacking.

The only nonstop and no-go decay factors that had been characterized in *C. elegans* were two components of the SKI complex, SKIH-2 (Ski2) and TTC-37 (Ski3), and the ribosome rescue factor PELO-1 (Dom34/Pelota) (Arribere and Fire, 2018). By homology search it was clear that homologs of other nonstop and no-go machinery exist in *C. elegans*, but none of the homologs had been characterized. Thus, the main objective of this work was to use *C. elegans* to gain insight into the mechanisms of nonstop and no-go decay.

CHAPTER 2: NONU-1 ENCODES A CONSERVED ENDONUCLEASE REQUIRED FOR MRNA TRANSLATION SURVEILLANCE

ABSTRACT

Cellular translation surveillance rescues ribosomes that stall on problematic mRNAs. During translation surveillance, endonucleolytic cleavage of the problematic mRNA is a critical step in rescuing stalled ribosomes. Here we identify NONU-1 as a factor required for translation surveillance pathways including no-go and nonstop mRNA decay. We show that (1) NONU-1 reduces nonstop and no-go mRNA levels; (2) NONU-1 contains an Smr RNase domain required for mRNA decay; (3) the domain architecture and catalytic residues of NONU-1 are conserved throughout metazoans and eukaryotes, respectively; and (4) NONU-1 is required for the formation of mRNA cleavage fragments in the vicinity of stalled ribosomes. We extend our results in *C. elegans* to homologous factors in *S. cerevisiae*, showing the evolutionarily conserved function of NONU-1. Our work establishes the identity of a factor critical to translation surveillance and will inform mechanistic studies at the intersection of translation and mRNA decay.

INTRODUCTION

Numerous mechanisms exist to protect cells from the negative effects of errors in gene expression. Among these are translation surveillance pathways in which a ribosome identifies an early stop codon (nonsense-mediated mRNA decay [NMD]), a lack of stop codons (nonstop decay), or a block during translation

elongation (no-go decay). Central to both nonstop and no-go decay is the process of ribosome stalling. Recent work has also shown that ribosomes stall during NMD, effectively funneling NMD targets into nonstop decay (Hashimoto et al., 2017; Arribere and Fire, 2018). Despite substantial mechanistic insight into translation surveillance pathways (reviewed by Joazeiro, 2017), how ribosomal stalling communicates with mRNA decay machinery remains a central unsolved question.

Mounting evidence points to endonucleolytic cleavage of the mRNA in the vicinity of stalled ribosomes as an important early event in translation surveillance (e.g., Doma and Parker, 2006; Guydosh and Green, 2014; Ikeuchi et al., 2019; D'Orazio et al., 2019; Navickas et al., 2020; Schaeffer and van Hoof, 2011). Subsequent to mRNA cleavage, target mRNAs are eventually cleared in part by 3'>5' degradation facilitated by the SKI RNA helicase in conjunction with the exosome (Doma and Parker 2006; van Hoof et al., 2002; Hashimoto et al., 2017; Arribere and Fire, 2018). Knowledge of the identities and functions of factors that interface between translation and mRNA decay will illuminate a critical junction in gene expression and regulation. Identification of the nuclease(s) at this junction would therefore significantly advance our understanding of translation, surveillance, and targeted mRNA decay.

Here we identify a mutation that blocks nonstop and no-go mRNA decay in *C. elegans*. The mutation identifies a conserved gene, *nonu-1*, whose structure predicts that it encodes a conserved nuclease component of translation surveillance. NONU-1 contains an Smr domain with the IF3-C fold previously implicated in processing

RNA. Homologs of NONU-1 include the recently identified *S. cerevisiae CUE2* and the uncharacterized *YPL199C*, which we show function redundantly in nonstop mRNA decay. Our results identify a critical component of the translation surveillance machinery in two model organisms and suggest why this factor has been recalcitrant to discovery in *S. cerevisiae*.

RESULTS

nonu-1 encodes a conserved factor required for nonstop mRNA decay

We previously developed a phenotypic reporter in *C. elegans* that allowed us to identify nonstop mRNA decay factors via reverse and forward genetics (Figure 2.1A; Arribere and Fire, 2018). Briefly, the reporter was constructed using the *unc-54* locus, as expression and function of this gene have been extensively studied (Brenner, 1974; Epstein et al., 1974; Dibb et al., 1985, 1989; Moerman et al., 1982; Bejsovec and Anderson, 1988; Anderson and Brenner, 1984) and *unc-54* has been used in previous suppressor screens (Hodgkin et al., 1989). The nonstop reporter has GFP integrated at the C terminus of UNC-54, a ribosomal skipping T2A sequence between GFP and the 3' UTR, and all stop codons removed from the 3' UTR. The T2A sequence is a viral-derived peptide that cotranslationally releases the upstream protein and allows UNC-54::GFP to escape nonstop protein decay (so-called ribosome quality control; Bengtson and Joazeiro, 2010; Shao et al., 2013; Shen et al., 2015). We hereafter refer to the *unc-54::gfp::t2a::nonstop* reporter as *unc-54(nonstop)*. Animals with the *unc-54(nonstop)* reporter deficient in nonstop mRNA decay exhibit

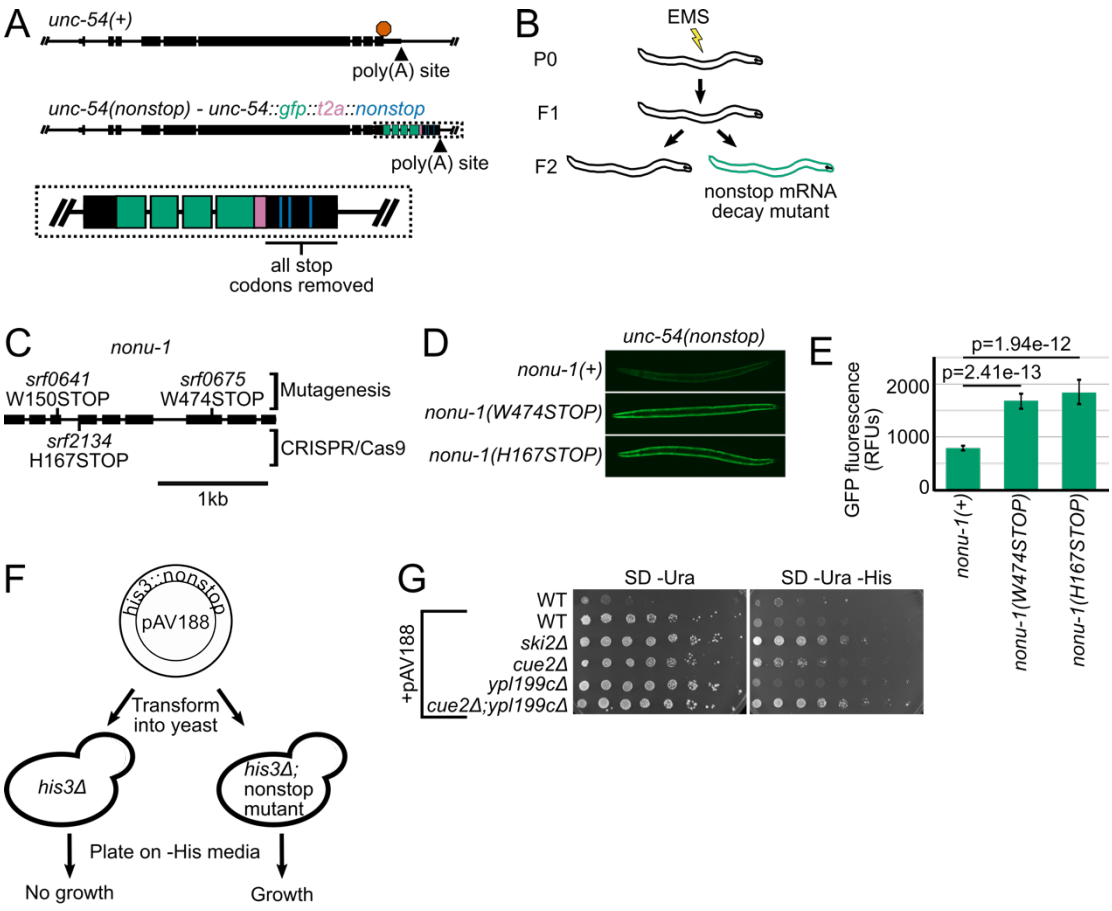

Figure 2.1: NONU-1 and its homologs have a conserved function in nonstop decay
A. Gene diagrams showing annotated exons (black rectangles) at the wild type *unc-54 locus* (top) and the *unc-54(nonstop)* reporter (bottom). Red octagon indicates the stop codon; triangles indicate poly(A) sites. Inset shows zoom in with GFP (green), T2A (pink), and re-coded stop codons (blue).
B. Cartoon of the genetic screen to identify nonstop mRNA decay mutants.
C. Gene diagram showing annotation of the *nonu-1* locus. Mutations made via EMS and CRISPR/Cas9 are above and below the gene, respectively.
D. Images of GFP expression in the indicated strains. See Methods.
E. Quantification of GFP expression for strains shown in (D). Each bar represents an average image of at least 5 different animals; 95% Confidence Interval shown as error bars. P-values from Student's T-test comparing mutants to *nonu-1(+)*. RFUs, Relative Fluorescence Units.
F. Diagram of the S. cerevisiae nonstop decay assay. See text for details.
G. The indicated strains were transformed with the reporter plasmid and strains were serially diluted and plated on the indicated media. Pictures are representative of experimental triplicates.

derepression of the locus, as evidenced by increased GFP fluorescence, mRNA expression, and egg laying (*unc-54* encodes a muscle myosin required in the vulva for egg laying) (Figure 2.1B; Arribere and Fire, 2018). Although our initial screen successfully identified *C. elegans' skih-2* and *ttc-37* (homologs of *S. cerevisiae SKI2*

and *SKI3*, respectively), it did not identify a factor that could function as an endonuclease.

We repeated the genetic screen and isolated an additional 36 mutants. We genetically mapped the causative locus in each strain by backcrossing to a polymorphic strain (also called Hawaiian variant mapping; Figure S2.1; Arribere and Fire, 2018; Doitsidou et al., 2010). The majority of mutants mapped to loci homologous to known nonstop mRNA decay factors in other systems. However, two strains (WJA0675 and WJA0641) harbored mutations that mapped to an area lacking obvious known nonstop mRNA decay components (Figure S2.1). Visual inspection revealed that strain WJA0675 contained a Trp > STOP mutation in predicted ORF *f26a1.13*, and strain WJA0641 contained a Trp > STOP mutation in the neighboring ORF *f26a1.14* (Figure S2.2A). Our subsequent analyses showed that *f26a1.13* and *f26a1.14* are a single gene that is required for nonstop mRNA decay (Figure S2.2; Lee et al., 2018), and we hereafter refer to this gene as *nonu-1* (*nonu* [nonstop nuclease]). Homology searches with the encoded NONU-1 protein identified homologous proteins in diverse eukaryotes, but no homolog known to function in nonstop mRNA decay. During review of this manuscript, one homolog of NONU-1 in *S. cerevisiae (CUE2)* was identified as a factor involved in no-go mRNA decay (D'Orazio et al., 2019).

S. cerevisiae homologs of NONU-1 are required for nonstop mRNA decay

A previous genetic screen in *S. cerevisiae* failed to identify a homolog of NONU-1 (Wilson et al., 2007). We performed a homology search and identified two candidate homologs in *S. cerevisiae*: *YPL199C* and *CUE2*. Of the two, *CUE2* was recently identified as a factor involved in no-go mRNA decay (D'Orazio et al., 2019), but the relationship of *YPL199C* to *CUE2* and *nonu-1* has not been studied. To determine whether *CUE2* and/or *YPL199C* function in nonstop decay, we assayed the ability of mutant strains to derepress a *his3::nonstop* reporter previously used to identify and study factors required for nonstop decay in *S. cerevisiae* (Wilson et al., 2007; van Hoof et al., 2002). When transformed into a *his3Δ* strain, the *his3::nonstop* reporter allows the selective growth of nonstop decay mutants (Figure 2.1F).

Consistent with previous work, we observed substantial derepression of the reporter in a *ski2* mutant (Figure 2.1G). In either a *cue2Δ* or *ypl199cΔ* mutant, we observed suppression of the *his3::nonstop* reporter. The magnitude of the suppression was significantly less than that conferred by a *ski2* mutation but was reproducible across independent isolates and technical replicates. The small magnitude of growth suppression compared with other mutants (e.g., *ski2*) may have precluded either gene from being identified in a previous genetic screen (Wilson et al., 2007). Analysis of a *cue2Δ ypl199cΔ* double-mutant strain revealed an even greater suppression of nonstop decay than either single mutant, pointing to a functional redundancy that likely precluded detection from prior loss-of-function screens. We conclude that NONU-1 and its homologs in *S. cerevisiae* have a conserved function in nonstop

decay. Although *CUE2* and *YPL199C* each had a consistent effect on the *his3::nonstop* reporter, we note that the magnitude of this effect was below that of other factors (i.e., *SKI2*), suggesting multiple independent mechanisms exist to repress nonstop mRNAs.

Domain architecture of NONU-1

To gain insight into NONU-1 function, we examined the domain structure of the protein and its metazoan orthologs and found that they contain several conserved domains (from N terminus to C terminus; Figures 2.2A and S2.3). The NONU-1 protein family is characterized by the following:

(1) An N-terminal basic region similar to a ribosome-binding motif at the N terminus of the ribosomal protein S26AE. This basic stretch is only observed in the chordate versions of NONU-1 and is thus not pictured in Figure 2.2A. The basic stretch suggests that NONU-1 might interact directly with ribosomes.

(2) A domain of the P loop kinase superfamily belonging to the polynucleotide kinase (PNK) clade. These kinase domains are known to phosphorylate RNA/DNA ends (Leipe et al., 2003; Burroughs and Aravind, 2016). The P loop kinase domain suggests NONU-1 may modify nonstop mRNAs or their degradation products.

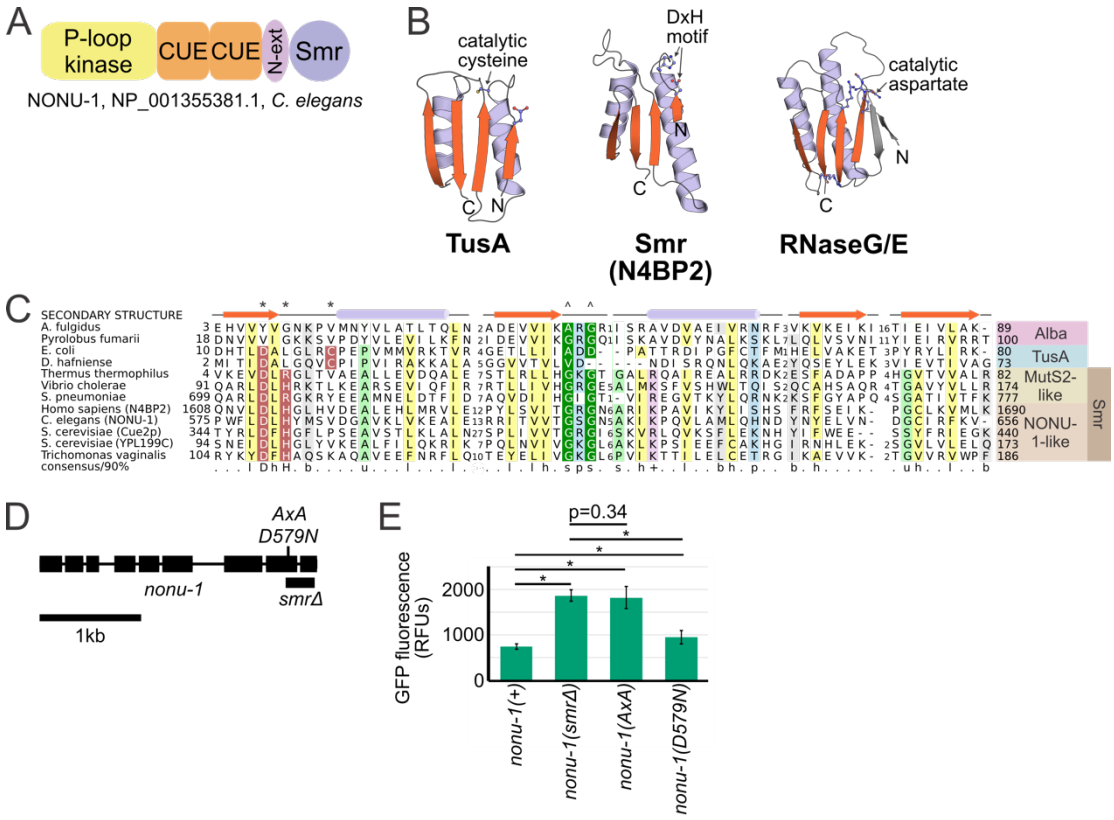

Figure 2.2: *nonu-1* contains a conserved Smr domain required for nonstop mRNA decay

A. Protein domain schematic of NONU-1. See text for details.

B. Structures of representatives of the IF3-C fold domain, including the Smr domain from the human homolog of NONU-1, N4BP2. See also Figure S2.3C.

C. Multiple sequence alignment of the TusA-Alba-Smr assemblage with protein secondary structure diagram and conserved amino acids highlighted. * and ^ indicate amino acids involved in catalysis and substrate recognition (respectively) in TusA or MutS2-like proteins. See also Figure S2.3A.

D. Gene diagram showing the *nonu-1* locus and mutations generated by CRISPR/Cas9.

E. Quantification of GFP expression for the indicated strains (as in Figure 2.1E). P-values from Student's T-test; * = p<10e-6. Compare to Figure 2.1E. See also Figure S2.3.

(3) Two ubiquitin-binding coupling of ubiquitin to ER degradation (CUE) domains of the UBA-like fold (Kang et al., 2003). Ub chains are an important signal for ribosomal stalling and suggest a mechanism of specificity for NONU-1 recruitment to stalled ribosomes (Ikeuchi et al., 2019; Simms et al., 2017; Garzia et al., 2017; Juszkiewicz et al., 2018; Saito et al., 2015).

(4) An Smr domain, homologous in structure and sequence to domains known to bind, cleave, or process RNA (Figures 2.2B, 2.2C, and S2.3A; Aravind et al., 2003). Smr domains of some proteins function as an endoribonuclease (Bhandari et al., 2011; Zhou et al., 2017;Wu et al., 2016), and the Smr domain of *CUE2* was recently identified as being critical for no-go mRNA decay in *S. cerevisiae* (D'Orazio et al., 2019). The NONU-1 Smr domain co-occurs with a highly charged, small helical extension that likely represents an extension of the Smr domain (''N-ext,'' also known as ''DUF1771''). The existence of a domain known to function as an endoribonuclease makes NONU-1 a prime candidate for an endonuclease involved in translation surveillance.

The combination of these domains characterizes the NONU-1 family of proteins found throughout metazoans and choanoflagellates as an endoribonuclease with a conserved role in diverse cell types and organisms.

Catalysis by the Smr domain of NONU-1 is required for nonstop mRNA decay

Given the above observations, we investigated whether the Smr domain is important for NONU-1 function in nonstop mRNA decay. We used CRISPR/Cas9 to delete the Smr domain, generating *nonu-1(srf0780)*, which we hereafter refer to as *nonu-1(smrΔ)* (Figure 2.2D). Expression, splicing, and stability of the *nonu-1* transcript was not grossly perturbed in *nonu-1(smrΔ)* as assayed using RNA sequencing (RNA-seq). When combined with the *unc-54(nonstop)* reporter, *nonu-*

1(smrΔ) conferred derepression of GFP expression comparable with the *nonu-1* premature stop codon mutations originally isolated in the genetic screen (Figure 2.2E). We thus conclude that the NONU-1 Smr domain is required for nonstop mRNA decay.

We analyzed the sequence and structure of the NONU-1 Smr domain to better understand its potential catalytic mechanism. Sequence alignment of NONU-1 homologs across eukaryotes identified a highly conserved aspartate-x-histidine (DxH, where x is typically a hydrophobic amino acid) motif (Figures 2.2C and S2.3A) shared with two related endoribonucleases (Bhandari et al., 2011; Zhou et al., 2017). The DxH motif occupies a position in the Smr domain similar to the location of active site residues of other catalytic versions of the IF3-C fold (Figure 2.2B) and was also identified as being critical for *CUE2* function in *S. cerevisiae* (D'Orazio et al., 2019). Given the defining DxH motif, we investigated if this motif is required for NONU-1's role in nonstop decay. Alanine substitutions at this location (DxH > AxA) exhibited a defect in nonstop decay comparable with the *nonu-1(smrΔ)* as well as *nonu-1* premature stop codon mutations (Figures 2.1E and 2.2E). Taken together, these observations are consistent with the idea that the DxH motif contributes to the active site of the NONU-1 endoribonuclease.

It was recently reported that endonucleolytic cleavage during no-go decay occurs via an unknown metal-independent nuclease resulting in a 3' phosphate and 5' hydroxl (Navickas et al., 2020). Although the catalytic mechanism of Smr is unknown, the emerging picture of Smr endoribonuclease activity is consistent with

what is known about cleavage during no-go/nonstop. First, in vitro RNA cleavage with Smr domain-containing proteins is inhibited by metals (Zhou et al., 2017). Second, metal-dependent nucleases typically require negatively charged amino acids (Asp or Glu) to chelate the positively charged metal. The one residue in NONU-1 that could conceivably function in this manner is Asp579 of the DxH motif, but the isosteric mutation *nonu-1(D579N)* was still functional (Figure 2.2E). Functional substitution of Asp579 with an asparagine is most readily consistent with a metal-independent role for this residue in catalysis.

Our results are consistent with the model that NONU-1 is an endoribonuclease that acts during nonstop mRNA decay, with metal-independent cleavage being carried out by the highly conserved DxH motif within the Smr domain.

NONU-1 reduces nonstop mRNA levels

The *unc-54(nonstop)* reporter contains a T2A "self-cleaving" peptide after the open reading frame that allows the nascent peptide to leave the ribosome and escape repression from ribosome quality control (Arribere and Fire, 2018). That we identified *nonu-1* as a phenotypic suppressor of the *unc-54(nonstop)* reporter suggests that *nonu-1* acts in nonstop mRNA decay rather than in ribosome quality control (Figure 2.3A). Consistent with this, by RNA-seq, we detected a 2.4-fold increase of the *unc-54(nonstop)* reporter mRNA in *nonu-1(smrΔ)* (Figures 2.3B and S2.4A). We thus conclude that *nonu-1* acts to reduce nonstop mRNA levels.

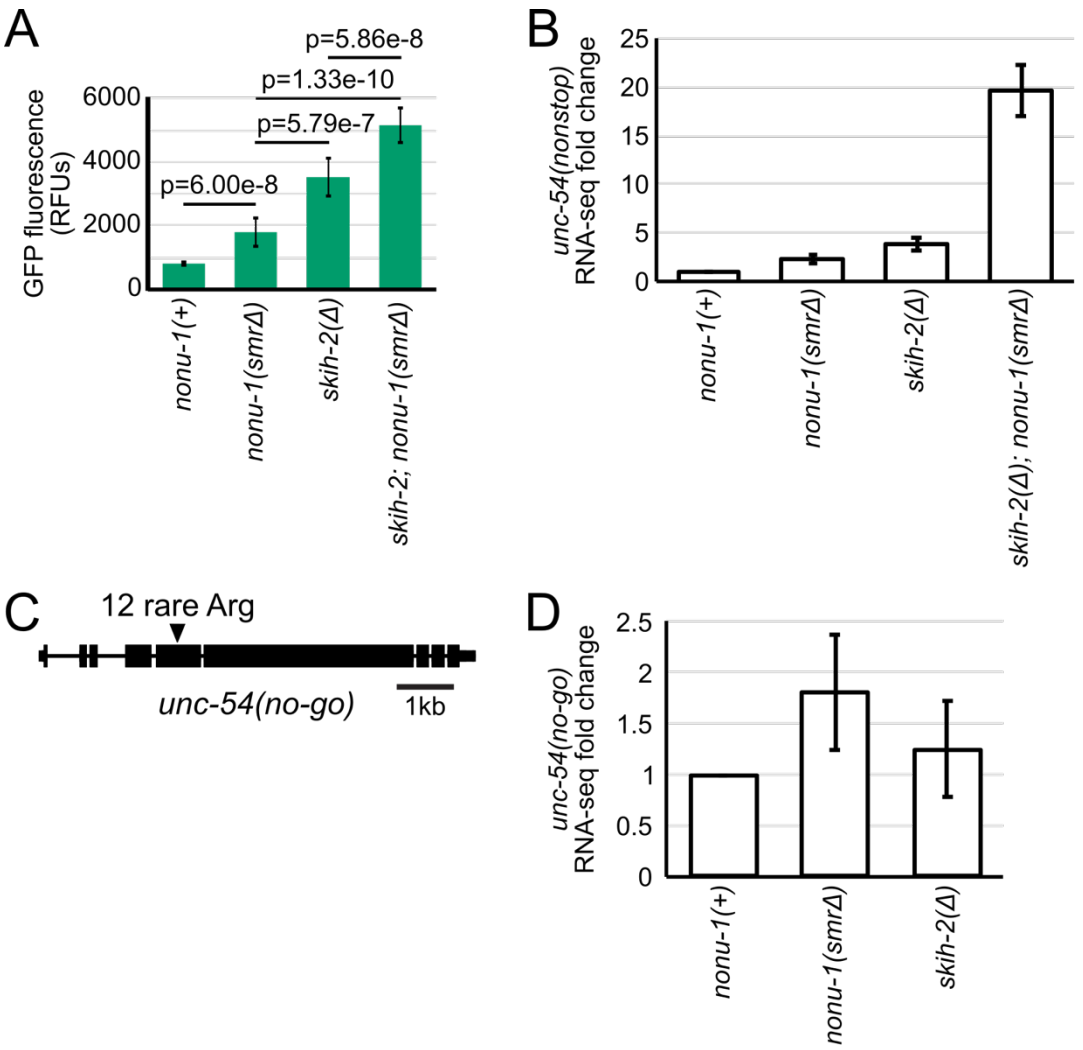

Figure 2.3: NONU-1 reduces mRNA levels of nonstop and no-go reporters
A. Quantification of GFP expression for the indicated strains (as in Figure 2.1E). P-values from Student's T-test.
B. RNA-seq shown as average fold change of *unc-54(nonstop)* relative to *nonu-1(+)* with 95% Confidence Interval shown as error bars.
C. Gene diagram of *unc-54* no-go decay reporter. Triangle indicates an insertion of 12 rare arginine codons (allele *srf0788*).
D. RNA-seq for *unc-54(no-go)* with 95% Confidence Interval as error bars. See also Figure S2.4.

We compared the phenotypic effect on *unc-54(nonstop)* conferred by mutations in *nonu-1* relative to mutations in other nonstop mRNA decay components. The phenotype of *nonu-1* mutants was distinct from *skih-2*-null mutants, as assayed

by the level of GFP fluorescence and *unc-54(nonstop)* mRNA expression (Figures 2.3A and 3B). Interestingly, the *skih-2 nonu-1* double mutant exhibited even greater nonstop suppression than either single mutant alone, as assayed by nonstop mRNA levels, nonstop protein levels, and suppression of *unc-54*'s egg-laying phenotype (Figures 2.3A, 2.3B, and S2.4B). This result is consistent with the idea that phenotypic suppression by *skih-2* and *nonu- 1* do not strictly depend on each other. It is unclear how much of the SKI complex's repressive effect in nonstop mRNA decay is a direct result of accelerated mRNA decay versus other effects (e.g., on mRNA translation initiation and/or recycling; Searfoss and Wickner, 2000; Searfoss et al., 2001; Schmidt et al., 2016).

Because the above analysis of *unc-54* mRNA expression was done using RNA-seq, we were able to address the question of whether *skih-2* and/or *nonu-1* are required for normal expression of endogenous mRNAs. There are endogenous mRNAs targeted by the nonstop decay pathway in other organisms (e.g., Sparks and Dieckmann, 1998). Although we were able to detect mRNAs that increased in either *skih-2* or *nonu-1*, our subsequent analyses support the idea that these mRNAs change as a result of secondary effects (Figure S2.4; Hendriks et al., 2014).

NONU-1 acts in no-go mRNA decay

In addition to nonstop decay, endonucleolytic cleavage of the mRNA is thought to be an important step in no-go decay (Doma and Parker, 2006). No-go

decay results from blocks in translation elongation such as rare codons, polybasic amino acid stretches, and RNA structures (Doma and Parker, 2006). We generated a no-go decay reporter in *C. elegans* by inserting 12 rare arginine codons in-frame in the *unc-54 gene* (*unc-54[no-go]*)(Figure 2.3C). We observed 2-fold derepression of the *unc-54(no-go)* mRNA in *nonu-1(smrΔ)*-mutant animals (Figure 2.3D). Thus NONU-1 is required for repression during no-go decay, and this function resides in the Smr domain. This result points to NONU-1 as a general player in translation surveillance.

We and others have recently shown that nonstop mRNA decay components including SKI and PELO act in NMD after a committed step of mRNA degradation (Hashimoto et al., 2017; Arribere and Fire, 2018). As with *skih-2* and *pelo-1*, we failed to detect derepression of endogenous NMD targets using RNA-seq in *nonu-1* mutants. Once there is additional information on the biochemistry, function, and relationship of NONU-1 to other translation surveillance events, it will become possible to directly test the hypothesis that NONU-1 functions in NMD.

NONU-1 is required for some RNA cleavages in the vicinity of stalled ribosomes

A simple model to explain NONU-1's function in translational surveillance is that it acts as an endonuclease after ribosome stalling. To test this model, we decided to characterize cleavage fragments during nonstop and no-go decay.

We first set out to characterize the role of NONU-1 in mRNA degradation during nonstop mRNA decay. Unfortunately, limitations preclude some techniques

from being used to examine cleavage products in the *unc-54(nonstop)* mRNA reporter: the *unc-54(nonstop)* mRNA is huge (>6 kb), making northern analysis of small cleavage differences difficult, and the A/T-rich nature of the *unc-54* 3' UTR causes short Ribo-seq reads to be lost during PCR (Arribere and Fire, 2018). For this reason we turned to a technique (3'RACE [3' rapid amplification of cDNA ends]) that allows longer read lengths and 3' end identification with single-nucleotide precision. To enhance the stability of cleavage products for detection, we performed these analyses in a *skih-2 pelo-1* mutant background, which slows 3' >5' decay.

Our initial analysis of 3'RACE reads mapping to the *unc- 54(nonstop)* 3' UTR revealed no major *nonu-1*-dependent differences (Figure 2.4A). Interestingly, we observed a population of 3' ends coinciding with the position of known ribosomal stalls (Arribere and Fire, 2018). The lack of a *nonu-1*-dependence to these cleavages points to the existence of *nonu-1*-independent decay mechanisms active during nonstop mRNA decay.

A caveat of the above analysis is that any cleavages occurring in the ~80 nt poly(A) tail (Lima et al., 2017) of *unc-54* would generate unmappable reads that would be lost. Consistent with this idea, a manual inspection revealed several unmapped reads that matched the *unc-54* 3' UTR and contained untemplated adenosines at the annotated poly(A) site (Figure 2.4B). Although we observed a

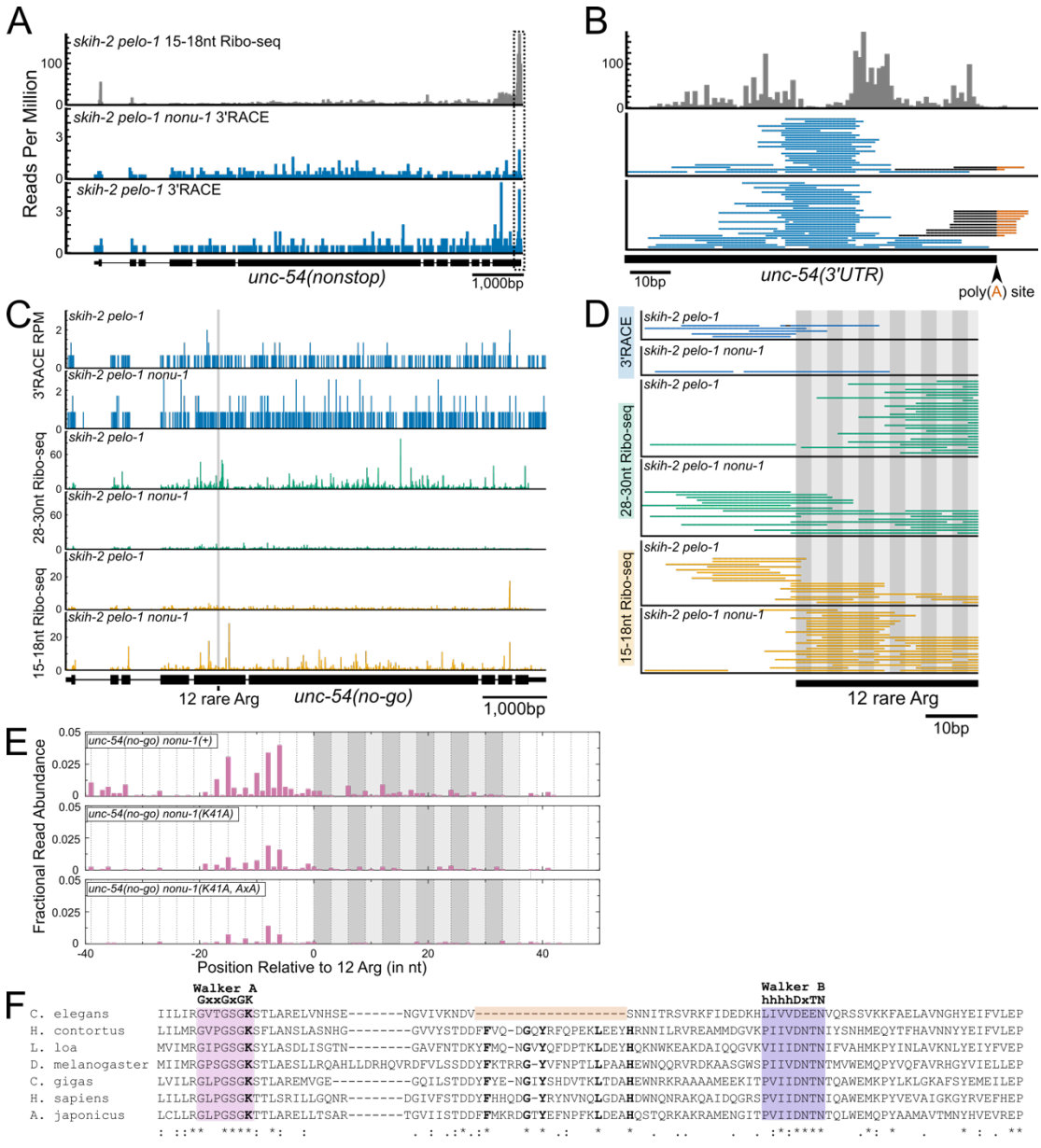

Figure 2.4: *nonu-1*-dependent mRNA cleavage occurs in the vicinity of stalled ribosomes

A. 15-18nt Ribo-seq reads from (Arribere and Fire, 2018) on top (gray) and 3'RACE data from this study on bottom (blue). 5'ends of Ribo-seq and 3'ends of 3'RACE reads were mapped to *unc-54(nonstop)*, with read counts displayed per million uniquely-mapping reads (RPM).

B. Zoomed-in view of the boxed area in part (A). Reads aligned to the poly(A) junction are shown with the sequence mapping to the 3'UTR in black and poly(A) sequence in red. 3'ends of Ribo-seq reads shown.

C. 3'RACE reads on top panel (3'ends, blue), 28-30nt Ribo-seq reads on middle panel (5'ends, green), and 15-18nt Ribo-seq reads on bottom panel (5'ends, orange).

D. Zoomed-in view from part (C) showing region upstream of and including the 12 rare arginines, alternating gray boxes.

E. 5'RACE reads mapped to *unc-54(no-go)*. 5'ends of reads are displayed as fractional read abundance (Methods).

F. Multiple sequence alignment of the P-loop kinase domain of NONU-1 and its homologs. See text.

general decrease in such reads in the *nonu-1(AxA)* mutant, the limited number of such reads makes it difficult to draw strong conclusions.

Given the difficulties in detecting poly(A)-internal cleavage events, we decided to analyze *nonu-1*'s role in no-go mRNA decay. We performed two variations on Ribo-seq: 15–18 nt Ribo-seq, which captures the products of terminally stalled ribosomes at cleavage sites, and 28–30 nt Ribo-seq, which captures some elongating ribosomes (Ingolia et al., 2009; Guydosh and Green, 2014; Arribere and Fire, 2018). The *unc-54(no-go)* reporter contains AGG and CGG arginine codons in a non-random order so as to allow unique mapping of short RNA fragments at and around the stretch of 12 arginines.

Expression analysis showed active translation throughout the *unc-54(no-go)* reporter, with no substantial difference in 28–30 nt Ribo-seq reads for the thousands of bases before and after the stall (Figure 2.4C). Consistent with this, we failed to observe a large discrete peak in either the 3'RACE or 15–18 nt Ribo-seq data. Taken together, these datasets are consistent with the idea that ribosomal stalling by arginine codons is relatively inefficient in *C. elegans*, with most ribosomes translating through the 12 consecutive arginines. We note this is in contrast to *S. cerevisiae*, in which even two rare arginine (CGA) codons are sufficient to induce stalling (Letzring et al., 2010).

Next we closely analyzed reads in the vicinity of the arginine stall. In a *skih-2 pelo-1* background, we observed an absence of 28–30 nt Ribo-seq reads just upstream of the stall, coincident with the appearance of 15–18 nt Ribo-seq and 3'RACE reads

in this region (Figure 2.4D). A simple model to explain this observation is that some elongating ribosomes stall and experience cleavage. This effect was lost in the *nonu-1* mutant; instead 28–30 nt Ribo-seq reads accumulated upstream of the stall, and 3'RACE and 15–18 nt Ribo-seq reads were absent. We note that the low read counts in this region are consistent with the idea that stalling and cleavage is a relatively inefficient event. Nevertheless, the data from the three techniques fit a model in which *nonu-1* facilitates mRNA cleavage after ribosomal stalling.

We next turned our attention to detection of the downstream fragment associated with cleavage. Using a gene-specific 5'RACE protocol, we detected 5' ends upstream of the rare arginine stretch in the same region in which we observed *nonu-1*-dependent 3' ends via 3'RACE and 15–18 nt Ribo-seq (Figure 2.4E). Also consistent with the 3'RACE and 15–18 nt Ribo-seq data, we failed to detect a single discrete site, instead observing a distribution of 5' ends spanning up to ~18 nt upstream upstream of the arginines. The detection of both 5' and 3' ends just upstream of the rare arginine stretch is consistent with endonucleolytic cleavage in this region. We note that our 5'RACE protocol was 5' hydroxyl dependent, adding further evidence to support the idea that the captured ends are the product of a metal-independent cleavage reaction.

We also analyzed the effect of *nonu-1* mutations on the presence of 5' ends. First we characterized the effect of mutation of a highly conserved lysine (K41) present in the Walker A motif of the NONU-1 PNK domain known to be essential for kinase activity (Wang et al., 2002, 2012). In a model in which the kinase domain

phosphorylates the 5’ OH end for subsequent degradation, one would expect an increase in 5’ ends at ribosome stall sites in a PNK domain mutant. Curiously, this was not the case; instead there was a slight reduction in the abundance of 5’ ends in the *nonu-1(K41A)* mutant (Figure 2.4E). Inspection of the PNK domain of *C. elegans* NONU-1 revealed that it contains a large (19 amino acid) in-frame deletion spanning a region of the protein including five residues that are otherwise universally conserved in animals (Figure 2.4F). Further analysis revealed this deletion to be present throughout the *Caenorhabditis* lineage but not in other nematodes. We thus conclude that the *Caenorhabditis* lineage suffered a deletion possibly inactivating the PNK domain of NONU-1, complicating an analysis of PNK domain function in this system.

We also tested the effect of the *nonu-1(AxA)* mutant on the abundance of 5’ ends (*nonu-1(K41A, AxA)* mutant). We saw a slight reduction in the abundance of 5’ ends, consistent with a role for NONU-1 in their generation (Figure 2.4E). However, we noted a persistent low level of reads in the *nonu-1(K41A, AxA)* mutant, thus demonstrating that not all 5’ ends in this region depend on the DxH motif of *nonu-1* for their generation. This result demonstrates that although *nonu-1* is important for cleavage in the vicinity of stalled ribosomes, at least some cleavages persist in its absence, consistent with other results (e.g., Figures 2.4A–2.4D) and data from other labs in other systems pointing to multiple nucleases (Ikeuchi et al., 2019; Navickas et al., 2020).

Evolution of NONU-1 and Smr-domain proteins

Given that previous studies have only partly examined the evolution of Smr domains in eukaryotes (Liu et al., 2013), we conducted an in-depth sequence and structure analysis of the Smr domain. Smr is an IF3-C fold domain that also includes the nucleic acid-binding Alba, and the tRNA thiotransfer-catalyzing TusA (Figures 2.2B, 2.2C, S2.3A, and S2.3B). One unifying sequence feature of this assemblage of IF3-C fold domains is a strongly conserved sxs motif (where s is a small residue, with the second s typically a glycine) in the extended loop region between the second strand and the second helix thought to be involved in substrate binding (Figures 2.2B, 2C, and S3A; Guo et al., 2014). Among the catalytically active versions of the Smr-TusA-Alba assemblage, a conserved aspartate is observed at the C-terminal end of the initial core strand (Figures 2.2B, 2.2C, and S2.3A). This aspartate is near a histidine in NONU-1 and forms the conserved DxH motif. More distant branches of the IF3-C fold include domains that bind, cleave, or process RNA, including the RNaseG/E nucleases (Fukui et al., 2008), the synaptojanin/calcineurin domain phosphoesterases and nucleases (Burroughs and Aravind, 2016), the Schlafen domain endoribonucleases (Makarova et al., 2001; Li et al., 2018; Yang et al., 2018), and the RtcA RNA end cyclases (Figure S2.3B; Palm et al., 2000).

At least one NONU-1-like protein is traceable to the last eukaryotic common ancestor and is in practically all major lineages, suggesting a widespread and ancient role for Smr domain surveillance endonucleases in eukaryotes. NONU-1 homologs show a diversity of domain architectures across eukaryotes, including fusions to

RNA-binding (CCCH, PWI), 20-30 cyclic phosphoesterase (2H), and ubiquitin-binding and conjugation (UIM, UBL, and RING) domains (Figure S2.3C). We also noted multiple instances of rapidly evolving lineage-specific expansions of NONU-1 homologs. These include multiple paralogs (25 or more) with distinct domain architectures in nematodes of the *Caenorhabditis* lineage. Some of these have predicted signal peptides, suggesting that they are secreted (e.g., in *Caenorhabditis remanei* and *Entamoeba*). The combination of lineage-specific expansions, rapid evolution, and secretion is a hallmark of proteins deployed as effectors in defensive or offensive roles in biological conflicts (Krishnan et al., 2018; Zhang et al., 2016; Lespinet et al., 2002). In light of this, we hypothesize that several eukaryotic Smr proteins, especially the expanded versions, might function beyond translation surveillance as effectors deployed against viral or parasitic RNA. This is consistent with the discovery of a comparable role for the structurally related Schlafen domain in tRNA processing and retroviral RNA restriction (Li et al., 2012; Yang et al., 2018), as well as numerous studies showing that cellular RNA processing and translation surveillance factors have antiviral functions (Toh-E et al., 1978; Garcia et al., 2014; Balistreri et al., 2014).

DISCUSSION

NONU-1 and its homologs in *S. cerevisiae* are the first factors with a nuclease domain to be identified as required for nonstop/no-go mRNA decay. The Smr domain is conserved throughout eukaryotes, and its function in translation surveillance is

conserved between *S. cerevisiae* and *C. elegans*, establishing NONU-1 as an ancient factor critical to ribosome rescue and mRNA decay. Our identification and characterization of NONU-1 sheds light on the poorly understood intersection of translation and mRNA decay and sets the stage for a more complete molecular understanding of ribosome rescue.

Our analyses support a model in which NONU-1 is required for some mRNA cleavages upstream of ribosomal stalls. This is consistent with the idea that NONU-1 acts on a trailing ribosome that collides with a stalled ribosome, lending support to the idea of ribosomal collisions as an important signal in translational surveillance (Simms et al., 2017). We also note this role of NONU-1 is conserved to *S. cerevisiae*, where the NONU-1 homolog Cue2p is required for cleavage upstream of a ribosomal stall (D'Orazio et al., 2019).

Our analysis also revealed a population of nonu-1-independent 15–18 nt Ribo-seq reads internal to the stall (Figures 2.4C and 2.4D). Arginine-internal ribosomal stalls have not been reported in *S. cerevisiae*, perhaps because stalling at CGA is so efficient (Letzring et al., 2010), and because the repetitive nature of the $(CGA)_{12}$ reporter commonly used prevents read mapping internal to the stall. Additional work will help illuminate the diversity of ribosome stalling events and downstream cellular responses.

Interestingly, we note that NONU-1 is not required for full repression of the mRNA targets of translation surveillance. Even in presumed *nonu-1*-null mutants, we observed substantial repression of nonstop/no-go targets that could be relieved with

other suppressors (e.g., *skih-2*). Two simple, non-mutually exclusive models are as follows: (1) NONU-1 may function redundantly with other endonucleases in translation surveillance. Recent work in *S. cerevisiae* points to the existence of at least two nucleases active during no-go decay, though their identities remain unknown (Ikeuchi et al., 2019; Navickas et al., 2020). Our analyses here corroborate this idea, as we observed some cleavages that persisted in *nonu-1* mutants (Figure 2.4). (2) There may be cleavage-independent mechanisms that repress the mRNA targets of translation surveillance. Whether through additional nucleases or cleavage-independent mechanisms, our work supports a redundancy in translation surveillance that ensures robust repression of its targets and efficient rescue of stalled ribosomes.

Our results support the idea that NONU-1 acts in translation surveillance largely independently of the SKI complex. We observed multiplicative effects in *skih-2 nonu-1* double mutants, and in both *C. elegans* and *S. cerevisiae*, we observed a greater derepression of nonstop reporters in *skih-2/ski2Δ* mutants relative to *nonu-1/cue2D/ypl199cΔ* mutants. This is surprising given the prevailing model in the field that SKI accelerates 3'>5' decay after endonucleolytic cleavage. One possibility is that NONU-1 may function redundantly with other endonucleases to create SKI substrates. Another possibility is that SKI's role in surveillance is misunderstood. Although it is widely known that one function of the SKI complex is to destabilize the upstream (5') mRNA fragment during translation surveillance (e.g., Doma and Parker, 2006; Hashimoto et al., 2017), it is unclear if this effect is responsible for the phenotypic suppression of nonstop reporters by SKI. Alternative models include

functional suppression by SKI's effects on ribosome recycling, initiation, or mRNA extraction from the ribosome (Searfoss and Wickner, 2000; Searfoss et al., 2001; Zinoviev et al., 2020), which is also consistent with recent structural data showing a direct role for SKI on the ribosome and near the 5' ends of ORFs (Schmidt et al., 2016).

In *S. cerevisiae*, endonucleolytic cleavage during no-go creates a 5' hydroxyl that is phosphorylated by Rlg1/Trl1 to facilitate 5' >3' digestion by Xrn1 (Navickas et al., 2020). Although Rlg1/ Trl1 is widely conserved in several eukaryotic lineages, including fungi, plants, alveolates, and kinetoplastids (Burroughs and Aravind, 2016), its absence in the animal/choanoflagellate lineage raises the question of what protein carries out this RNA repair. Interestingly, the animal/choanoflagellate NONU-1 homologs have acquired a P loop kinase domain that is related to but distinct from the kinase domain of Rlg1/Trl1. The acquisition of a P loop kinase domain in NONU-1 in organisms that have lost Rlg1/Trl1 suggests a model in which NONU-1 phosphorylates its own cleavage products to facilitate degradation by Xrn1. Although we were unable to test this model in *C. elegans*, we expect that it will inform efforts to understand the fate of cleaved fragments in other animal systems such as humans.

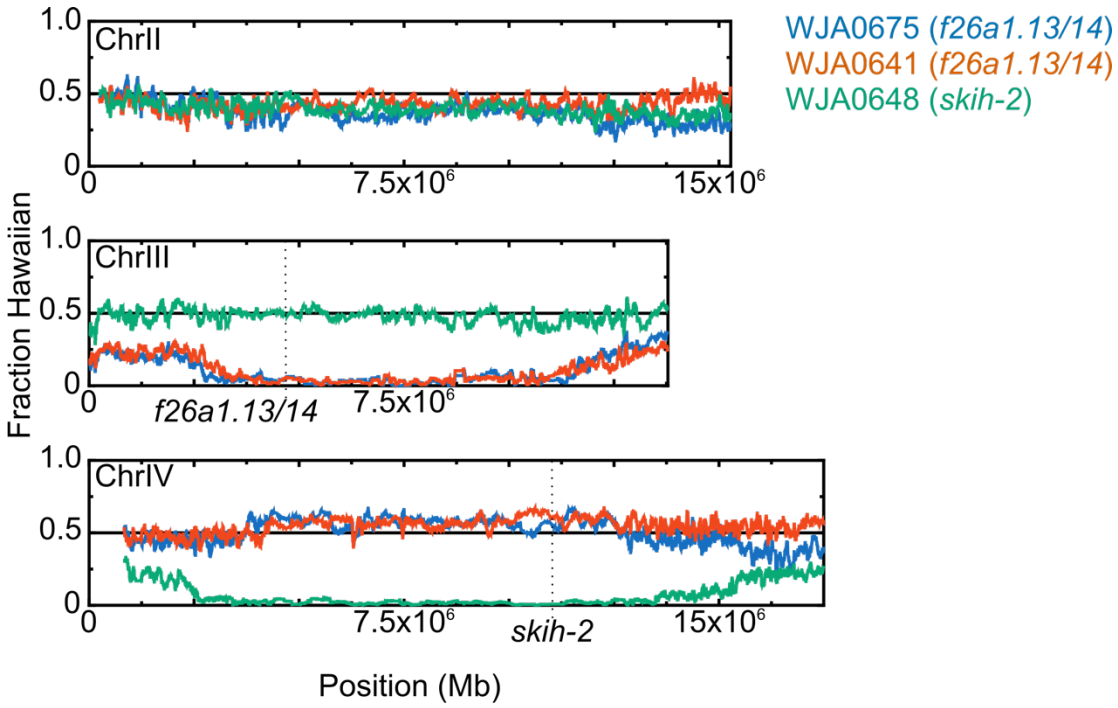

Figure S2.1: Two strains show linkage to an area of chromosome III lacking known nonstop mRNA decay factors (related to Figure 2.1)

Genetic maps for three strains showing linkage (and lack thereof) to chromosomes II, III, and IV. WJA0648 contains a mutation in *skih-2* on chromosome IV. WJA0675 and WJA0641 contain mutations in *f26a1.13/14* (renamed *nonu-1*) on chromosome III. X-axis shows position along the chromosome in megabases (Mb). See Methods for a description of the Hawaiian mapping procedure and variant calling. This technique narrows down the causative mutation to a large swath of one chromosome, after which we manually inspected the region of interest to identify possible mutations (subsequently verified by CRISPR/Cas9).

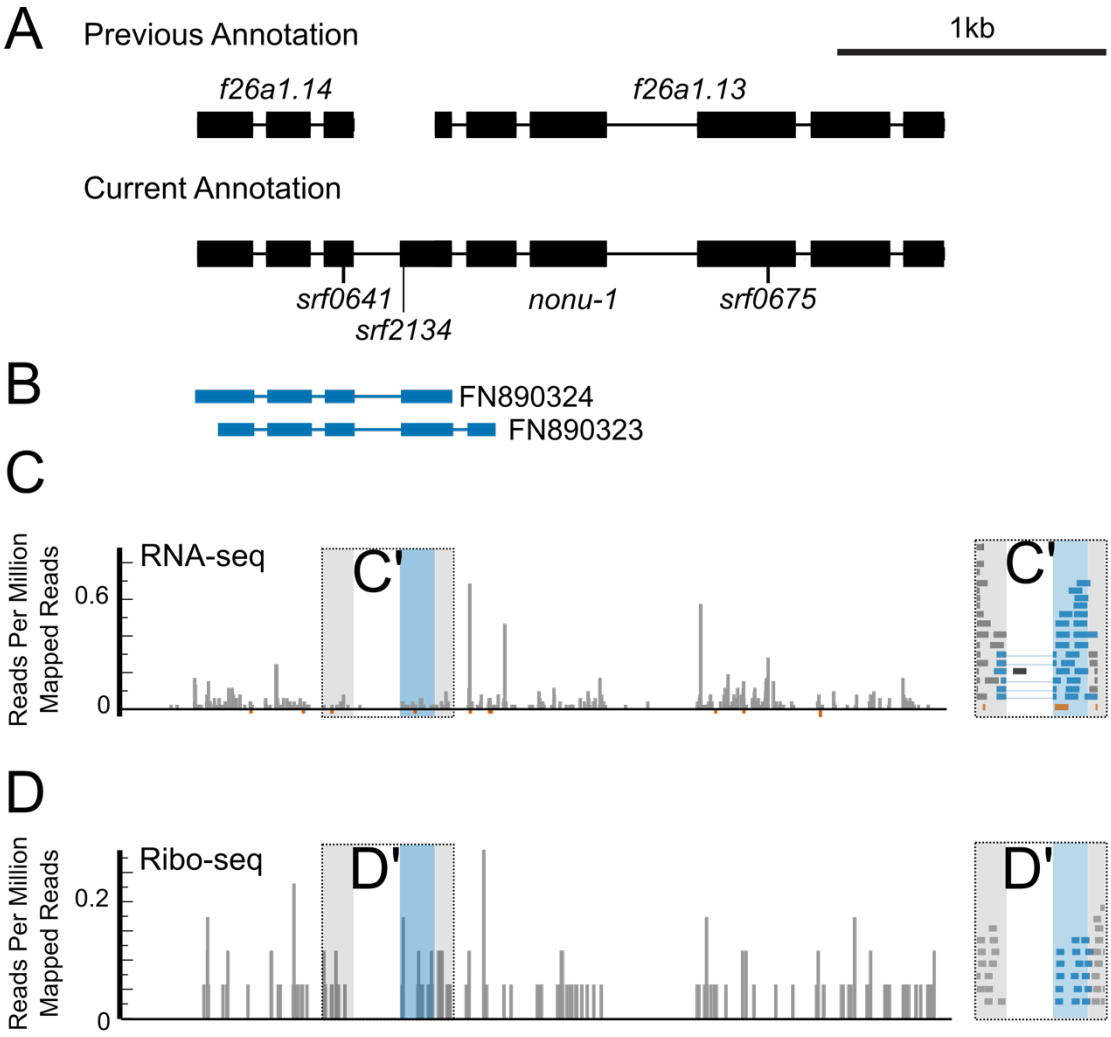

Figure S2.2: *f26a1.13/14* encode a single functional gene (related to Figure 2.1)
A. Gene diagrams for *f26a1.13* and *f26a1.14*. Prior annotations indicated on top, with rectangles and lines representing exons and introns, respectively. New annotation below, along with the location of each of three premature stop codon mutations (*srf* alleles) that exhibit identical phenotypes in a nonstop mRNA reporter strain. Data in parts (B-D) are vertically aligned with annotations in part (A).
B. Public ESTs that span the proposed previously unannotated splice junction.
C. Published RNA-seq data from (Hendriks et al., 2014) showing reads spanning the proposed previously unannotated splice junction. Inset (C') zooms in on the region of interest, with reads supporting the junction highlighted (blue). Antisense reads in red.
D. Published Ribo-seq data from (Hendriks et al., 2014) showing ribosome footprints spanning the proposed previously unannotated splice junction. Inset (D') zooms in on the region of interest, with reads supporting the junction highlighted (blue). Note there is a similar density of Ribo-seq reads throughout the entire gene body of both *f26a1.13* and *f26a1.14*, consistent with the idea they represent a single translational unit.

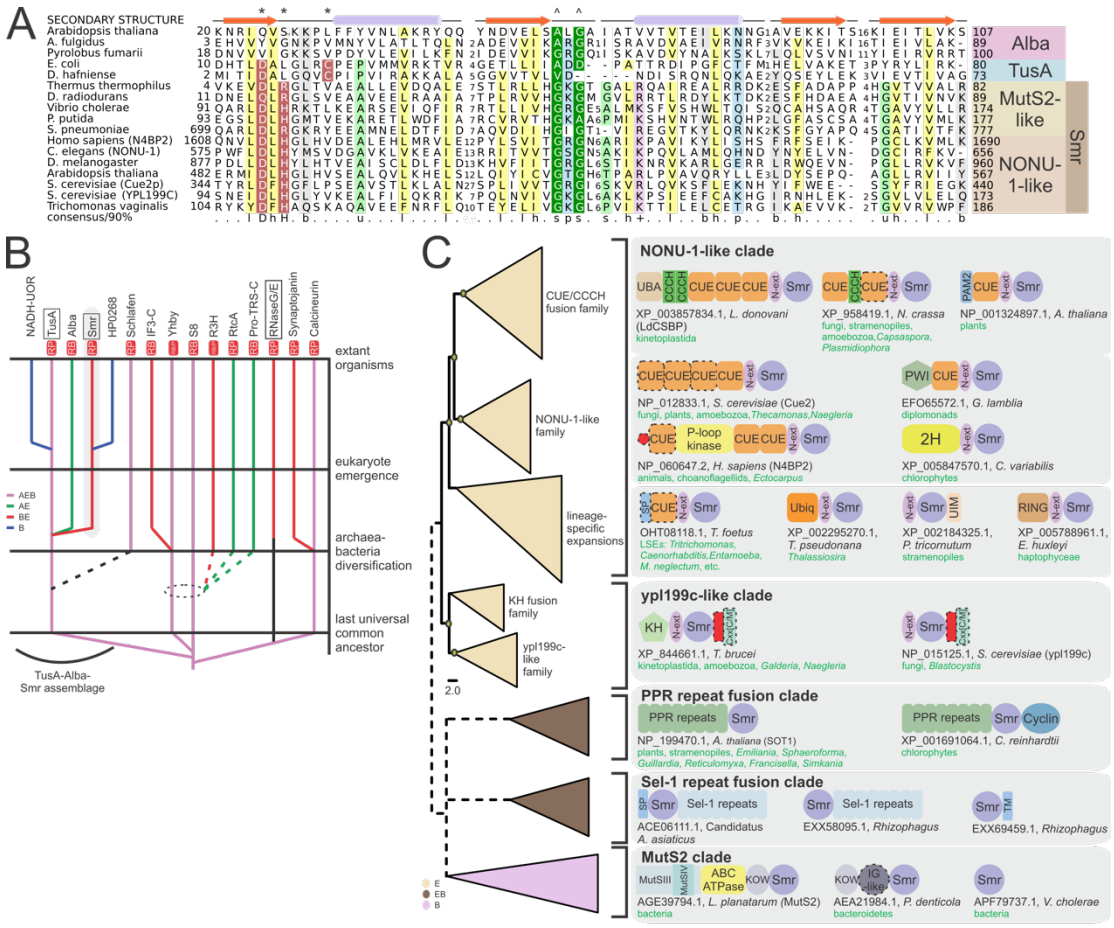

Figure S2.3: Conservation and evolution of the Smr domain in the IF3-C fold framework (related to Figure 2.2)

A. Extended multiple sequence alignment of representatives of domains from the TusA-Alba-Smr assemblage. Secondary structure shown on top, and consensus on which alignment is colored provided on bottom line.

B. Phylogenetic tree of evolutionary relationships between different IF3-C fold domains, with key evolutionary transitions labeled to the left of the diagram. Tree branches are colored according to occurrence of the domain in the respective kingdom (Archaea, Bacteria, and/or Eukarya). Some evolutionary relationships are uncertain (dotted lines). Structural renderings of boxed domains (TusA, Smr, RNaseG/E) are shown in Figure 2.2B. Functional annotations for lineages in red boxes below names are as follows: 'RB', RNA-binding; 'RP', RNA-processing. Here, top-down view of RNaseG/E is provided to emphasize the importance of dimerization in the metal-binding nuclease active site.

C. Broader phylogeny depicted as stylized tree of all known Smr domain families. Nodes supported by bootstrap >75% are marked by brown circles. Dotted lines in tree indicate uncertainty in phylogenetic placement. Representative domain architectures observed within each family provided to the right of monophyletic, collapsed tree branches. Individual domains found within a single polypeptide are represented by distinct shapes labeled by name. Dotted lines around a domain indicate absence in some organisms of the listed phylogenetic distribution for each architecture, provided below architectural depiction. Red circle represents the N-terminal basic stretch described in the text. Red box represents a variable-length charged region characteristic of members of the ypl199c-like clade.

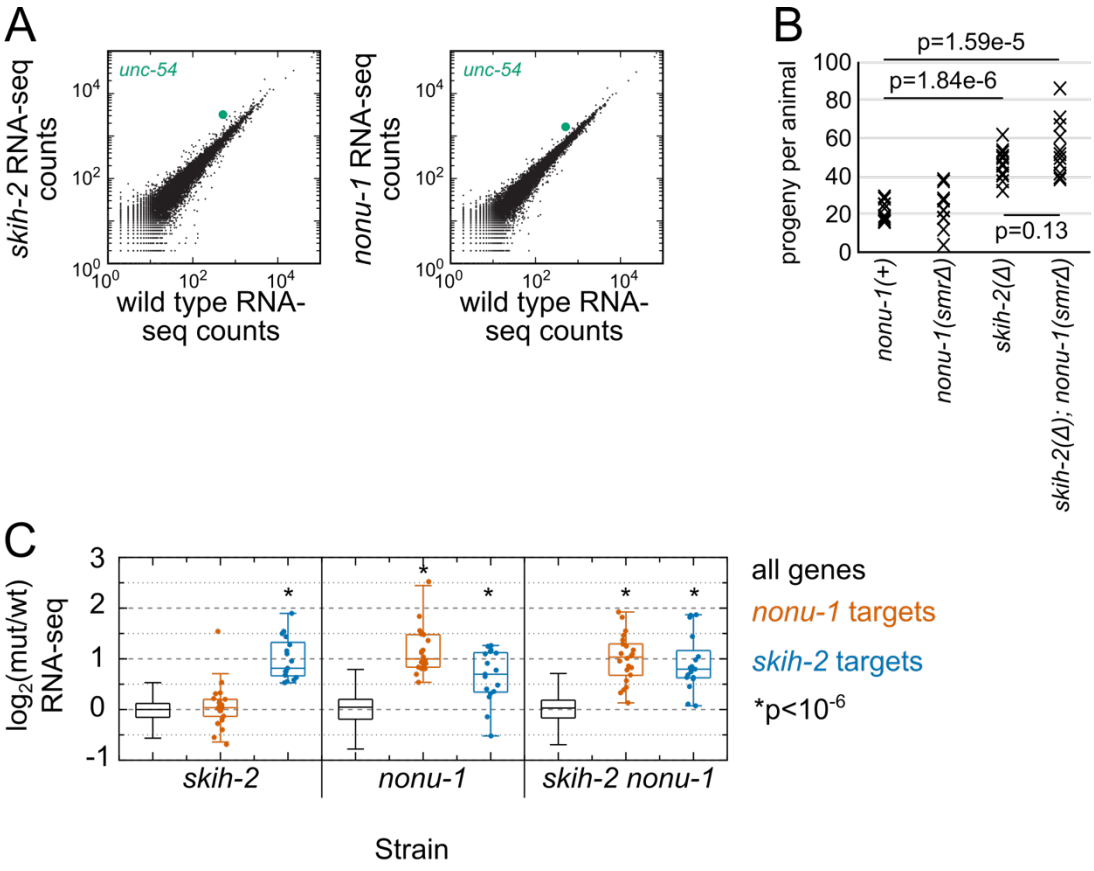

Figure S2.4: Multiplicative and non-multiplicative effects of *skih-2* and *nonu-1* on phenotypes (related to Figure 2.3)

A. RNA-seq read counts in the indicated strains. RNA-seq was performed (see Methods), and read counts for all mRNAs is shown (black dots) with *unc-54* highlighted (green dot). Off-diagonal genes indicate increased mRNA expression in one strain relative to the other. Note axes are log-scaled.

B. Brood sizes for the indicated strains. Each X represents the number of progeny from a single animal from that strain. 12 animals were examined per strain. P-values from Student's T-test.

C. Y-axis shows log2 fold change for gene expression changes between the indicated mutant strains and wild type for all genes with at least 30 reads in wild type (different read cutoffs in wild type yielded similar results). *nonu-1* (red) and *skih-2* (blue) targets are defined as mRNAs that are upregulated in the respective mutant strains relative to wild type (as determined by DESeq, see Methods). P-value from Mann Whitney U test comparing the indicated subset of genes to all genes. Note that unlike *unc-54*, targets of *nonu-1* and *skih-2* fail to exhibit a further increase in mRNA expression in the double mutant. A biological replicate of these data produced similar results.

CHAPTER 3: *k07a12.4* IS A HOMOLOG OF *HBS1* THAT DOES NOT ENCODE A Ski7-LIKE PROTEIN

ABSTRACT

Nonstop mRNA decay is a translation surveillance pathway that degrades transcripts with no in-frame stop codons, so-called nonstop mRNAs. Ribosomes translate nonstop mRNAs and stall in the poly-A tail or on the 3' end of the mRNA, triggering mRNA decay and ribosome rescue. Hbs1 is a GTPase that is required for ribosome rescue during nonstop decay and here we identify the *C. elegans* homolog, K07A12.4, via a genetic screen with a phenotypic nonstop mRNA decay reporter. Ski7 is a paralog of Hbs1 that is required to degrade nonstop mRNAs in yeast by mediating interactions between the SKI helicase complex and the 3'>5' RNA exosome. In many eukaryotes a Ski7-like protein is expressed as an alternative splice isoform of the *HBS1* gene. However, we did not detect a Ski7-like isoform in *C. elegans*. If *C. elegans* expresses a Ski7-like protein, we hypothesize that the protein is highly diverged from Ski7-like proteins identified in other organisms. Our genetic screen also identified new alleles of genes encoding components of the SKI complex, *skih-2* and *ttc-37*. All identified *skih-2* alleles are individual point mutations that will prove useful in dissecting where SKIH-2 functions during translation surveillance.

INTRODUCTION

mRNA translation consists of initiation, elongation, termination, and recycling, with the ultimate goal of faithfully synthesizing the protein encoded in the mRNA. As ribosomes translate mRNAs, they also act as sensors to detect aberrations

in the mRNA and initiate translation surveillance pathways (reviewed in Simms et al., 2017). Nonstop mRNA decay regulates transcripts lacking stop codons that result in ribosomal stalling in the poly-A tail or on the 3' end of the mRNA (Frischmeyer et al., 2002; van Hoof et al., 2002). When ribosomal stalling occurs, a second trailing ribosome collides with the first stalled ribosome, triggering degradation of the aberrant mRNA and rescue of the stalled ribosomes (Simms et al., 2017; Juszkiewicz et al., 2018; D'Orazio et al., 2019; Ikeuchi et al., 2019; Navickas et al., 2020).

Interestingly, stalled ribosomes do not participate in canonical termination and recycling, because the canonical machinery only recognizes ribosomes with a stop codon in the A site (reviewed in Loh and Song, 2010). The ribosome release factors eRF1 and eRF3 have paralogs in most eukaryotes, Dom34/Pelota and Hbs1, respectively (Atkinson et al., 2008; Graille et al., 2008; Chen et al., 2010). Dom34/Pelota contains M and C domains that are structurally similar to the M and C domains of eRF1, though the M domain lacks the GGQ motif that is critical for peptide hydrolysis (Atkinson et al., 2008; Graille et al., 2008; Chen et al., 2010). Dom34/Pelota also lacks the eRF1 NIKS motif that recognizes stop codons, allowing Dom34/Pelota to interact with ribosomes in a codon-independent manner (Atkinson et al., 2008; Graille et al., 2008; Chen et al., 2010). Comparable to the mechanism of eRF3 delivering eRF1 to the A site of terminating ribosomes, the GTPase Hbs1 delivers Dom34/Pelota to the A site of stalled ribosomes during nonstop decay (Tsuboi et al., 2012; Saito et al., 2013; Hilal et al., 2016). Significant conformational changes occur when GTP-bound Hbs1 binds Dom34/Pelota, causing Dom34/Pelota to

adopt a tRNA-like structure that increases A site affinity (Shao et al., 2016). After GTP hydrolysis by Hbs1, the ribosome recycling factor ABCE1 is recruited to work with Dom34/Pelota to split the ribosome into subunits (Pisareva et al., 2011; Shoemaker and Green, 2011; Becker et al., 2012; Shao et al., 2016).

In yeast there is another paralog of eRF3 and Hbs1, Ski7 (Marshall et al., 2018). Hbs1 and Ski7 arose from a whole genome duplication and have distinct cellular functions (van Hoof et al., 2002; Tsuboi et al., 2012; Saito et al., 2013; Marshall et al., 2018). Ski7 operates in mRNA decay, directly binding to the SKI helicase complex and the RNA exosome (Araki et al., 2001; Wang et al., 2005; Kowalinski et al., 2016). Structural studies are consistent with Ski7 mediating mRNA delivery from the SKI complex into the cytoplasmic exosome to allow for mRNA degradation (Kowalinski et al., 2016). In many eukaryotes, a Ski7-like protein is encoded by an alternatively spliced isoform of *HBS1* (Marshall et al., 2013; Kalisiak et al., 2017; Marshall et al., 2018). Interestingly, the Ski7-like isoforms are incredibly diverse and have poor alignment via multiple sequence alignment. Yeast Ski7 is discernible from Hbs1 by three short motifs, though only one of the motifs, the S3 motif that forms part of the exosome binding domain, is recognizable in all identified Ski7-like proteins (Marshall et al., 2018). Furthermore, the exosome binding domain of Ski7-like proteins is in a weakly conserved, elongated stretch of the protein lacking a three-dimensional fold and the SKI binding domain is predicted to exhibit similar properties (Wang et al., 2005; Marshall et al., 2018). There is also poor conservation of the domain organization of Ski7-like proteins, inhibiting simple identification of

Ski7-like proteins via homology searches. Consequently, a Ski7-like protein is yet to be identified in *C. elegans*.

The SKI complex is required for nonstop mRNA decay and is composed of Ski2, Ski3, and Ski8, though only homologs of Ski2 (SKIH-2) and Ski3 (TTC-37) have been characterized in *C. elegans* (Anderson and Parker, 1998; Brown et al., 2000; van Hoof et al., 2002; Arribere et al., 2018). Ski2 is a 3'>5' RNA helicase that has been shown to feed mRNA into the RNA exosome via Ski7 for degradation (Widner and Wickner, 1993; Araki et al., 2001; Wang et al., 2005; Kowalinski et al., 2016). After ribosomes stall and collide on mRNAs, endonucleolytic cleavage of the offending mRNA occurs and the prevailing model is that the 5' cleavage fragment is degraded by SKI with the exosome (van Hoof et al., 2002; Doma and Parker, 2006; Hashimoto et al., 2017; Arribere and Fire, 2018). SKI appears to also have an alternative Ski7-independent function of extracting mRNA from ribosomes and may remove nonstop mRNAs from stalled ribosomes in a cleavage-independent manner, though this is yet to be tested *in vivo* (Zinoviev et al., 2020).

Here we identify the homolog of Hbs1, K07A12.4, as being required for nonstop decay in *C. elegans*. Our phenotypic data is consistent with K07A12.4 functioning as Hbs1 in ribosome rescue and mutations in the critical GTPase domain of K07A12.4 block nonstop decay. Although there are two isoforms of K07A12.4, they are extremely similar and neither of them encode a Ski7-like protein. We also identified new alleles of *skih-2* and *ttc-37* that will provide insight into how SKI's helicase activity represses nonstop mRNAs. Identification of Hbs1 and novel SKI

alleles in *C. elegans* will provide a better understanding for mRNA degradation and ribosome rescue during nonstop decay.

RESULTS

k07a12.4 is required for nonstop mRNA decay in *C. elegans*

We performed a genetic screen with a phenotypic reporter in *C. elegans* to identify nonstop mRNA decay factors, which led to the identification of *skih-2*, *ttc-37*, and *nonu-1* (see Chapter 2). During analysis of additional mutants from the screen, we found that two mutants mapped to an uncharacterized *C. elegans* gene, *k07a12.4*. The strain WJA0646 contained a G275R mutation and the strain WJA0670 contained a splice site acceptor c.2773G>A mutation (Figure 3.1A). Homology searches identified the K07A12.4 protein as a homolog of the translational GTPase Hbs1. Hbs1 has been characterized in other eukaryotes and works in conjunction with Dom34/Pelota to rescue stalled ribosomes during nonstop and no-go decay (Becker et al., 2011; Shao et al., 2013; Shao and Hegde, 2014; Guydosh and Green, 2014; Hilal et al., 2016).

The nonstop reporter used for the genetic screen was integrated at the *unc-54* locus, harboring GFP followed by a ribosomal skipping T2A sequence and all stop codons removed from the 3' UTR. The *unc-54(nonstop)* reporter is derepressed when nonstop mRNA decay is blocked, leading to increased GFP fluorescence. Both mutations in *k07a12.4* conferred derepression of GFP to a similar extent as a

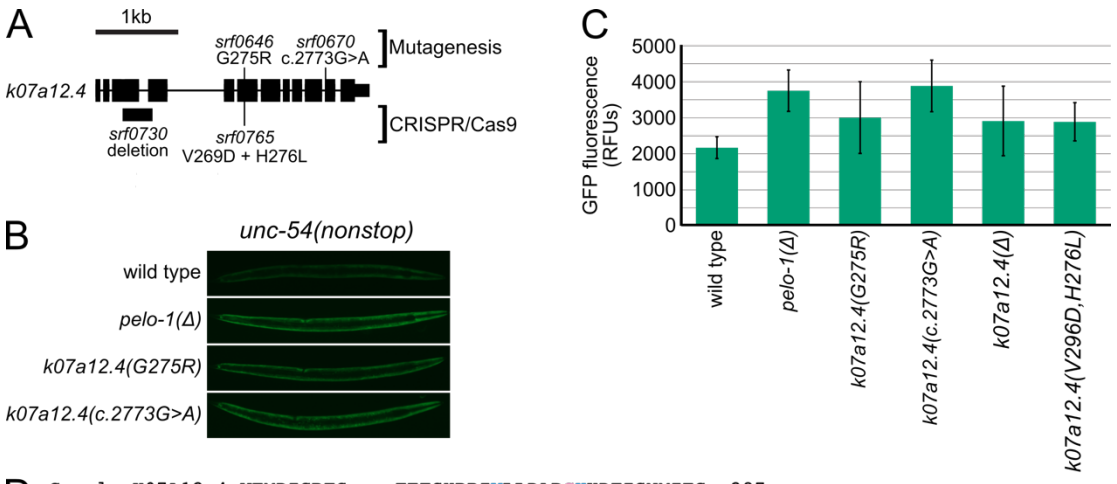

D

```
C. ele K07A12.4 VTMDIGRTS----FETSHRRIVLLDAPGHKDFISNMITG- 287
S. cer Ski7     FSMFKKVIQVENDLLPPSSTLTLIDTPGSIKYFNKETLNS 371
S. cer Hbs1     VTVSICTSH----FSTHRANFTIVDAPGHRDFVPNAIMG- 266
C. ele ERFA-3   KTVEVGRAY----FETEKRHFTILDAPGHKSFVPNMIVG- 208
S. cer Sup35    KTIEVGKAY----FETEKRRYTILDAPGHKMYVSEMIGG- 359
                 ::          :       .::*:**   :. :   .
```

Figure 3.1: K07A12.4 is required for nonstop mRNA decay
A. Gene diagram showing annotated exons (black rectangles) at the *k07a12.4* locus. Mutations made via EMS and CRISPR/Cas9 are above and below the gene, respectively.
B. Images of UNC-54::GFP expression in the indicated strains.
C. Quantification of GFP expression for strains shown in (B) and two strains made by CRISPR/Cas9. Each bar represents an average image of at least 5 different animals; 95% Confidence Interval shown as error bars. RFUs, Relative Fluorescence Units.
D. Multiple sequence alignment of the GTPase domain of K07A12.4 with the GTPase domain of Ski7, Hbs1, ERFA-3, and Sup35. Ski7's GTPase domain is inactive due to loss of the catalytic histidine. 'C. ele' is *C. elegans* and 'S. cer' is *S. cerevisiae*. Bold residues mutated by EMS (pink) or CRISPR/Cas9 (blue).

knockout of the ribosome rescue factor *pelo-1*, which is Hbs1's functional partner (Figure 3.1B and 3.1C).

Upon closer analysis of the mutations in *k07a12.4*, we found that the G275R mutation mapped to the GTPase domain. Both Hbs1 and Ski7 have a GTPase domain required for function in nonstop decay, though Ski7's GTPase domain is inactive for GTP hydrolysis due to loss of a catalytic residue (Kowalinski et al., 2015; Horikawa et al., 2016; Marshall et al., 2018). We performed a multiple sequence alignment of K07A12.4's GTPase domain with *S. cerevisiae* Hbs1 and Ski7, in addition to the homologs of the translational GTPase eRF3, *C. elegans* ERFA-3 and *S. cerevisiae*

Sup35 (Figure 3.1D). G275 is highly conserved and directly upstream of a histidine residue that catalyzes GTP hydrolysis, suggesting that G275R inhibited GTP hydrolysis. We also independently created two mutant alleles of *k07a12.4* via CRISPR/Cas9: a V269D; H276L mutation *(k07a12.4(V269D;H276L))* and a large deletion near the N-terminus expected to completely knockout expression of all isoforms *(k07a12.4(Δ))*. Both *k07a12.4(G275R)* and *k07a12.4(V269D;H276L)* derepressed GFP from the *unc-54(nonstop)* reporter to the same degree as *k07a12.4(Δ)*, indicating that K07A12.4 lacking GTPase activity functions as a null allele (Figure 3.1C). Therefore, we conclude that the GTPase activity of K07A12.4 is critical for nonstop mRNA decay.

The splice site acceptor mutation found in *k07a12.4* mapped to the 5' side of exon 11 (Figure 3.1A). We hypothesize that this mutation either caused complete skipping of exon 11 or use of a cryptic splice site nearby. If a cryptic splice site in a different reading frame was chosen, *k07a12.4* could be targeted for Nonsense Mediated Decay (NMD) (reviewed in Lykke-Andersen and Jensen, 2015). There is an out of frame UAA near the 3' end of exon 11 that could be recognized as a premature termination codon by the NMD machinery, leading to destruction of the mRNA and decreased expression of K07A12.4. Alternatively, if exon 11 was completely skipped there would not be a premature termination codon within the mRNA. This would suggest that exon 11 is crucial for K07A12.4 function. Exon 11 falls within domain III of K07A12.4 which interacts with the central domain and the C-terminal domain of Dom34/Pelota (Chen et al., 2010; Becker et al., 2011; Hilal et al., 2016). Structural

studies from yeast show extensive interactions between Dom34/Pelota and R517, P518, and H558 of Hbs1 domain III (Hilal et al., 2016). While the equivalent residues of K07A12.4 are not encoded by exon 11, skipping of the exon may disrupt multiple contacts with the *C. elegans* homolog of Dom34/Pelota, PELO-1. RNAseq will be crucial to understand the effect of the splice site mutation on K07A12.4. Importantly, the *k07a12.4(c.2773G>A)* allele derepressed GFP from the *unc-54(nonstop)* reporter to the same degree as *k07a12.4(Δ)*, demonstrating that the splice site mutation results in a null allele of K07A12.4 (Figure 3.1C).

k07a12.4 does not encode a Ski7-like protein

In yeast, Ski7 is a paralog of Hbs1 and these factors are encoded by different genes (Marshall et al., 2013; Marshall et al., 2018). However, in many other eukaryotes Hbs1 and a Ski7-like protein are encoded by a single gene that is alternatively spliced to create two isoforms (Marshall et al., 2013; Kalisiak et al., 2017; Marshall et al., 2018). While it was originally hypothesized that Hbs1 only functions in the translation surveillance pathway no-go decay, studies have shown that both Hbs1 and Ski7 are required for nonstop decay, with Hbs1 functioning in ribosome rescue and Ski7 functioning in mRNA decay (van Hoof et al., 2002; Doma and Parker, 2006; Tsuboi et al., 2012; Saito et al., 2013). We considered the possibility that K07A12.4 is alternatively spliced to produce both Hbs1 and Ski7. There are two annotated splice isoforms of *k07a12.4* that are extremely similar and neither encodes a Ski7-like protein. The protein encoded by each *k07a12.4* transcript

lacks an S3 motif, a motif that is critical for interactions with the RNA exosome and is found in all Ski7-like proteins identified in eukaryotes (Marshall et al., 2018). We then considered the possibility that additional unannotated isoforms of *k07a12.4* may exist and analyzed published nanopore mRNA reads (Roach et al., 2020). While the two annotated isoforms were confirmed, no additional isoforms were identified (Figure 3.2).

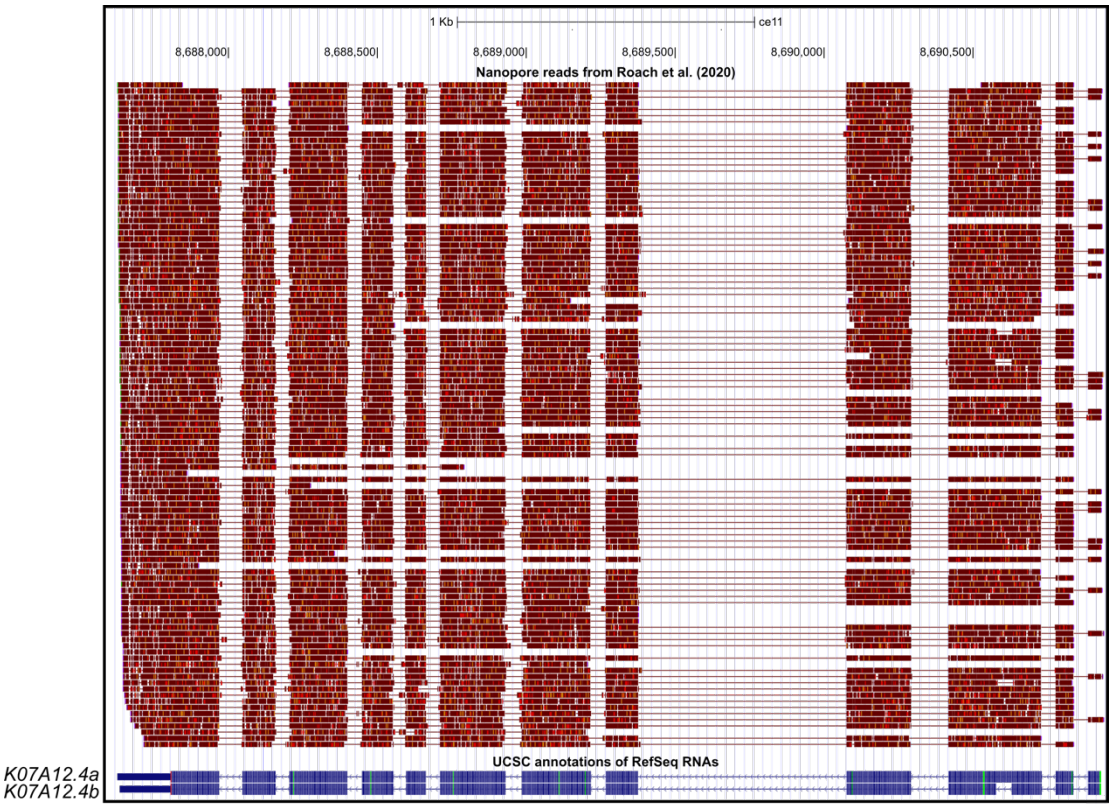

Figure 3.2: *k07a12.4* encodes two similar splice isoforms
Nanopore reads (red) from (Roach et al. 2020) aligned to *k07a12.4* locus of *C. elegans* genome (ce11). Annotated transcripts shown on botton (blue), with exons as boxes and introns as lines with arrowheads indicating the direction of transcription.

Consistent with these findings, we failed to isolate mutant alleles of *k07a12.4* that exhibit a SKI phenotype. The *unc-54(nonstop)* reporter expresses varying levels

of GFP when different genes are mutated, depending on where the gene's function is in nonstop decay. Mutations in mRNA decay factors such as the SKI complex express bright UNC-54::GFP, while mutations in ribosome rescue factors such as PELO-1 express dim UNC-54::GFP (Figure S3.1A and S3.1B). All mutant alleles of *k07a12.4* express dim UNC-54::GFP, including the deletion allele *(k07a12.4(Δ))*. This phenotypic evidence supports the idea that *k07a12.4* encodes Hbs1 and not Ski7 function.

New alleles of *skih-2* and *ttc-37*

The majority of mutants identified by the nonstop mRNA decay genetic screen mapped to homologs of *SKI2* and *SKI3*, *skih-2* and *ttc-37,* respectively (Figure 3.3A and 3.3B). *skih-2* and *ttc-37* were previously shown to be required for nonstop decay in *C. elegans* (Arribere and Fire, 2018). Structures of the yeast SKI complex revealed that Ski3 acts as a scaffold for Ski2 and Ski8 (Halbach et al., 2013; Schmidt et al., 2016) (Figure 3.3C). All four of the mutations in *ttc-37* were premature stop mutations, likely targeting the *ttc-37* transcripts for degradation by NMD (reviewed in Lykke-Andersen and Jensen, 2015). However, the R1037stop mutation is in the last exon of *ttc-37* and thus may not be an NMD target. Instead, the R1037stop mutation may truncate the TTC-37 protein such that the C-terminus loses the ability to bind Ski8, though the homolog of Ski8 has not been identified in *C. elegans*.

We identified eight missense mutations in *skih-2*. Each mutation was in a residue that is conserved between *C. elegans* SKIH-2 and *S. cerevisiae* Ski2p, therefore we mapped each mutation onto the yeast ribosome:SKI cryo-EM structure

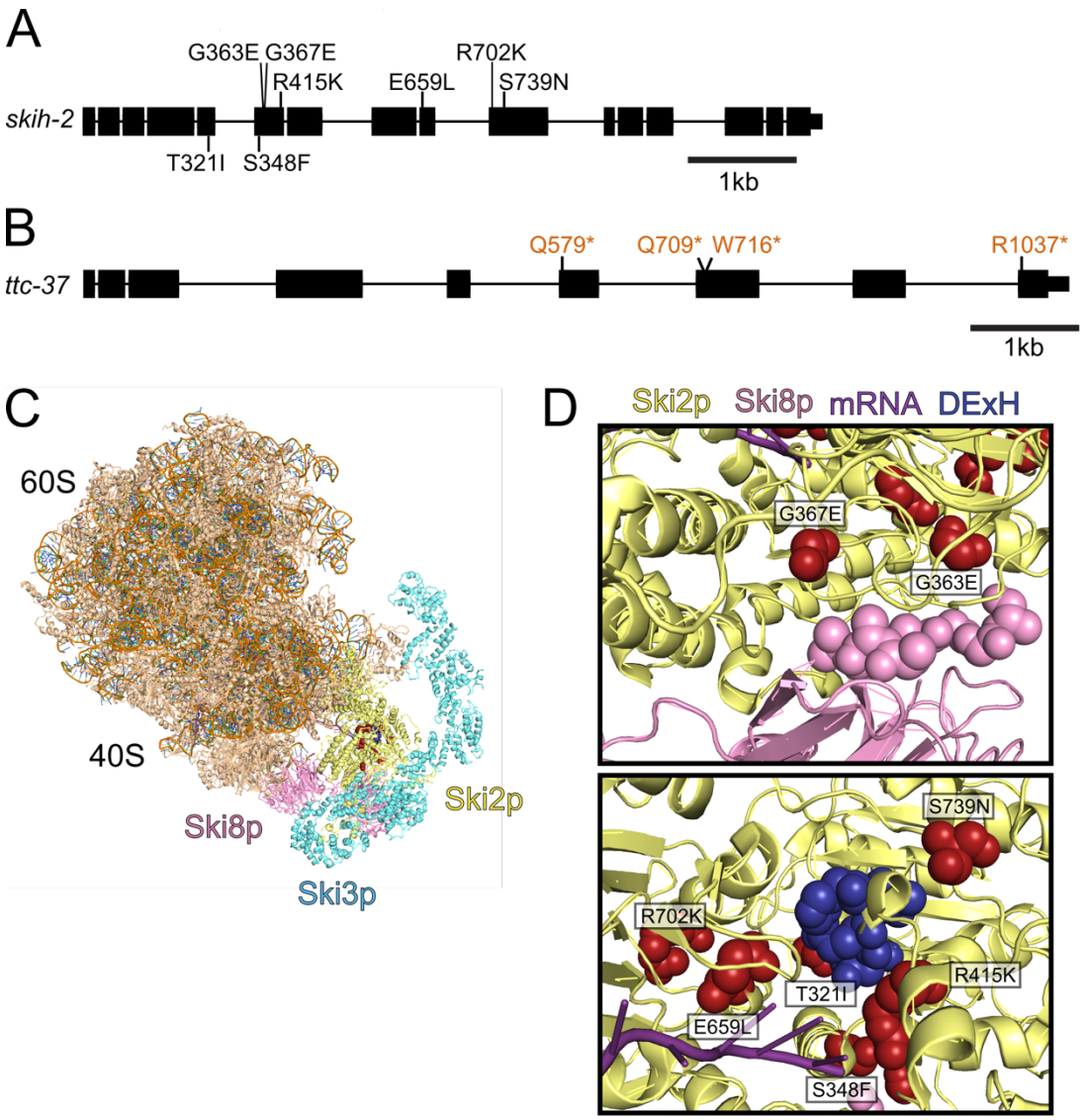

Figure 3.3: Mutations identified in *skih-2* and *ttc-37* that block nonstop mRNA decay
A. Gene diagram of *skih-2* with mutations identified in the nonstop mRNA decay screen.
B. Gene diagram of *ttc-37* with mutations identified in the nonstop mRNA decay screen.
C. Cryo-EM structure of *S. cerevisiae* 80S-Ski2-Ski3-Ski8 complex from (Schmidt et al. 2016). Ribosomal proteins in tan and rRNA backbone in orange. Ski2p in yellow with residues homologous to identified missense residues in *C. elegans* highlighted in red. Ski3p in blue and Ski8p in pink.
D. Zoom ins of Ski2p-Ski8p interface (top) and Ski2p-mRNA interface (bottom). mRNA in purple and DExH catalytic core in dark blue. Identified *C. elegans* missense residues highlighted in red and annotated.

to analyze possible consequences of these mutations on SKIH-2 function (Schmidt et al.) (Figure 3.3C and 3.3D). The helicase region of SKIH-2 comprises two RecA domains that face each other flanked by a helical domain, creating a central RNA channel (Halbach et al., 2013; Schmidt et al., 2016). Five of the single amino acid substitutions (T321I, S348F, G363E, G367E, R415K) lie within the RecA1 domain and the remaining three mutations (E659L, R702K, S739N) lie within the RecA2 domain. SKIH-2 requires ATP to repress nonstop mRNAs and the adenosine of ATP has been shown to bind P328 and R767 of Ski2p (Halbach et al., 2013). R703 of SKIH-2 is homologous to R767 of Ski2p and mutation of the adjacent R702 may affect ATP binding. R415 and S739 are positioned close to the DExH catalytic core of SKIH-2 and could conceivably disrupt catalysis. While some mutations likely affect SKI complex formation, such as G363E and G367E located close to Ski8p, others may disrupt RNA binding, including S348F and E659L, which are proximal to the mRNA channel. Analysis on RNA binding and SKI complex activity with these mutants will help us understand exactly how each mutation inhibits nonstop mRNA repression.

DISCUSSION

Nonstop mRNA decay may have unique aspects in nematodes that are uncommon in other eukaryotes. While most eukaryotes either express Hbs1 and Ski7 from independent genes or express two alternatively spliced isoforms from a single gene, we failed to identify a Ski7-like protein in *C. elegans*. We identified the *HBS1*

homolog in *C. elegans* and confirmed that the two isoforms expressed from the *k07a12.4* locus are highly similar with neither encoding a Ski7-like protein. These results are consistent with findings from the van Hoof lab in which they determined *C. elegans* lacks an obvious Ski7 sequence homolog (Marshall et al., 2018).

The van Hoof lab performed extensive transcriptomic analysis and homology searches in diverse eukaryotes to study Ski7 diversification, though they failed to identify a potential Ski7-like gene in *C. elegans* (Marshall et al., 2018). Comparison of Ski7-like proteins revealed poorly conserved domain inclusion and organization, complicating homology searches. Therefore, it is believed that nematodes either lost Ski7 or have a highly diverged and unrecognizable Ski7-like protein. Remarkably, Ski7 is required to bind Ski2 and the exosome in many eukaryotes (Araki et al., 2001; Kalisiak et al., 2017). It is possible that nematodes have evolved a nonstop decay pathway that does not require Ski7 to mediate interactions between the SKI complex and the exosome, though this model has not been tested. Future research on the composition of the *C. elegans* SKI complex and its interface with the RNA exosome will inform the mechanism of nonstop mRNA decay.

Components of the SKI complex were originally identified by their *superkiller* phenotype in yeast and were later found to be required for nonstop mRNA decay, though it remains elusive how SKI represses nonstop mRNAs (Toh-E et al., 1978; van Hoof et al., 2002). Obtaining new mutant alleles of the *ski* class of genes will bolster the effort to understand SKI's mechanism. We isolated novel alleles of *skih-2* that block nonstop mRNA decay, harboring mutations in residues that have not been

functionally characterized. By mapping the mutations onto the yeast SKI:ribosome cryo-EM structure, we modeled the positions of the mutated residues and hypothesized the possible consequences on SKIH-2 function.

Despite components of the SKI complex being discovered over 40 years ago, we still have a poor understanding of how SKI functions in translation surveillance. The predominant model is that after ribosome collision-induced mRNA cleavage, SKI works in conjunction with the 3'>5' exosome to degrade the 5' fragment (van Hoof et al., 2002; Doma and Parker, 2006; Hashimoto et al., 2017; Arribere and Fire, 2018). However, there is emerging evidence implicating SKI in cleavage-independent suppression mechanisms: (1) the Pestova Lab showed SKI extracting mRNA from stalled ribosomes in a cleavage-independent manner (Zinoviev et al., 2020); (2) there were multiplicative effects on nonstop reporter derepression in *skih-2 nonu-1* double mutants (Chapter 2); and (3) by RNA-seq in a *skih-2(Δ)* background there was stabilization of the entire no-go reporter mRNA, not just the 5' cleavage fragment. Understanding where SKI loads on nonstop/no-go mRNAs will elucidate how SKI functions during nonstop/no-go decay and the collection of *skih-2* mutants isolated from the genetic screen will help this effort. Mutants lacking ATPase activity could conceivably bind nonstop/no-go mRNAs but not translocate once bound, which would allow us to trap SKI-bound mRNAs and identify where SKI binds. An ATPase-deficient mutant of *skih-2* could also be used in conjunction with a *nonu-1(Δ)* mutant to investigate cleavage-dependent vs. cleavage-independent mechanisms of SKI. If SKI is found to bind directly downstream of stalled ribosomes during no-go

decay, it would suggest that SKI is directly recruited to stalled ribosomes to repress the full-length mRNA. Interestingly, SKI can extract mRNA from stalled ribosomes with as few as 19 (but not 13) 3'-terminal nucleotides from the P site of the ribosome, implying SKI cannot extract mRNAs from ribosomes stalled on 3' ends during nonstop decay. However, the multiplicative effects on the nonstop reporter derepression in *skih-2 nonu-1* double mutants implicates SKI in a cleavage-independent mechanism and results from a SKI binding assay would make sense of this.

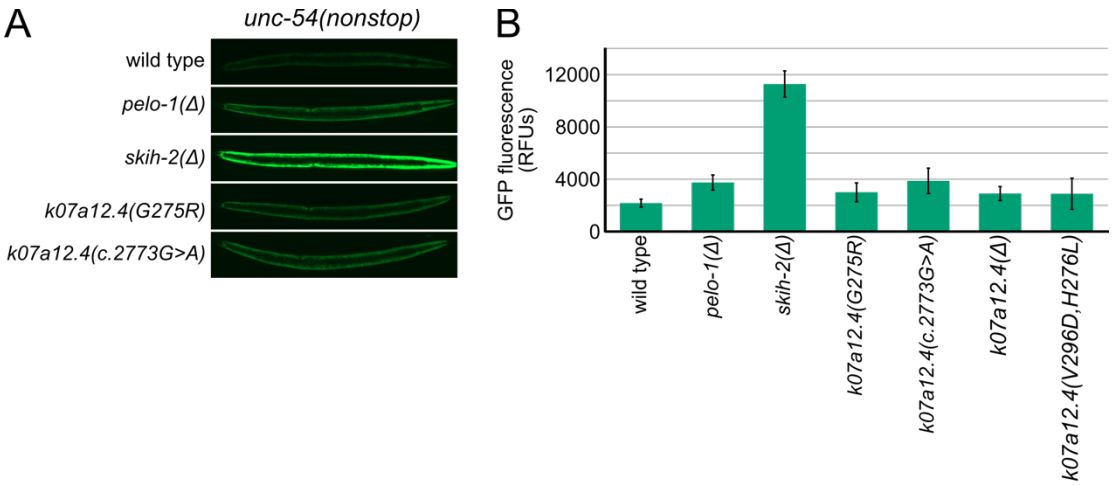

Figure S3.1: *unc-54(nonstop)* derepression is stronger for mRNA decay mutants than ribosome rescue mutants (related to Figure 3.1)

A. Images of UNC-54::GFP expression in the indicated strains.

B. Quantification of GFP expression for strains shown in (B) and two strains made by CRISPR/Cas9. Each bar represents an average image of at least 5 different animals; 95% Confidence Interval shown as error bars. RFUs, Relative Fluorescence Units.

CHAPTER 4: CONCLUSIONS AND FUTURE DIRECTIONS

For over a decade evidence showed that endonucleolytic cleavages occur during nonstop and no-go mRNA decay. Genetic screens using a deletion collection had been performed in *S. cerevisiae* to identify factors required for nonstop decay and the screens failed to identify candidate endonucleases. In hindsight, the screens in *S. cerevisiae* may have been hindered by the existence of two redundant homologs of the conserved endonuclease NONU-1, Cue2 and YPL199C. Consistent with this logic, during the discovery and characterization of NONU-1, Cue2 was identified by the Green Lab via an overexpression screen in *S. cerevisiae* (D'Orazio et al., 2019). These salient findings finally illuminated how ribosome collisions interface with mRNA decay and have provided a better understanding of nonstop and no-go decay mechanisms. The discovery on a nonstop/no-go endonuclease has opened the door to many different future research ideas.

Since the discovery of both nonstop and no-go decay, it has been shown that the SKI complex is required to repress nonstop/no-go mRNAs. The predominant model is that SKI helps degrade 5' cleavage fragments, though recent evidence challenges this. Understanding where SKI binds nonstop/no-go mRNAs will help elucidate the requirement for SKI in translation surveillance. Furthermore, it is unclear how the *C. elegans* SKI complex interacts with the RNA exosome during translation surveillance. In other eukaryotes Ski7 mediates interactions between SKI and the exosome, though a Ski7-like protein is yet to be identified in nematodes.

Determining SKI complex interactions will help us understand how SKI works with the exosome to degrade aberrant mRNAs.

How is NONU-1 recruited to collided ribosomes?

An outstanding question is how NONU-1 is recruited to ribosome collisions. One possible mechanism is that the ubiquitin-binding CUE domains of NONU-1 recognize the ubiquitins deposited on the 40S ribosomal proteins of collided ribosomes. While it is unknown if both ribosomes of the disome get ubiquitinated, there are multiple sites on the ribosome that get ubiquitinated. Both eS10 and uS10 are ubiquitinated by ZNF598, which could potentially be recognized by NONU-1. Moreover, deletion of ZNF598 abolishes ubiquitination and affects mRNA cleavage.

Mutating the CUE domains of NONU-1 would test the hypothesis that NONU-1 recognizes collided ribosomes via ubiquitinated ribosomal proteins. By deleting one or both CUE domains, the effects on NONU-1:ribosome interactions as well as mRNA cleavages could be addressed. However, deletion of a whole domain may cause issues with expression or protein folding. Alternatively, the highly conserved residues required for the ubiquitin binding activity of CUE domains could be mutated to ensure minimal side effects. It is curious why NONU-1 and many homologs have multiple CUE domains. The results from this proposed assay could reveal if a single CUE domain is sufficient for NONU-1 function or if multiple CUE domains are required for efficient recruitment to collided ribosomes.

Another approach to test if NONU-1's CUE domains bind ubiquitinated ribosomes is to identify *trans* factors required for NONU-1 to recognize collided ribosomes. Analyzing the ability of NONU-1 to bind ribosomes and cleave mRNA in a ZNF598 knockout would shed light on the necessity of ubiquitination for recruitment of NONU-1. There may be a certain combination of ubiquitins that are required for NONU-1, such as two residues on eS10, or one residue on eS10 and one on uS10. Furthermore, CUE domains can dimerize to bind ubiquitin, thus NONU-1 may only require a single ubiquitin. To test this, each ubiquitination target could be mutated from lysine to arginine, which inhibits ubiquitination by ZNF598. The effects on NONU-1:ribosome binding and mRNA cleavage could then be addressed to determine the exact combination of ubiquitin marks that may be required to recruit NONU-1 to collided ribosomes.

Is there an additional nuclease required for nonstop and no-go decay?

There is strong evidence that there is an unidentified nuclease acting on nonstop and no-go mRNAs. Analysis of cleavage fragments by Ribo-seq, 3' RACE, and 5' RACE showed persistence of some cleavage events in a *nonu-1* catalytic mutant. This is consistent with data from other labs as well (D'Orazio et al., 2019; Ikeuchi et al., 2019; Navickas et al., 2020), in which cleavage events varied in different conditions. There are currently no candidates for another nuclease, but further studies may shed light on this.

If NONU-1 is partially redundant with another nuclease that shares the common goal of targeting nonstop and no-go mRNAs for degradation, then a synthetic lethal screen may identify potential candidate nucleases. Human K562 cells would be ideal for a synthetic lethal screen because genome-wide CRISPR gRNA libraries have already been validated and optimized in K562s. By homology searches we identified N4BP2 as the human homolog of NONU-1. The CRISPR gRNA library could be introduced to both wildtype and N4BP2 knockout cells to identify genes that cause a diminished growth phenotype in N4BP2 knockout cells. All identified genes could then be characterized to determine their relationship to N4BP2 and possible function in nonstop and no-go decay.

Does the P-loop kinase domain of N4BP2 phosphorylate downstream cleavage fragments?

NONU-1 cleavage generates a downstream mRNA fragment with a 5'hydroxyl, which is not a substrate for the 5'>3' exonuclease that presumably degrades it. The exonuclease XRN-1 requires a 5'monophosphate, indicating that a phosphorylation event must occur prior to degradation. We hypothesized that NONU-1 could be responsible for phosphorylating its own cleavage products to enable degradation by XRN-1. However, the highly conserved lysine residue of NONU-1's P-loop kinase domain was shown to not be required for degradation of downstream cleavage fragments. *C. elegans* exhibits a 19 amino acid deletion in its P-loop kinase

domain, which may have inactivated the domain. It is possible that there is a different residue required for NONU-1's kinase activity, but this was not researched further.

The human homolog of NONU-1, N4BP2, contains a P-loop kinase domain without a deletion, therefore investigating phosphorylation activity of N4BP2 may be informative. An N4BP2 allele with mutation of the highly conserved lysine residue could be integrated into the endogenous locus in N4BP2 knockout cells containing a no-go reporter. Effects on downstream cleavage fragments could then be assessed by capturing 5'hydroxyl RNA ends to determine if the P-loop kinase domain of N4BP2 is required to phosphorylate no-go mRNA cleavage products.

How does the *C. elegans* SKI complex function?

Unlike many eukaryotes, a Ski7-like protein has not been identified in nematodes. It is possible that *C. elegans* expresses a Ski7-like protein that is highly diverged and unrecognizable. An alternative model is that *C. elegans* lacks a Ski7-like protein and the SKI complex directly binds to the RNA exosome to degrade nonstop and no-go mRNAs, which is consistent with recent *in vitro* evidence from Pestova and colleagues showing the SKI:exosome complex extracting mRNAs from stalled ribosomes independent of Ski7 (Zinoviev et al., 2020). Interestingly, the results from the Pestova group also implicated SKI in an endonucleolytic cleavage-independent mechanism of mRNA repression, supporting the multiplicative effects that we observed in *skih-2 nonu-1* double mutants. It remains elusive if SKI can

function with the exosome independently of Ski7 *in vivo* and where SKI binds nonstop and no-go mRNAs.

To determine how the *C. elegans* SKI complex interacts with the exosome, a co-immunoprecipitation could be performed. By using a tagged allele of SKIH-2 or TTC-37, binding partners could be identified through co-immunoprecipitation and mass spectrometry. If components of the exosome are not recovered, a tagged version of the exosome factor DIS-3 could be used for the reciprocal experiment. This would not only clarify if *C. elegans'* SKI:exosome interaction does not require a Ski7-like protein, but could also identify the homolog of Ski8. Identified binding partners could then be mutated to determine if the factors are required for nonstop and no-go mRNA decay. Kalisiak et al. (2017) performed a similar experiment in human cells with tagged isoforms of exosome components and detected the functional homologs of Ski7 and Ski8, HBS1LV3 and WDR61, respectively. Thus, it would be informative to use this method to identify components of the *C. elegans* SKI complex.

Although SKI functions as a 3'>5' helicase to feed cleaved mRNA into the exosome for degradation, it is hypothesized that SKI participates in additional mechanisms to suppress aberrant mRNAs. However, this has yet to be tested *in vivo*. Determining where the SKI complex binds mRNAs could help shed light on SKI's function. The ATPase-deficient mutants of *skih-2* isolated from our nonstop decay screen would be useful to trap SKI on mRNAs. Performing iCLIP against SKI and ribosome profiling would illuminate where SKI binds mRNA in relation to collided ribosomes. If SKI binds downstream of disomes, it would support the *in vitro* data

showing SKI functioning independently of endonucleolytic cleavage and would be consistent with SKI repressing entire no-go transcripts, not just 5' cleavage fragments.

Furthermore, the structure of the yeast SKI complex bound to the ribosome indicates that SKI interacts with the ribosome near the mRNA entry tunnel. However, it remains elusive if this interaction is required for mRNA decay facilitated by SKI. Residues on the yeast SKI:ribosome interface are identifiable from the cryo-EM structure and the homologous residues on the *C. elegans* SKI complex could be mutated to determine if SKI's function is inhibited. If SKI does have multiple functions during nonstop decay, separation of function mutants will be imperative in understanding SKI's role.

APPENDIX A: COMPUTATIONAL ANALYSES

INTRODUCTION

Technological advances have been crucial to progress in molecular biology. Sequencing advances in particular have allowed researchers to easily obtain imperative sequence information. However, the ability to sequence genomes and transcriptomes has vastly surpassed our ability to interpret the data. Analyzing sequencing data requires use of a computer to run specific algorithms, depending on the sequence analysis being performed. While wet-lab skills are critical for preparing sequencing libraries, one must know how to accurately apply computational techniques to successfully analyze the data. Consequently, I was determined to learn and understand how to use Python to perform computational analyses.

Computational biology allows researchers to look at problems from a unique perspective by distilling large amounts of complex data into meaningful information. Intriguingly, novel information about biological processes can be gleaned from existing data. Therefore, I utilized existing data and learned Python to investigate two biological questions related to mRNA translation.

(1) The first project involved analysis of a ribosome profiling dataset to determine if *C. elegans* undergoing RNAi exhibit ribosomal phasing. We found that a 3nt periodicity of translation can be detected, but no other ribosomal phasing occurs due to the diffuseness of primary cleavage events during RNAi.

(2) The second project took advantage of publicly available coronavirus sequencing data to compare SARS-CoV, MERS-CoV, and SARS-CoV2. While no substantial differences were found in amino acid usage, relative synonymous codon usage, or nucleotide usage, we did notice a U-ending codon bias for all three viruses that is consistent with previous studies.

RESULTS

Analysis of ribosome phasing during RNAi

Silencing of specific genes can be initiated by introduction of exogenous double-stranded RNA (dsRNA) (Fire et al., 1998). The endonuclease DICER processes the dsRNA into short interfering RNAs (siRNAs), which are unwound into single-stranded RNAs (ssRNAs) (Zamore et al., 2000; Bernstein et al., 2001). One of the ssRNAs is degraded while the other gets incorporated into the RNA-induced silencing complex (RISC) (Liu et al., 2003; Matranga et al., 2005; Pratt and MacRae, 2009). The ssRNA pairs with the complementary sequence in a mRNA, bringing RISC to its cleavage target (Haley and Zamore, 2004). Argonaute 2 is the catalytic component of RISC, which cleaves the target mRNA to silence expression (Liu et al., 2004; Tsai et al., 2015). This process of RNA interference (RNAi) creates substrates for nonstop mRNA decay, as cleavage in the open reading frame of the mRNA generates a stop codon-less mRNA (Hashimoto et al., 2017; Szádeczky-Kardoss et al., 2018; Pule et al., 2019). Ribosomes undergoing translation prior to cleavage by

RISC translate to and stall on the 3' edge of the cleavage fragment, initiating nonstop decay (Pule et al., 2019).

During nonstop mRNA decay, the SKI complex is responsible for clearing cleavage fragments in a 3'>5' manner and PELO-1 rescues stalled ribosomes (van Hoof et al., 2002; Shoemaker et al., 2010; Pisareva et al., 2011; Arribere and Fire, 2018). Both SKI and PELO-1 are required to relieve stalled ribosome:mRNA complexes during RNAi and the absence of SKI/PELO-1 causes accumulation of stalled ribosomes upstream of the RNAi trigger (Hashimoto et al., 2017; Szádeczky-Kardoss et al., 2018; Pule et al., 2019). This manifests as an increase in truncated ribosome footprints (15-18nt) by Ribo-seq due to ribosomes stalling on the 3' edge of an mRNA (Pule et al., 2019). Generally when RNA cleavage is combined with SKI/PELO-1-mediated decay, secondary cleavage events are phased by the length of a ribosome footprint (Guydosh et al., 2017; Simms et al., 2017; Arribere and Fire, 2018). Therefore, we asked if there is ribosomal phasing during RNAi in *C. elegans* when SKI and PELO-1 are knocked out.

We used computational analysis of 15-18nt Ribo-seq reads from strains undergoing RNAi to determine if ribosomal phasing was observed. An RNAi trigger was used against *unc-22*, *unc-54*, and *unc-15* independently and we only detected 3nt periodicity from translation (Figure A1, only *unc-54* shown for simplicity). This result was not unexpected, as the dsRNA triggers used for RNAi are complementary to a large region (hundred to thousands of bases) of the target mRNA. The siRNAs that are processed from the dsRNA can therefore induce cleavage at any one of a

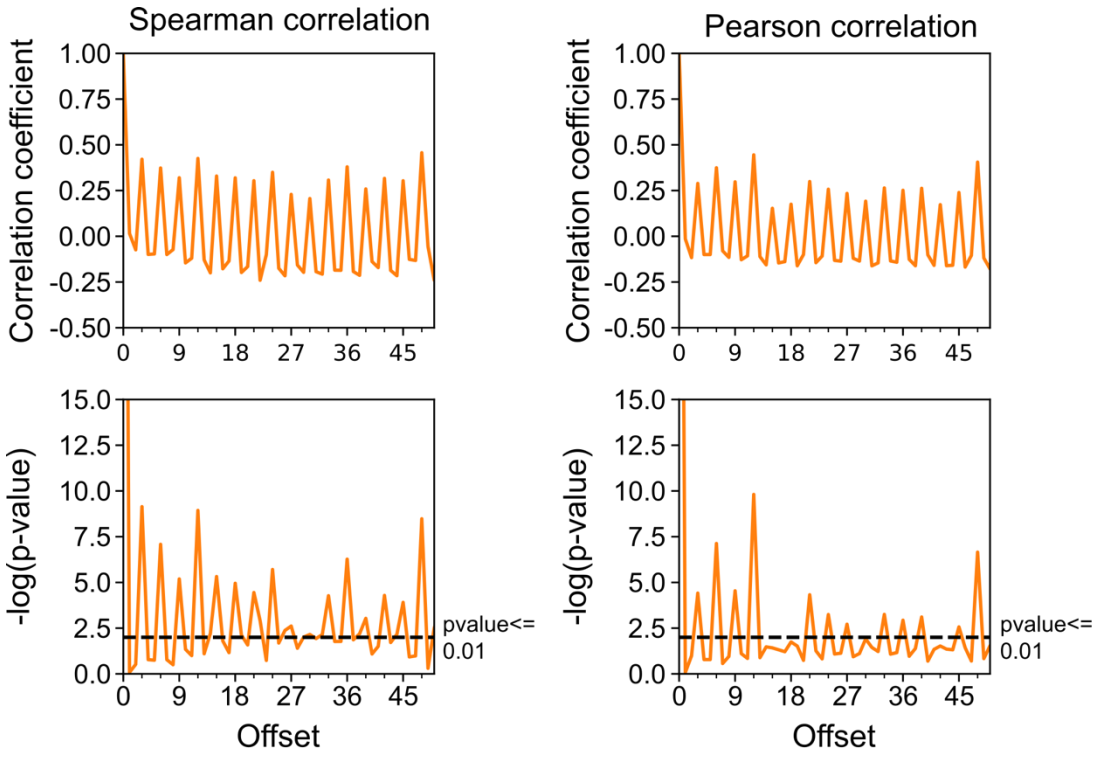

Figure A1: Ribosome phasing analysis of 15-18nt Ribo-seq reads
Spearman and Pearson autocorrelation for 15-18nt Ribo-seq reads upon RNAi against *unc-54* in *skih-2 pelo-1*. Correlation was determined with itself at offsets ranging from 0-50nt.

number of bases that are complementary to the dsRNA trigger, unlike nonstop decay where the initial cleavage event occurs at a discrete site. When siRNA-mediated cleavage occurs over a large region opposed to a discrete site, ribosome stalling is more diffuse and phasing events cannot be assessed by bulk analysis. Therefore, each mRNA may display 15-18nt phasing, but the read densities are not at the same position on each mRNA and phasing is lost during bulk analysis.

Sequence analysis of coronaviruses

Coronaviruses (CoVs) are positive-sense single-stranded RNA viruses that are pathogenic for humans (reviewed in Woo et al., 2009). While some CoVs only cause mild respiratory infections, others such as severe acute respiratory syndrome CoV (SARS-CoV), Middle East respiratory syndrome (MERS-CoV), and the novel SARS-CoV2 can cause serious respiratory illness (Fehr and Perlman, 2015; Grant et al., 2020). Interestingly, there are also major differences in virulence and mortality between SARS-CoV, MERS-CoV, and SARS-CoV2. The basis for these differences remains elusive and little is known on how CoV gene expression is regulated.

The genetic code has redundancies, with 18 of the 20 amino acids being encoded by more than one synonymous codon. During evolution, organisms develop biases for particular synonymous codons where the most frequently used codons are generally decoded by the most abundant tRNAs (Spencer and Barral, 2012). Codon usage can therefore affect protein expression levels. Viruses do not encode their own translational machinery, but instead rely on the host's machinery to express the proteins encoded in the viral mRNA (Lodish et al., 2000). Thus, viruses commonly adapt their genomes to take advantage of their host's molecular machinery while also evading detection by the immune system (Agudelo-Romero et al., 2008). Analysis of CoV sequence features can shed light on the regulation of CoV gene expression, which could conceivably be an aspect that influences the virulence and mortality of the virus.

To analyze differences in coding sequences between SARS-CoV, MERS-CoV, SARS-CoV2, we compared amino acid usage, relative synonymous codon usage, and nucleotide usage. We also determined these values for the human genome coding sequences. Each of the CoVs analyzed exhibited highly similar amino acid usage, which is also similar to that of humans (Figure A2.A) Although we observed that relative synonymous codon usage (RSCU) was fairly similar between each CoV, there were clear differences in the human RSCUs (Figure A2.B). This could potentially be a mechanism for the virus to avoid competition for human tRNAs. Interestingly, we also noticed that each CoV had a bias for U-ending codons. To investigate this further, we looked for biases in nucleotide usage (Figure A2.C). Each virus had similar nucleotide usage with a strong A/U bias and when looking at the nucleotide usage at each codon position, the U bias was the strongest at the third position (Figure A2.D). This supports the RSCU results showing a bias for U-ending codons. While this is not novel information, it is consistent with reports from others (Dilucca et al, 2020; Hou, 2020; Hussain et al., 2020). It is thought that cytosine deamination contributes to the U-ending codon bias by creating accumulation of C-to-U mutations, which is likely a mechanism for the viral RNA to evade the immune system and not be recognized as non-self RNA (Takata et al., 2017; Dilucca et al, 2020; Hussain et al., 2020).

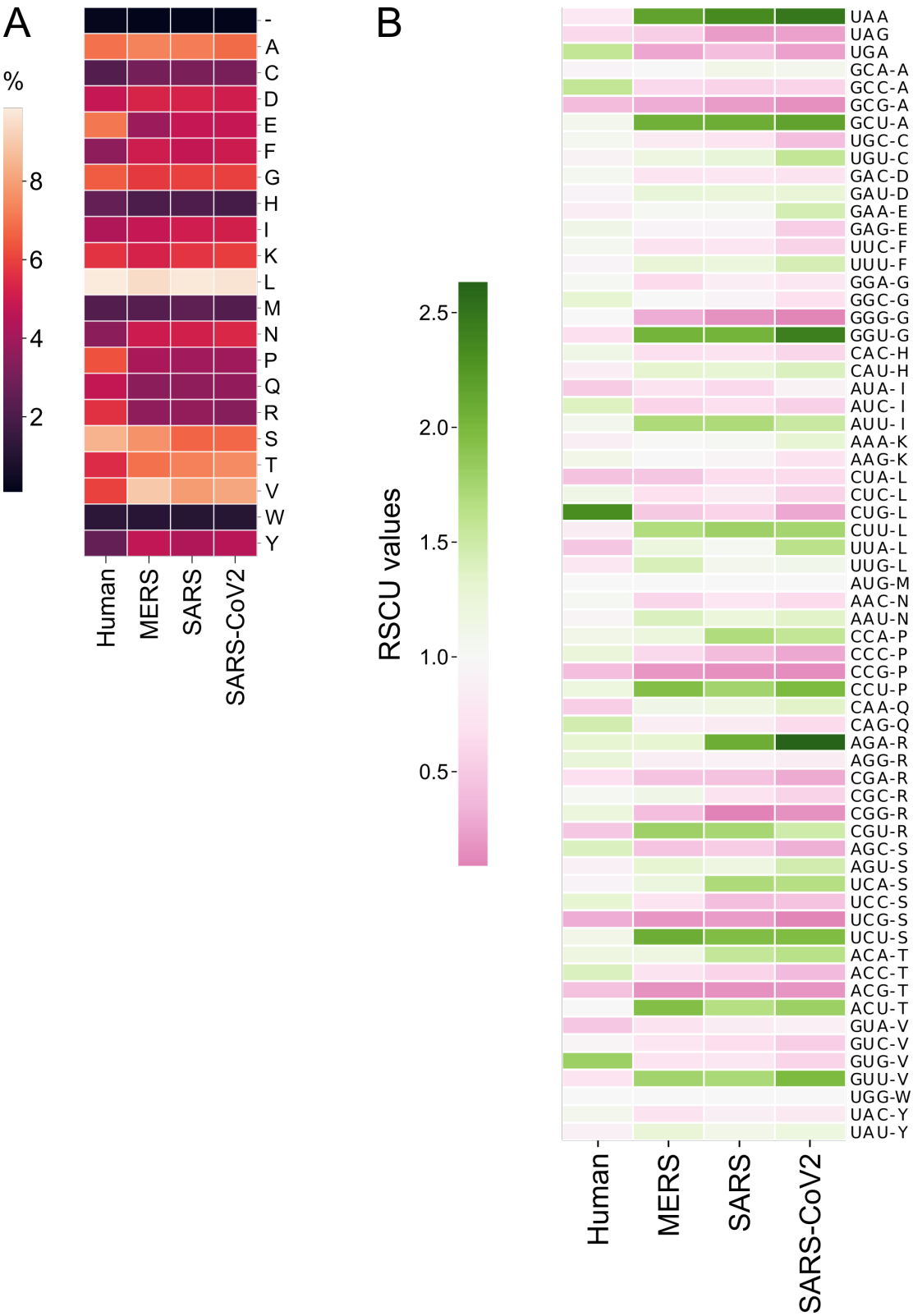
A
%
8
6
4
2
-
A
C
D
E
F
G
H
I
K
L
M
N
P
Q
R
S
T
V
W
Y
Human
MERS
SARS
SARS-CoV2
B
RSCU values
2.5
2.0
1.5
1.0
0.5
UAA
UAG
UGA
GCA-A
GCC-A
GCG-A
GCU-A
UGC-C
UGU-C
GAC-D
GAU-D
GAA-E
GAG-E
UUC-F
UUU-F
GGA-G
GGC-G
GGG-G
GGU-G
CAC-H
CAU-H
AUA-I
AUC-I
AUU-I
AAA-K
AAG-K
CUA-L
CUC-L
CUG-L
CUU-L
UUA-L
UUG-L
AUG-M
AAC-N
AAU-N
CCA-P
CCC-P
CCG-P
CCU-P
CAA-Q
CAG-Q
AGA-R
AGG-R
CGA-R
CGC-R
CGG-R
CGU-R
AGC-S
AGU-S
UCA-S
UCC-S
UCG-S
UCU-S
ACA-T
ACC-T
ACG-T
ACU-T
GUA-V
GUC-V
GUG-V
GUU-V
UGG-W
UAC-Y
UAU-Y
Human
MERS
SARS
SARS-CoV2

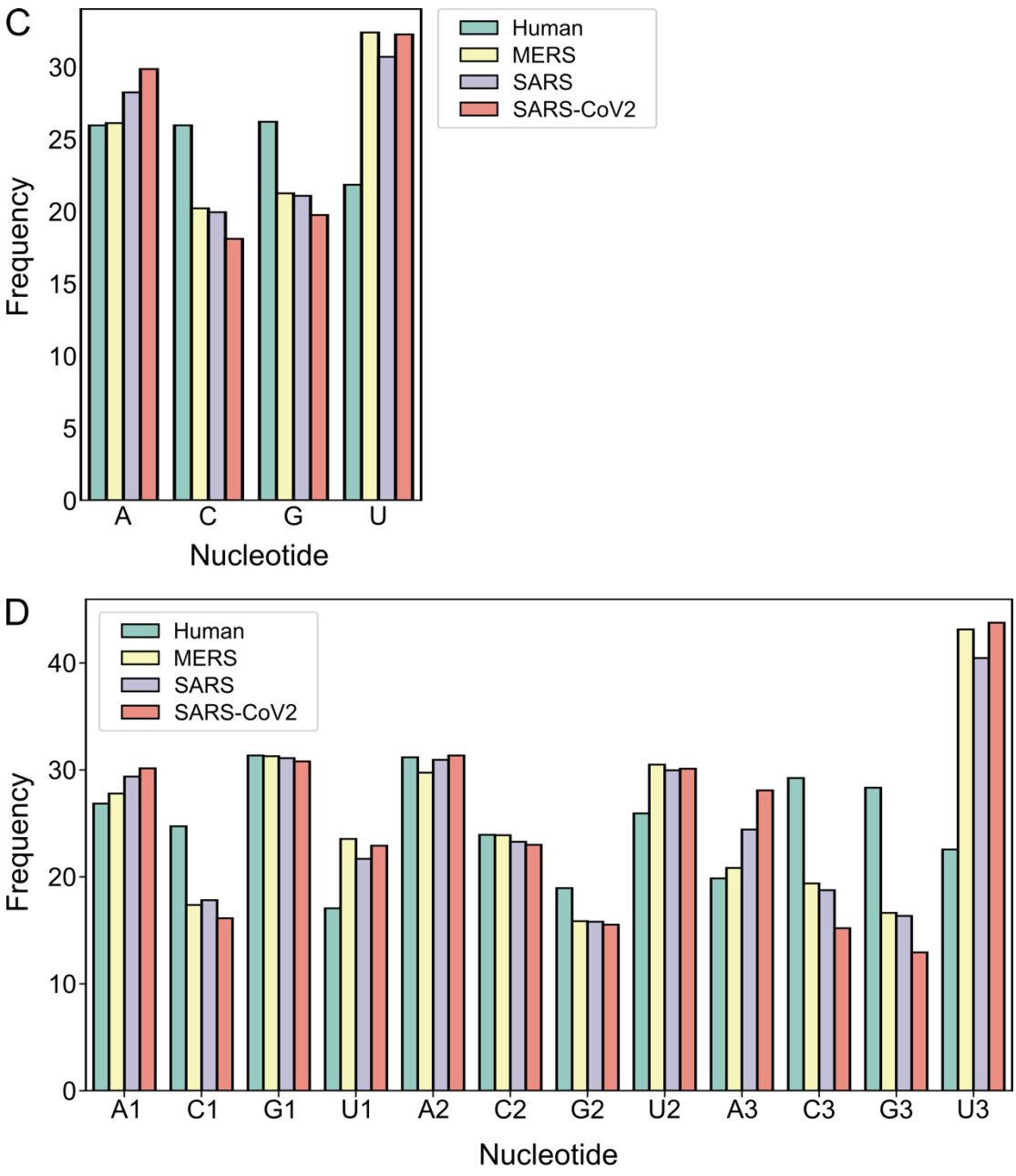

Figure A2: Sequence analysis of human, MERS, SARS, and SARS-CoV2 coding sequences

A. Heat map of amino acid frequencies for the species indicated.

B. Heat map of relative synonymous codon usage values for the species indicated.

C. Nucleotide frequencies of coding sequences for the species indicated.

D. Nucleotide frequencies of coding sequences at each codon position for the species indicated.

MATERIALS AND METHODS

C. elegans growth and propagation

Strains were derived from N2 background (VC2010 [Thompson et al., 2013]). Hermaphroditic animals were grown at 22C on NGM plates using OP50 as a food source per standard *C. elegans* husbandry (Brenner, 1974). Some strains were provided by the CGC, which is funded by NIH Office of Research Infrastructure Programs (P40 OD010440). A full list of strains, sources, and constructions is available in Table 1.

S. cerevisiae husbandry

S. cerevisiae strains were grown on YPAD media at 30C. A full list of strains, sources, and constructions is available in Table 2. All mutations were verified by at least two independent PCR primers.

EMS mutagenesis

EMS mutagenesis was performed essentially as described (Arribere and Fire, 2018). Briefly, a large population of *unc-54(cc4092)* was washed with M9 and resuspended in a final volume of 4mL M9. EMS was added to a final concentration of ~1mM and animals incubated for 4 hr at room temperature with rotation. Animals were washed and allowed to recover overnight on plates with OP50. The next day animals were washed and eggs isolated via sodium hypochlorite treatment. 100-200 eggs were placed on a single small NGM plate and allowed to develop. Plates were

screened for individuals with increased GFP fluorescence at the F2/F3 generation. Only a single isolate was kept per small NGM plate, ensuring independence of mutations identified.

Mutation mapping

We crossed each isolated suppressor to Hawaiian *unc-54(cc4112)* males (expressing an UNC-54::mCherry fusion engineered by CRISPR/Cas9). Cross progeny were picked to new plates to self-fertilize. From among the F2, we picked ~30 GFP+ progeny to a new plate and allowed the animals to self-fertilize and starve. Upon starvation, animals were washed off the plate with 1mL EN50, and further washed with EN50 to remove residual *E. coli*. Genomic DNA was extracted after proteinase K treatment and resuspended in 50uL TE pH7.4. 50ng genomic DNA was used as input for Nextera (Tn5) sequencing libraries. Libraries were sequenced at the Vincent J. Coates Genomics Sequencing Laboratory at UC Berkeley.

Reads were mapped to the *C. elegans* genome using bowtie2 (version 2.3.4.1). Reads were assigned using GATK (McKenna et al., 2010) and a previously published dataset of Hawaiian SNPs (Thompson et al., 2013). The fraction of reads that were assignable to Hawaiian or N2 animals was calculated across the genome, and linkage was identified by portions of the genome that went to 0% Hawaiian. Regions of linkage were then manually inspected to identify candidate lesions/loci.

CRISPR/Cas9 mutagenesis

CRISPR/Cas9 was performed as previously described (Arribere et al., 2014). A full list of gRNAs is available in Table 3, and exact sequences of mutant alleles is provided alongside *C. elegans* strains in Table 1. Multiple genetic isolates of each mutation were obtained and observed to have identical phenotypes.

Microscopy and image quantification

L4 worms were anesthetized in 2uL 1mM levamisole in a microscope well slide with a 0.15mm coverslip. A Zeiss AxioZoom microscope was used with a 1.0x objective and a GFP fluorescence light source to acquire all images. The *unc-54(cc4092); skih-2(cc2854)* strain was used to set parameters (exposure time 330ms., shift 50%, zoom 80%) and the same parameters were used for all images. Five representative worms were imaged for each strain. All comparisons shown are between images obtained during the same imaging session.

We used FIJI to define the area of the worm, subtract the background, and determine mean pixel intensity for the area of each worm. A mean fluorescence intensity was calculated for each strain based upon quantification of 5 representative images per strain. We calculated two standard deviations above and below the mean to obtain a 95% confidence interval.

RNA-seq and analysis

25-50 day 1 adults were picked from a blank plate into S-basal solution and washed to remove *E. coli*. Animals were dissolved in trizol and total RNA extracted. Ribosomal RNA was depleted from 250 ng of total RNA using an NEBNext rRNA Depletion Kit (Human/Mouse/Rat) and libraries were constructed using an NEBNext Ultra RNA Library Prep Kit for Illumina sequencing. Libraries were sequenced at the University of California, Santa Cruz using the Illumina NextSeq platform.

RNA-seq reads were trimmed with cutadapt and mapped using STAR (version 2.5.0a) to the *C. elegans* genome (WBCel235) with the *unc-54* locus modified to match the *unc-54(cc4092)* allele. Reads that mapped within the annotated bounds of a protein coding gene were assigned to that gene. Multiply-mapping reads or reads that could not be unambiguously assigned to a gene (e.g., due to overlapping genes) were discarded. Read counts were median-normalized using DESeq (Anders and Huber, 2010).

For differential expression of endogenous mRNAs in *skih-2* and *nonu-1*, genes with mRNAs that increased in biological duplicates (*skih-2*) or triplicates (*nonu-1*) were identified with DESeq. mRNA levels were deemed significantly different if they exhibited an adjusted p value < 0.05 (*skih-2*) or < 0.001 (*nonu-1*). Varying these cutoffs changed the number genes identified as *skih-2* or *nonu-1* targets, but did not alter our conclusions.

S. cerevisiae nonstop decay assay

Cells were transformed with the *his3::nonstop* reporter plasmid (pAV188) via lithium acetate transformation and plated on selective media (SD-Ura). Two Ura+ transformants were taken for each strain, and results were reproducible across these independent isolates. Cells were subsequently grown on SD-Ura plates and in SD-Ura liquid media to maintain the plasmid. For the *his3::nonstop* reporter assay, 100mL liquid cultures were grown overnight and harvested at mid-log phase (OD600 ~0.5). Cells were pelleted and resuspended in 3mL media. The OD600 was measured and the same OD600 was used as the starting number of cells for all strains. Cells were serially diluted 1:6 and plated on selective media (SD-Ura and SD-Ura-His). Plates were photographed after 4 days of growth at 30C.

Sequence analysis

Domain sequence similarity searches were performed using PSI-BLAST program (Altschul et al., 1997) against the non-redundant (nr) database housed at the NCBI and the HHpred program (Zimmermann et al., 2018) against pfam and pdb databases (Finn et al., 2016, Burley et al., 2019). Structure similarity searches were performed using the DALI server (Holm and Sander, 1995). Multiple sequence alignments were built using the Kalign2 program, with manual adjustments based on profile-profile and high-scoring pair sequence similarity search results (Lassmann et al., 2009). Domain architectures Smr domain-containing proteins were elucidated by first running rpsblast searches against a PSSM library constructed from the pfam

profile database (Marchler-Bauer and Bryant, 2004). Regions lacking any annotation were then used as seeds in further rounds of iterative similarity searches. Phylogenetic analyses were carried out using approximate-maximum-likelihood as enacted by the FastTree 2.1 program with default parameters for amino acid sequences (Price et al., 2010).

3′RACE

Strains for 3′RACE in Figures 2.4A and 2.4B were grown up as populations of mixed developmental stages (L1-adult); animals in Figures 2.4C and 2.4D were grown as populations of synchronized L4/young adult animals. Animals were passed through a 5% sucrose cushion, washed with N50 to remove *E. coli*, and snap frozen in liquid nitrogen. Frozen animal pellets were dissolved in trizol and total RNA was extracted and stored in TE pH7.4. 1ug of RNA was treated with T4 PNK (NEB) to remove 3′phosphates. RNA was then extracted with phenol chloroform and precipitated into TE pH7.4. AF-JA-34 was ligated onto RNA 3′ends with T4 RNA Ligase 1 (NEB). Adaptor cleanup was performed with 5′ deadenylase (NEB) and RecJ (NEB), followed by RNA extraction as before. RNA was fragmented with 2x AF buffer (10mM Na_2CO_3, 90mM $NaHCO_3$, 0.5mM EDTA) and then ran on a 15% polyacrylamide gel. AF-JA-126 was used for reverse transcription on gel purified RNA with Superscript II RT (Thermo Fisher). RNA was hydrolyzed with 1N NaOH and the remaining cDNA product was run on 15% polyacrylamide gel. Gel purified cDNA was circularized with circligase (Lucigen) and then used for PCR. Libraries

were agarose gel purified and sequenced at the Vincent J. Coates Genomics Sequencing Laboratory at UC Berkeley.

Ribo-seq

Strains for Ribo-seq were harvested at the L4/young adult stage. Animals were passed through a 5% sucrose cushion and washed in N50 to remove *E. coli*, and snap frozen in liquid nitrogen. Frozen animal pellets were ground in PLB (20mM Tris pH8.0, 140mM KCl, 1.5mM $MgCl_2$, 1% Triton) with 0.1mg/mL cycloheximide and liquid nitrogen with a mortar and pestle. Ground powder was mixed with PLB and 100ug/mL cycloheximide and clarified via a 10' spin at 10,000 rcf. RNA in the supernatant was quantified with a nanodrop and OD units were used to calculate the amount of RNaseI to use (total OD x 0.3). RNA was treated with RNaseI (Ambion) and loaded onto a 10%–50% sucrose gradient. Gradients were spun in an SW41 Ti rotor in an ultracentrifuge at 35,000 rpm for 4.5hrs. Monosomes were collected on a fractionator and digested with proteinase K. Monosome RNA was cleaned up by acid phenol chloroform extraction and stored in TE pH7.4. 2ug was ran on 15% polyacrylamide gel and size-selected for 15-18nt or 28-30nt footprints. Gel purified RNA was treated with T4 PNK (NEB) to remove 3′phosphates. The remaining library preparation was as per 3′RACE, except no fragmentation was performed.

5′RACE

Strains for 5′RACE were grown up as populations of mixed developmental stages (L1-adult). Animals were passed through a 5% sucrose cushion, washed with N50 to remove *E. coli*, and snap frozen in liquid nitrogen. Frozen animal pellets were dissolved in trizol and total RNA was extracted and stored in TE pH7.4. 400 pmole of 5′adaptor (/5Phos/ACACGACGCTCTTCCGATCT [barcode] GC rNrNrNrNrNrNrN/3Phos/) was ligated to free 5′OH ends of 1ug RNA with RtcB ligase (NEB). We used distinct 5′ adaptors (JA-AA-313, JA-AA-314, JA-AA-315, and JA-AA-316) for each sample, each with an internal barcode of 6nts that allowed us to sort reads into their respective samples after sequencing. This approach normalized for sample-specific differences in the downstream enzymatic steps (RT, PCR) and the UMI allowed us to collapse PCR duplicates after sequencing. JA-AA-275 binds downstream of the 12 rare arginines in the *unc-54(no-go)* reporter and was used for reverse transcription with Superscript II RT (Thermo Fisher). Two rounds of nested PCR were performed with oligos upstream of the RT oligo to reduce products not derived from *unc-54*, first with PCR primers JA-AA-276 and JA-AA-277, and then with primers for Illumina barcoding. Biological and technical replicates with 5′adaptors flipped yielded similar data to that shown in Figure 2.4E. Libraries were gel purified and sequenced at the Vincent J. Coates Genomics Sequencing Laboratory at UC Berkeley.

Fractional Read Abundance (Figure 2.4E) was calculated as follows: reads were assigned to samples based on the six nucleotide barcode, and then mapped and

collapsed based on common UMIs allowing for up to two mutations in their UMI (this was found to be necessary due to bottlenecking in the PCR which coupled with the error rate of PCR/sequencing led to extraneous UMIs one nucleotide mismatched from a far more abundant UMI). The "fractional read abundance" is the read abundance at each position divided by the total number of unique (UMI-collapsed) reads across all three samples. This metric allows for detection of differences in *unc-54* expression across samples. This metric was also found to be reproducible across biological and technical replicates.

Quantification and statistical analysis

Statistical details for experiments can be found in Figure Legends and STAR Methods. Briefly, p values were determined by Student's t test when data were normally distributed (Figures 2.1E, 2.2E, 2.3A, and S2.4B), and by Mann Whitney U when data were not normally distributed (Figure S2.4C). All 95% confidence intervals were mean ± two standard deviations from the mean.

Data and code availability

The accession number for the data reported in Chapter 2 is SRA: PRJNA548154.

Autocorrelation for periodicity

A 15-18nt Ribo-seq dataset of *C. elegans* encountering RNAi was used to analyze periodicity upstream of different RNAi triggers. A list of normalized read densities was generated for 200nt upstream of each RNAi trigger. Pearson autocorrelation and Spearman autocorrelation were performed with each list of read densities to determine correlation with itself at offsets ranging from 0 to 50 nt. For each offset, correlation coefficients and p-values were calculated. A correlation coefficient measures the degree to which two variables change together, and a coefficient of -1 or +1 demonstrates perfect correlation.

Sequence analysis of coronaviruses

Coding sequences (CDS) for human, MERS, SARS, and SARS-CoV2 genomes were downloaded from Ensembl. For each coronavirus CDS, nucleotide frequencies were determined by counting how many times each nucleotide is used and dividing that number by the total number of nucleotides in the CDS. The same process was done to determine codon and amino acid frequencies for each coronavirus. The relative synonymous codon usage (RSCU) was calculated for each coronavirus and for the human CDS. RSCU is calculated by dividing the observed frequency of a codon by the expected frequency if there is equal usage of synonymous codons. This was achieved by using the equation $RSCU_{ij} = \frac{X_{ij}}{\frac{1}{n_i}\sum_{j=1}^{n_i} X_{ij}}$

where X_{ij} is the frequency of the jth codon for the ith amino acid and n_i is the number of synonymous codons for the ith amino acid.

Table 1: *C. elegans* strains

Strain #	Genotype	Strain Construction	Sequence around any CRISPR/Cas9-introduced mutations
WJA0438	*unc-54(cc4092; unc-54::GFP::T2A::nonstop)I*	Arribere and Fire 2018	
WJA0458	*unc-54(cc4112; unc-54::mCherry)/unc-54(cc4106; unc-54::GFP)I*	Arribere and Fire 2018	
WJA0675	*unc-54(cc4092; unc-54::GFP::T2A::nonstop)I; nonu-1(srf0675; W474STOP)III*	EMS mutagenesis	
WJA0641	*unc-54(cc4092; unc-54::GFP::T2A::nonstop)I; nonu-1(srf0641; W150STOP)III*	EMS mutagenesis	
WJA0552	*unc-54(cc4092; unc-54::GFP::T2A::nonstop)I; skih-2(cc2854; NtermΔ)IV*	Arribere and Fire 2018	
WJA0780	*unc-54(cc4092; unc-54::GFP::T2A::nonstop)I; nonu-1(srf0780; SmrΔ)III*	CRISPR with gRNAs from JA-MG-34/35 and JA-MG-36/37, donor template JA-MG-40. Isolate #1.	GAAAGAACTTGATCGGAAAATTCGAGAAGCCCACAACAATAGATCTTAGCTAAGTGATGATGGATGTATAAGATTCAAAGTCTAGcatatcgtattctctcaaatatctctgcttttctttgcgctgtatttttga
WJA0781	*unc-54(cc4092; unc-54::GFP::T2A::nonstop)I; nonu-1(srf0781; SmrΔ)III*	CRISPR with gRNAs from JA-MG-34/35 and JA-MG-36/37, donor template JA-MG-40. Isolate #2.	GAAAGAACTTGATCGGAAAATTCGAGAAGCCCACAACAATAGATCTTAGCTAAGTGATGATGGATGTATAAGATTCAAAGTCTAGcatatcgtattctctcaaatatctctgcttttctttgcgctgtatttttga
WJA0782	*unc-54(cc4092; unc-54::GFP::T2A::nonstop)I; nonu-1(srf0782; SmrΔ)III*	CRISPR with gRNAs from JA-MG-34/35 and JA-MG-36/37, donor template JA-MG-40. Isolate #3.	GAAAGAACTTGATCGGAAAATTCGAGAAGCCCACAACAATAGATCTTAGCTAAGTGATGATGGATGTATAAGATTCAAAGTCTAGcatatcgtattctctcaaatatctctgcttttctttgcgctgtatttttga

Strain #	Genotype	Strain Construction	Sequence around any CRISPR/Cas9-introduced mutations
WJA0783	*unc-54(cc4092; unc-54::GFP::T2A::nonstop)I; nonu-1(srf0783; SmrΔ)III*	CRISPR with gRNAs from JA-MG-34/35 and JA-MG-36/37, donor template JA-MG-40. Isolate #4.	GAAAGAACTTGATCGGAAAATTCGAGAAGCCCACAACAATAGATCTTAGCTAAGTGATGATGGATGTATAAGATTCAAAGTCTAGcatatcgtattctctcaaatatctctgcttttctttgcgctgtatttttga
WJA2133	*unc-54(cc4092; unc-54::GFP::T2A::nonstop)I; nonu-1(srf2133; H167STOP)III*	CRISPR with gRNA from JA-MG-29/30, donor temple JA-MG-31. Isolate #1.	acattaaaaatacaattttcagaATTTCAAACTTCTAGATCGATACGGAGattaccagtgtcctgtgtaaatcaccaatc
WJA2134	*unc-54(cc4092; unc-54::GFP::T2A::nonstop)I; nonu-1(srf2134; H167STOP)III*	CRISPR with gRNA from JA-MG-29/30, donor temple JA-MG-31. Isolate #2.	acattaaaaatacaattttcagaATTTCAAACTTCTAGATCGATACGGAGattaccagtgtcctgtgtaaatcaccaatc
WJA3012	*unc-54(cc4092; unc-54::GFP::T2A::nonstop)I; nonu-1(srf3012; D579N)III*	CRISPR with gRNAs from JA-MG-32/33 and JA-MG-34/35 and JA-MG-45/46, donor template JA-MG-47	GAAAGAACTTGATCGGAAAATTCGAGAAGCCCACAACAATCCCTGGTTTCTAAATTTACATTACATGTCAGTTGACGGAGCAGTTAAACTTGTGAAAGAAGCGATTGAAGCA
WJA3015	*unc-54(cc4092; unc-54::GFP::T2A::nonstop)I; nonu-1(srf3015; D579A,H581A)III*	CRISPR with gRNAs from JA-MG-32/33 and JA-MG-34/35 and JA-MG-45/46, donor template JA-AA-198	GAAGTGAAAGAACTTGATCGGAAAATTCGAGAAGCCCACAACAAc CCg TGG TTc tTg Gcc TTg GcT TAt ATG TCg GTTGATGGAGCAGTTAAACTTGTGAAAGAAGCGATTGAAGCA
WJA0037	*skih-2(cc2854; NtermΔ)IV*	Arribere and Fire 2018	
WJA0785	*unc-54(cc4092; unc-54::GFP::T2A::nonstop)I; skih-2(cc2854; NtermΔ)IV; nonu-1(srf0780; SmrΔ)III*	Crossed *skih-2(cc2854; NtermΔ)IV* from WJA0037 into WJA0780	
WJA0788	*unc-54(srf0788; 12rareArg)I*	CRISPR with gRNAs from JA-AF-268/269 and JA-AF-270/271, donor template JA-AA-176	AGATGGTACCGATGAGGCCGAGAAGGCATCCAACATGTACAGATCT cgg cgg agg cgg agg agg cgg cgg agg cgg cgg agg ATCGGATGCGAGGAGTTCCTCAAGGCTTTGACCAAGCCAC

Strain #	Genotype	Strain Construction	Sequence around any CRISPR/Cas9-introduced mutations
WJA0789	*unc-54(srf0788; 12rareArg)I; nonu-1(srf0780; SmrΔ)III*	Crossed *nonu-1(srf0780; SmrΔ)III* from WJA0780 into WJA0788	
WJA0790	*unc-54(srf0788; 12rareArg)I; skih-2(cc2854; NtermΔ)IV*	Crossed *skih-2(cc2854; NtermΔ)IV* from WJA0037 into WJA0788	
WJA0791	*unc-54(srf0788; 12rareArg)I; nonu-1(srf0791; K41A)III*	CRISPR with gRNAs from JA-AA-184/185 and JA-AA-186/187, donor template JA-AA-188	AAGGTCATCGCACAATTATTTT AATTCGCGGAGTTACGGGAagtG GtgccTCAACATTAGCTCGAGAG TTGGTAAACCATTCCGAAAA
WJA0802	*unc-54(cc4092; unc-54::GFP::T2A::nonstop)I; nonu-1(srf0802; K41A,D579A,H581A)III*	CRISPR with gRNAs from JA-AA-184/185 and JA-AA-186/187, donor template JA-AA-188, into WJA3015	AAGGTCATCGCACAATTATTTT AATTCGCGGAGTTACGGGAagtG GtgccTCAACATTAGCTCGAGAG TTGGTAAACCATTCCGAAAA
WJA0812	*unc-54(srf0788; 12rareArg)I; nonu-1(srf0802; K41A,D579A,H581A)III*	Crossed *nonu-1(srf0802; K41A,D579A,H581A)III* from WJA0802 into WJA0788	
WJA0579	*unc-54(cc4092; unc-54::GFP::T2A::nonstop)I; pelo-1(cc2849; ex3,4,5KO-BglII)III; skih-2(cc2854; NtermΔ)IV*	Arribere and Fire 2018	
WJA0809	*unc-54(cc4092; unc-54::GFP::T2A::nonstop)I; nonu-1(srf3015; D579A;H581A) pelo-1(srf0809)III*	CRISPR with gRNAs from JA-AF-138/139 and JA-AF-143/144, donor template JA-AF-152, into WJA3015	ACTTCATCTTTTGCAGATTCGT AGTTTTAATGGCGGAAGAGGC AGAGGATAGATCTATTTGTGAA AGACGCATTTATGCAGCATTTA ATAGCACATGCAGATGCAA

Strain #	Genotype	Strain Construction	Sequence around any CRISPR/Cas9-introduced mutations
WJA0811	*unc-54(cc4092; unc-54::GFP::T2A::nonstop)I; nonu-1(srf3015; D579A,H581A) pelo-1(srf0809; ex3,4,5KO-BglI)III; skih-2(cc2854; NtermΔ)IV*	Crossed *skih-2(cc2854; NtermΔ)IV* from WJA0037 into WJA0809	
WJA0043	*pelo-1(cc2849; ex3,4,5KO-BglII)III; skih-2(cc2854; NtermΔ)IV*	Arribere and Fire 2018	
WJA1002	*unc-54(srf0788; 12rareArg)I; pelo-1(cc2849; ex3,4,5KO-BglII)III; skih-2(cc2854; NtermΔ)IV*	Crossed *pelo-1(cc2849; ex3,4,5KO-BglII)III; skih-2(cc2854; NtermΔ)IV* from WJA0043 into WJA0788	
WJA0032	*pelo-1(cc2849; ex3,4,5KO-BglII)III*	Arribere and Fire 2018	
WJA2138	*nonu-1(srf0780; SmrΔ) pelo-1(cc2849; ex3,4,5KO-BglII)III*	CRISPR with gRNAs from JA-MG-34/35 and JA-MG-36/37, donor template JA-MG-40, into WJA0032	GAAAGAACTTGATCGGAAAATTCGAGAAGCCCACAACAATAGATCTTAGCTAAGTGATGATGGATGTATAAGATTCAAAGTCTAGcatatcgtattctctcaaatatctctgcttttctttgcgctgtatttttga
WJA0800	*nonu-1(srf0780; SmrΔ) pelo-1(cc2849; ex3,4,5KO-BglII)III; skih-2(cc2854; NtermΔ)IV*	Crossed *skih-2(cc2854; NtermΔ)IV* from WJA0037 into WJA2138	
WJA0815	*unc-54(srf0788; 12rareArg)I; nonu-1(srf0780; SmrΔ) pelo-1(cc2849; ex3,4,5KO-BglII)III; skih-2(cc2854; NtermΔ)IV*	Crossed *nonu-1(srf0780; SmrΔ)III; pelo-1(cc2849; ex3,4,5KO-BglII)III; skih-2(cc2854; NtermΔ)IV* from WJA0800 into WJA0788	

Strain #	Genotype	Strain Construction	Sequence around any CRISPR/Cas9-introduced mutations
WJA0730	*k07a12.4(srf0730; ex3,4KO)I*	CRISPR with gRNAs from JA-MG-5/6 and JA-MG-7/8, donor template JA-MG-9. Isolate #1.	ATCCTGGTATTCCATCATCATC GTATCATCCACCT CATATG TAG C TAA G TGA ATCTTCTGAAGTCGATTTAACA TCATTTCGACGCA
WJA0731	*k07a12.4(srf0731; ex3,4KO)I*	CRISPR with gRNAs from JA-MG-5/6 and JA-MG-7/8, donor template JA-MG-9. Isolate #2.	ATCCTGGTATTCCATCATCATC GTATCATCCACCT CATATG TAG C TAA G TGA ATCTTCTGAAGTCGATTTAACA TCATTTCGACGCA
WJA0732	*k07a12.4(srf0732; ex3,4KO)I*	CRISPR with gRNAs from JA-MG-5/6 and JA-MG-7/8, donor template JA-MG-9. Isolate #3.	ATCCTGGTATTCCATCATCATC GTATCATCCACCT CATATG TAG C TAA G TGA ATCTTCTGAAGTCGATTTAACA TCATTTCGACGCA
WJA0765	*k07a12.4(srf0765; V269D,H276L)I*	CRISPR with gRNAs from JA-MG-17/18 and JA-MG-19/20, donor template JA-MG-21. Isolate #1.	CATTGGAAGAACAAGCTTCGA AACTTCACATCGACGAATaGatC TTCTCGATGCTCCAGGcCtcAAA GATTTTATTTCAAATATGATCA CAGGAACGTCACAAG
WJA0766	*k07a12.4(srf0766; V269D,H276L)I*	CRISPR with gRNAs from JA-MG-17/18 and JA-MG-19/20, donor template JA-MG-21. Isolate #2.	CATTGGAAGAACAAGCTTCGA AACTTCACATCGACGAATaGatC TTCTCGATGCTCCAGGcCtcAAA GATTTTATTTCAAATATGATCA CAGGAACGTCACAAG
WJA0767	*k07a12.4(srf0767; V269D,H276L)I*	CRISPR with gRNAs from JA-MG-17/18 and JA-MG-19/20, donor template JA-MG-21. Isolate #3.	CATTGGAAGAACAAGCTTCGA AACTTCACATCGACGAATaGatC TTCTCGATGCTCCAGGcCtcAAA GATTTTATTTCAAATATGATCA CAGGAACGTCACAAG
WJA3004	*unc-54(cc4092; unc-54::GFP::T2A::nonstop)I; k07a12.4(srf0730; ex3,4KO)I*	Crossed *k07a12.4(srf0730; ex3,4KO)I* from WJA0730 into WJA0438	
WJA3005	*unc-54(cc4092; unc-54::GFP::T2A::nonstop)I; k07a12.4(srf0732; ex3,4KO)I*	Crossed *k07a12.4(srf0732; ex3,4KO)I* from WJA0732 into WJA0438	

Strain #	*Genotype*	Strain Construction	Sequence around any CRISPR/Cas9-introduced mutations
WJA3006	*unc-54(cc4092; unc-54::GFP::T2A::nonstop)I; k07a12.4(srf0765; V269D,H276L)I*	Crossed *k07a12.4(srf0765; V269D,H276L)I* from WJA0765 into WJA0438	
WJA3007	*unc-54(cc4092; unc-54::GFP::T2A::nonstop)I; k07a12.4(srf0765; V269D,H276L)I*	Crossed *k07a12.4(srf0765; V269D,H276L)I* from WJA0765 into WJA0438	
WJA3008	*unc-54(cc4092; unc-54::GFP::T2A::nonstop)I; k07a12.4(srf0765; V269D,H276L)I*	Crossed *k07a12.4(srf0765; V269D,H276L)I* from WJA0765 into WJA0438	

Table 2: *S. cerevisiae* strains

Strain #	Genotype	Background Genotype	Strain Construction
YJA001	*ski2Δ::KanMX*	*MATa his3Δ1 leu2Δ0 met15Δ0 ura3Δ0*	KO collection (Ares Lab)
YJA003	*cue2Δ::KanMX*	*MATa his3Δ1 leu2Δ0 met15Δ0 ura3Δ0*	KO collection (Ares Lab)
YJA004	*ypl199cΔ::KanMX*	*MATa his3Δ1 leu2Δ0 met15Δ0 ura3Δ0*	KO collection (Ares Lab)
YJA007	*cue2Δ::KanMX/CUE2*	*MATa/α his3Δ1/his3Δ1 leu2Δ0/leu2Δ0 LYS2/lys2Δ0 met15Δ0/MET15 ura3Δ0/ura3Δ0*	heterozygote KO collection (Hartzog Lab)
YJA008	wt	*MATa his3Δ1 leu2Δ0 met15Δ0 ura3Δ0*	Ares Lab
YJA009	*ski2Δ::KanMX [pAV188]*	*MATa his3Δ1 leu2Δ0 met15Δ0 ura3Δ0*	Transformation
YJA010	*ski2Δ::KanMX [pAV188]*	*MATa his3Δ1 leu2Δ0 met15Δ0 ura3Δ0*	Transformation
YJA011	*cue2Δ::KanMX [pAV188]*	*MATa his3Δ1 leu2Δ0 met15Δ0 ura3Δ0*	Transformation
YJA012	*cue2Δ::KanMX [pAV188]*	*MATa his3Δ1 leu2Δ0 met15Δ0 ura3Δ0*	Transformation
YJA013	*ypl199cΔ::KanMX [pAV188]*	*MATa his3Δ1 leu2Δ0 met15Δ0 ura3Δ0*	Transformation
YJA014	*ypl199cΔ::KanMX [pAV188]*	*MATa his3Δ1 leu2Δ0 met15Δ0 ura3Δ0*	Transformation
YJA015	wt [pAV188]	*MATa his3Δ1 leu2Δ0 met15Δ0 ura3Δ0*	Transformation
YJA016	wt [pAV188]	*MATa his3Δ1 leu2Δ0 met15Δ0 ura3Δ0*	Transformation
YJA 017	*ypl199cΔ::KanMX/YPL199C cue2Δ::KanMX/CUE2*	*MATa/α his3Δ1/his3Δ1 leu2Δ0/leu2Δ0 LYS2/lys2Δ0 met15Δ0/MET15 ura3Δ0/ura3Δ0*	Made by sporulating YJA007, identifying tetrads with 2:2 segregation of all markers, then tetrads of the appropriate auxotrophies. Took these spores and streaked onto YPD plate containing YJA004.
YJA 022	cue2Δ::KanMX ypl199cΔ::KanMX	*MATa his3Δ1 leu2Δ0 lys2Δ0 ura3Δ0*	Made by sporulating YJA017, replica plating tetrads, and picking colonies with 2:2 segregation of G418.

Strain #	Genotype	Background Genotype	Strain Construction
YJA 023	cue2Δ::KanMX ypl199cΔ::KanMX	*MATa his3Δ1 leu2Δ0 lys2Δ0 ura3Δ0*	Made by sporulating YJA017, replica plating tetrads, and picking colonies with 2:2 segregation of G418.
YJA 024	cue2Δ::KanMX ypl199cΔ::KanMX	*MATa his3Δ1 leu2Δ0 met15Δ0 ura3Δ0*	Made by sporulating YJA017, replica plating tetrads, and picking colonies with 2:2 segregation of G418.
YJA025	*cue2Δ::KanMX ypl199cΔ::KanMX [pAV188]*	*MATa his3Δ1 leu2Δ0 met15Δ0 ura3Δ0*	Transformation
YJA026	*cue2Δ::KanMX ypl199cΔ::KanMX [pAV188]*	*MATa his3Δ1 leu2Δ0 met15Δ0 ura3Δ0*	Transformation

Table 3: Oligos

Oligo	Sequence	Purpose
JA-MG-5	TCTTG GTGTTGGAGTTGATACAGG	Annealed with JA-MG-6 to make gRNA to make k07a12.4(ex3,4KO)I
JA-MG-6	AAAC CCTGTATCAACTCCAACAC C	Annealed with JA-MG-5 to make gRNA to make k07a12.4(ex3,4KO)I
JA-MG-7	TCTTG ATCGACTTCAGAAGATGGG	Annealed with JA-MG-8 to make gRNA to make k07a12.4(ex3,4KO)I
JA-MG-8	AAAC CCCATCTTCTGAAGTCGAT C	Annealed with JA-MG-7 to make gRNA to make k07a12.4(ex3,4KO)I
JA-MG-9	ATCCTGGTATTCCATCATCATCGTATCATC CACCT CATATG TAG C TAA G TGA ATCTTCTGAAGTCGATTTAACATCATTTCG ACGCA	Donor template for CRISPR/Cas9 to make k07a12.4(ex3,4KO)I
JA-MG-10	GGACGACGATTATGACGACG	PCR oligo to verify k07a12.4(ex3,4KO)I, use with JA-MG-11
JA-MG-11	CCTGCATCGACATGTCCAAC	PCR oligo to verify k07a12.4(ex3,4KO)I, use with JA-MG-10
JA-MG-17	TCTTG TCGTGCTTCTCGATGCTCC	Annealed with JA-MG-18 to make gRNA to make k07a12.4(V269D,H276L)I
JA-MG-18	AAAC GGAGCATCGAGAAGCACGA C	Annealed with JA-MG-17 to make gRNA to make k07a12.4(V269D,H276L)I
JA-MG-19	TCTTG TCTTTATGTCCTGGAGCAT	Annealed with JA-MG-20 to make gRNA to make k07a12.4(V269D,H276L)I
JA-MG-20	AAAC ATGCTCCAGGACATAAAGA C	Annealed with JA-MG-19 to make gRNA to make k07a12.4(V269D,H276L)I
JA-MG-21	CATTGGAAGAACAAGCTTCGAAACTTCAC ATCGACGAATaGatCTTCTCGATGCTCCAGG cCtcAAAGATTTTATTTCAAATATGATCACA GGAACGTCACAAG	Donor template for CRISPR/Cas9 to make k07a12.4(V269D,H276L)I
JA-MG-22	gtacagccctgatggcaacaac	PCR oligo to verify k07a12.4(V269D,H276L)I, use with JA-MG-23
JA-MG-23	GTTGCGGTGCTACGAAACTGTc	PCR oligo to verify k07a12.4(V269D,H276L)I, use with JA-MG-22

Oligo	Sequence	Purpose
JA-MG-29	TCTTG ggtaatctccgtatcgatg	Annealed with JA-MG-30 to make gRNA to insert STOP between f26a1.13 and f26a1.14
JA-MG-30	AAAC catcgatacggagattacc C	Annealed with JA-MG-29 to make gRNA to insert STOP between f26a1.13 and f26a1.14
JA-MG-31	acattaaaaatacaattttcaga ATTTCAAACTTCTAGATCGATACGGAG attaccagtgtcctgtgtaaatcaccaatc	Donor template for CRISPR/Cas9 insertion of STOP between f26a1.13 and f26a1.14
JA-MG-32	TCTTG AGAAGCCCACAACAATCCA	Annealed with JA-MG-33 to make gRNA to make nonu-1(D579N) and nonu-1(AxA)
JA-MG-33	AAAC TGGATTGTTGTGGGCTTCT C	Annealed with JA-MG-32 to make gRNA to make nonu-1(D579N) and nonu-1(AxA)
JA-MG-34	TCTTG AGAAACCATGGATTGTTGT	Annealed with JA-MG-35 to make gRNA to make nonu-1(smrΔ)
JA-MG-35	AAAC ACAACAATCCATGGTTTCT C	Annealed with JA-MG-34 to make gRNA to make nonu-1(smrΔ)
JA-MG-36	TCTTG ATTATGAACTCGTGAATGA	Annealed with JA-MG-37 to make gRNA to make nonu-1(smrΔ)
JA-MG-37	AAAC TCATTCACGAGTTCATAAT C	Annealed with JA-MG-36 to make gRNA to make nonu-1(smrΔ)
JA-MG-40	GAAAGAACTTGATCGGAAAATTCGAGAAG CCCACAACAAT AGATCT TAG C TAA G TGA TGATGGATGTATAAGATTCAAAGTCTAGcat atcgtattctctcaaatatctctgcttttctttgcgctgtatttttga	Donor template for CRISPR/Cas9 to make nonu-1(smrΔ)
JA-MG-41	tttcacgtgatagacgacgc	Forward PCR primer to verify insertion of STOP between f26a1.13 and f26a1.14
JA-MG-42	gacgtttctaaggggttatg	Reverse PCR primer to verify insertion of STOP between f26a1.13 and f26a1.14
JA-MG-43	GCACTCTGAAATGAACGACG	Forward PCR primer to verify nonu-1(smrΔ) and nonu-1(D579N) and nonu-1(AxA)
JA-MG-44	cctactgcagaggcataaga	Reverse PCR primer to verify nonu-1(smrΔ) and nonu-1(D579N) and nonu-1(AxA)

Oligo	Sequence	Purpose
JA-MG-45	TCTTG TACATTACATGTCAGTTGA	Annealed with JA-MG-46 to make gRNA to make nonu-1(D579N) and nonu-1(AxA)
JA-MG-46	AAAC TCAACTGACATGTAATGTA C	Annealed with JA-MG-45 to make gRNA to make nonu-1(D579N) and nonu-1(AxA)
JA-MG-47	GAAAGAACTTGATCGGAAAATTCGAGAAG CCCACAACAATCCCTGGTTTCTAAATTTAC ATTACATGTCAGT TGACGGAGCAGTTAAACTTGTGAAAGAAG CGATTGAAGCA	Donor template for CRISPR/Cas9 to make nonu-1(D579N)
JA-AF-34	/5rApp/NNNNNNAGATCGGAAGAGCACACG TCT/3ddC/	Oligo for 3'ligation of 3'RACE and Ribo-seq libraries
JA-AF-126	/5Phos/AGATCGGAAGAGCGTCGTGT/iSp18/C ACTCA/iSp18/GTGACTGGAGTTCAGACGTG TGCTCTTCCGATCT	RT for 3'RACE and Ribo-seq libraries
JA-AF-138	TCTTG GGAAGAGGCAGAGGATATG	Annealed with JA-AF-139 to make gRNA to make pelo-1(cc2849; ex3,4,5KO-BglII)
JA-AF-139	AAAC CATATCCTCTGCCTCTTCC C	Annealed with JA-AF-138 to make gRNA to make pelo-1(cc2849; ex3,4,5KO-BglII)
AF-JA-141	CAGAATCTGAAATTCATCATCAATC	Forward PCR primer to verify pelo-1(cc2849; ex3,4,5KO-BglII)
JA-AF-143	TCTTG TGCGTCTTTCACAAATCCA	Annealed with JA-AF-144 to make gRNA to make pelo-1(cc2849; ex3,4,5KO-BglII)
JA-AF-144	AAAC TGGATTTGTGAAAGACGCA C	Annealed with JA-AF-143 to make gRNA to make pelo-1(cc2849; ex3,4,5KO-BglII)
AF-JA-147	TTTTCATAGGAAAGCTTTGCAAA	Reverse PCR primer to verify pelo-1(cc2849; ex3,4,5KO-BglII)
JA-AF-152	ACTTCATCTTTTGCAGATTCGTAGTTTTAAT GGCGGAAGAGGCAGAGGATAGATCTATTT GTGAAAGACGCATTTATGCAGCATTTAATA GCACATGCAGATGCAA	Donor template for CRISPR/Cas9 pelo-1(cc2849; ex3,4,5KO-BglII)
JA-AF-268	TCTTG ATGTACGGAATCGGATGCG	Annealed with JA-AF-269 to make gRNA to make unc-54(No-Go)
JA-AF-269	AAAC CGCATCCGATTCCGTACAT C	Annealed with JA-AF-268 to make gRNA to make unc-54(No-Go)
JA-AF-270	TCTTG CATCCGATTCCGTACATGT	Annealed with JA-AF-271 to make gRNA to make unc-54(No-Go)

Oligo	Sequence	Purpose
JA-AF-271	AAAC ACATGTACGGAATCGGATG C	Annealed with JA-AF-270 to make gRNA to make unc-54(No-Go)
JA-AA-176	AGATGGTACCGATGAGGCCGAGAAGGCAT CCAACATGTAC AGATCT cgg cgg agg cgg agg agg cgg cgg agg cgg cgg agg ATCGGATGCGAGGAGTTCCTCAAGGCTTTG ACCAAGCCAC	Donor template for CRISPR/Cas9 to make unc-54(No-Go)
JA-AF-273	TTCTACCAAATCTACTCTGACTTCC	JA-AF-273/274 make 619 bp amplicon centered over unc-54(e1301) site
JA-AF-274	GGTTGAAGAATTGTTGGAGCTTC	JA-AF-273/274 make 619 bp amplicon centered over unc-54(e1301) site
JA-AA-184	TCTTG TTCGCGGAGTTACGGGATC	Annealed with JA-AA-185 to make gRNA to make nonu-1(K41A)
JA-AA-185	AAAC GATCCCGTAACTCCGCGAA C	Annealed with JA-AA-184 to make gRNA to make nonu-1(K41A)
JA-AA-186	TCTTG CGAGCTAATGTTGATTTTC	Annealed with JA-AA-187 to make gRNA to make nonu-1(K41A)
JA-AA-187	AAAC GAAAATCAACATTAGCTCG C	Annealed with JA-AA-186 to make gRNA to make nonu-1(K41A)
JA-AA-188	AAGGTCATCGCACAATTATTTTAATTCGCG GAGTTACGGGAagtGGtgccTCAACATTAGCT CGAGAGTTGGTAAACCATTCCGAAAA	Donor template for CRISPR/Cas9 to make nonu-1(K41A)
JA-AA-198	GAAGTGAAAGAACTTGATCGGAAAATTCG AGAAGCCCACAACAAc CCg TGG TTc tTg Gcc TTg GcT TAt ATG TCg GTT GATGGAGCAGTTAAACTTGTGAAAGAAGC GATTGAAGCA	Donor template for CRISPR/Cas9 to make nonu-1(AxA)
JA-AA-275	GATCCAGAGTGAGGTTACAC	oligo for gene-specific RT of unc-54 just downstream of e1301 site
JA-AA-276	ACACGACGCTCTTCCGATCT	Forward primer identical to the 5'end of JA-AA-313-316
JA-AA-277	GAGTAGAGACCCTTGGCCATGG	reverse primer for gene-specific PCR of unc-54 just downstream of e1301 site. Tm 64C.

Oligo	Sequence	Purpose
JA-AA-278	CAAGCAGAAGACGGCATACGAGAT GCGCATTA GTGACTGGAGTTCAGACGTGTGCTCTTCCG ATCT TCGGTTCCGACCTTGACACG	reverse primer with D708 barcode for illumina sequencing. Primes just downstream of e1301 site in unc-54
JA-AA-313	/5Phos/ACACGACGCTCTTCCGATCT CTACGT GC rNrNrNrNrNrNrNrN/3Phos/	Includes 6nt unique barcode, GC upstream of the N8, 5'blocking group (phosphate), 3'phosphate for Rtcb1 ligation.
JA-AA-314	/5Phos/ACACGACGCTCTTCCGATCT GATGAC GC rNrNrNrNrNrNrNrN/3Phos/	Includes 6nt unique barcode, GC upstream of the N8, 5'blocking group (phosphate), 3'phosphate for Rtcb1 ligation.
JA-AA-315	/5Phos/ACACGACGCTCTTCCGATCT TCGTCG GC rNrNrNrNrNrNrNrN/3Phos/	Includes 6nt unique barcode, GC upstream of the N8, 5'blocking group (phosphate), 3'phosphate for Rtcb1 ligation.
JA-AA-316	/5Phos/ACACGACGCTCTTCCGATCT AGCATA GC rNrNrNrNrNrNrNrN/3Phos/	Includes 6nt unique barcode, GC upstream of the N8, 5'blocking group (phosphate), 3'phosphate for Rtcb1 ligation.

BIBLIOGRAPHY

Agudelo-Romero, P., Carbonell, P., Perez-Amador, M. A., & Elena, S. F. (2008). Virus adaptation by manipulation of host's gene expression. *PLoS One*, *3*(6), e2397.

Algire, M. A., Maag, D., & Lorsch, J. R. (2005). Pi release from eIF2, not GTP hydrolysis, is the step controlled by start-site selection during eukaryotic translation initiation. *Mol Cell*, *20*(2), 251-262.

Alkalaeva, E. Z., Pisarev, A. V., Frolova, L. Y., Kisselev, L. L., & Pestova, T. V. (2006). In vitro reconstitution of eukaryotic translation reveals cooperativity between release factors eRF1 and eRF3. *Cell*, *125*(6), 1125-1136.

Altschul, S. F., Madden, T. L., Schaffer, A. A., Zhang, J., Zhang, Z., Miller, W., & Lipman, D. J. (1997). Gapped BLAST and PSI-BLAST: a new generation of protein database search programs. *Nucleic Acids Res*, *25*(17), 3389-3402.

Anders, S., & Huber, W. (2010). Differential expression analysis for sequence count data. *Genome Biol*, *11*(10), R106.

Anderson, J. S., & Parker, R. P. (1998). The 3' to 5' degradation of yeast mRNAs is a general mechanism for mRNA turnover that requires the SKI2 DEVH box protein and 3' to 5' exonucleases of the exosome complex. *EMBO J*, *17*(5), 1497-1506.

Anderson, P., & Brenner, S. (1984). A selection for myosin heavy chain mutants in the nematode Caenorhabditis elegans. *Proc Natl Acad Sci U S A*, *81*(14), 4470-4474.

Araki, Y., Takahashi, S., Kobayashi, T., Kajiho, H., Hoshino, S., & Katada, T. (2001). Ski7p G protein interacts with the exosome and the Ski complex for 3'-to-5' mRNA decay in yeast. *EMBO J*, *20*(17), 4684-4693.

Aravind, L., Iyer, L. M., & Anantharaman, V. (2003). The two faces of Alba: the evolutionary connection between proteins participating in chromatin structure and RNA metabolism. *Genome Biol*, *4*(10), R64.

Arribere, J. A., Bell, R. T., Fu, B. X., Artiles, K. L., Hartman, P. S., & Fire, A. Z. (2014). Efficient marker-free recovery of custom genetic modifications with CRISPR/Cas9 in Caenorhabditis elegans. *Genetics*, *198*(3), 837-846.

Arribere, J. A., & Fire, A. Z. (2018). Nonsense mRNA suppression via nonstop decay. *Elife*, *7*.

Atkinson, G. C., Baldauf, S. L., & Hauryliuk, V. (2008). Evolution of nonstop, no-go and nonsense-mediated mRNA decay and their termination factor-derived components. *BMC Evol Biol*, *8*, 290.

Balchin, D., Hayer-Hartl, M., & Hartl, F. U. (2016). In vivo aspects of protein folding and quality control. *Science*, *353*(6294), aac4354.

Balistreri, G., Horvath, P., Schweingruber, C., Zund, D., McInerney, G., Merits, A., Muhlemann, O., Azzalin, C., & Helenius, A. (2014). The host nonsense-mediated mRNA decay pathway restricts Mammalian RNA virus replication. *Cell Host Microbe*, *16*(3), 403-411.

Becker, T., Armache, J. P., Jarasch, A., Anger, A. M., Villa, E., Sieber, H., Motaal, B. A., Mielke, T., Berninghausen, O., & Beckmann, R. (2011). Structure of the no-go mRNA decay complex Dom34-Hbs1 bound to a stalled 80S ribosome. *Nat Struct Mol Biol*, *18*(6), 715-720.

Becker, T., Franckenberg, S., Wickles, S., Shoemaker, C. J., Anger, A. M., Armache, J. P., Sieber, H., Ungewickell, C., Berninghausen, O., Daberkow, I., Karcher, A., Thomm, M., Hopfner, K. P., Green, R., & Beckmann, R. (2012). Structural basis of highly conserved ribosome recycling in eukaryotes and archaea. *Nature*, *482*(7386), 501-506.

Behrmann, E., Loerke, J., Budkevich, T. V., Yamamoto, K., Schmidt, A., Penczek, P. A., Vos, M. R., Burger, J., Mielke, T., Scheerer, P., & Spahn, C. M. (2015). Structural snapshots of actively translating human ribosomes. *Cell*, *161*(4), 845-857.

Bejsovec, A., & Anderson, P. (1988). Myosin heavy-chain mutations that disrupt Caenorhabditis elegans thick filament assembly. *Genes Dev*, *2*(10), 1307-1317.

Bengtson, M. H., & Joazeiro, C. A. (2010). Role of a ribosome-associated E3 ubiquitin ligase in protein quality control. *Nature*, *467*(7314), 470-473.

Bernstein, E., Caudy, A. A., Hammond, S. M., & Hannon, G. J. (2001). Role for a bidentate ribonuclease in the initiation step of RNA interference. *Nature*, *409*(6818), 363-366.

Bhandari, D., Guha, K., Bhaduri, N., & Saha, P. (2011). Ubiquitination of mRNA cycling sequence binding protein from Leishmania donovani (LdCSBP) modulates the RNA endonuclease activity of its Smr domain. *FEBS Lett*, *585*(5), 809-813.

Brandman, O., Stewart-Ornstein, J., Wong, D., Larson, A., Williams, C. C., Li, G. W., Zhou, S., King, D., Shen, P. S., Weibezahn, J., Dunn, J. G., Rouskin, S., Inada, T., Frost, A., & Weissman, J. S. (2012). A ribosome-bound quality control complex triggers degradation of nascent peptides and signals translation stress. *Cell*, *151*(5), 1042-1054.

Brenner, S. (1974). The genetics of Caenorhabditis elegans. *Genetics*, *77*(1), 71-94.

Brown, A., Shao, S., Murray, J., Hegde, R. S., & Ramakrishnan, V. (2015). Structural basis for stop codon recognition in eukaryotes. *Nature*, *524*(7566), 493-496.

Brown, J. T., Bai, X., & Johnson, A. W. (2000). The yeast antiviral proteins Ski2p, Ski3p, and Ski8p exist as a complex in vivo. *RNA*, *6*(3), 449-457.

Budkevich, T., Giesebrecht, J., Altman, R. B., Munro, J. B., Mielke, T., Nierhaus, K. H., Blanchard, S. C., & Spahn, C. M. (2011). Structure and dynamics of the mammalian ribosomal pretranslocation complex. *Mol Cell*, *44*(2), 214-224.

Bulygin, K. N., Khairulina, Y. S., Kolosov, P. M., Ven'yaminova, A. G., Graifer, D. M., Vorobjev, Y. N., Frolova, L. Y., Kisselev, L. L., & Karpova, G. G. (2010). Three distinct peptides from the N domain of translation termination factor eRF1 surround stop codon in the ribosome. *RNA*, *16*(10), 1902-1914.

Burley, S. K., Berman, H. M., Bhikadiya, C., Bi, C., Chen, L., Di Costanzo, L., Christie, C., Dalenberg, K., Duarte, J. M., Dutta, S., Feng, Z., Ghosh, S., Goodsell, D. S., Green, R. K., Guranovic, V., Guzenko, D., Hudson, B. P., Kalro, T., Liang, Y., Lowe, R., Namkoong, H., Peisach, E., Periskova, I., Prlic, A., Randle, C., Rose, A., Rose, P., Sala, R., Sekharan, M., Shao, C., Tan, L., Tao, Y. P., Valasatava, Y., Voigt, M., Westbrook, J., Woo, J., Yang, H., Young, J., Zhuravleva, M., & Zardecki, C. (2019). RCSB Protein Data Bank: biological macromolecular structures enabling research and education in fundamental biology, biomedicine, biotechnology and energy. *Nucleic Acids Res*, *47*(D1), D464-D474.

Burroughs, A. M., & Aravind, L. (2016). RNA damage in biological conflicts and the diversity of responding RNA repair systems. *Nucleic Acids Res*, *44*(18), 8525-8555.

Chavatte, L., Seit-Nebi, A., Dubovaya, V., & Favre, A. (2002). The invariant uridine of stop codons contacts the conserved NIKSR loop of human eRF1 in the ribosome. *EMBO J*, *21*(19), 5302-5311.

Chen, L., Muhlrad, D., Hauryliuk, V., Cheng, Z., Lim, M. K., Shyp, V., Parker, R., & Song, H. (2010). Structure of the Dom34-Hbs1 complex and implications for no-go decay. *Nat Struct Mol Biol*, *17*(10), 1233-1240.

Cheng, Z., Saito, K., Pisarev, A. V., Wada, M., Pisareva, V. P., Pestova, T. V., Gajda, M., Round, A., Kong, C., Lim, M., Nakamura, Y., Svergun, D. I., Ito, K., & Song, H. (2009). Structural insights into eRF3 and stop codon recognition by eRF1. *Genes Dev*, *23*(9), 1106-1118.

Choe, Y. J., Park, S. H., Hassemer, T., Korner, R., Vincenz-Donnelly, L., Hayer-Hartl, M., & Hartl, F. U. (2016). Failure of RQC machinery causes protein aggregation and proteotoxic stress. *Nature*, *531*(7593), 191-195.

Choi, J., Grosely, R., Prabhakar, A., Lapointe, C. P., Wang, J., & Puglisi, J. D. (2018). How Messenger RNA and Nascent Chain Sequences Regulate Translation Elongation. *Annu Rev Biochem*, *87*, 421-449.

Chong, Y. P., Ia, K. K., Mulhern, T. D., & Cheng, H. C. (2005). Endogenous and synthetic inhibitors of the Src-family protein tyrosine kinases. *Biochim Biophys Acta*, *1754*(1-2), 210-220.

Cigan, A. M., Feng, L., & Donahue, T. F. (1988). tRNAi(met) functions in directing the scanning ribosome to the start site of translation. *Science*, *242*(4875), 93-97.

Consortium, C. e. S. (1998). Genome sequence of the nematode C. elegans: a platform for investigating biology. *Science*, *282*(5396), 2012-2018.

Corsi, A. K., Wightman, B., & Chalfie, M. (2015). A Transparent Window into Biology: A Primer on Caenorhabditis elegans. *Genetics*, *200*(2), 387-407.

D'Orazio, K. N., Wu, C. C., Sinha, N., Loll-Krippleber, R., Brown, G. W., & Green, R. (2019). The endonuclease Cue2 cleaves mRNAs at stalled ribosomes during No Go Decay. *Elife*, *8*.

Defenouillere, Q., Yao, Y., Mouaikel, J., Namane, A., Galopier, A., Decourty, L., Doyen, A., Malabat, C., Saveanu, C., Jacquier, A., & Fromont-Racine, M. (2013). Cdc48-associated complex bound to 60S particles is required for the clearance of aberrant translation products. *Proc Natl Acad Sci U S A*, *110*(13), 5046-5051.

des Georges, A., Hashem, Y., Unbehaun, A., Grassucci, R. A., Taylor, D., Hellen, C. U., Pestova, T. V., & Frank, J. (2014). Structure of the mammalian ribosomal

pre-termination complex associated with eRF1.eRF3.GDPNP. *Nucleic Acids Res*, *42*(5), 3409-3418.

Deshaies, R. J., & Joazeiro, C. A. (2009). RING domain E3 ubiquitin ligases. *Annu Rev Biochem*, *78*, 399-434.

Dever, T. E. (2002). Gene-specific regulation by general translation factors. *Cell*, *108*(4), 545-556.

Dever, T. E., Dinman, J. D., & Green, R. (2018). Translation Elongation and Recoding in Eukaryotes. *Cold Spring Harb Perspect Biol*, *10*(8).

Dever, T. E., & Green, R. (2012). The elongation, termination, and recycling phases of translation in eukaryotes. *Cold Spring Harb Perspect Biol*, *4*(7), a013706.

Dibb, N. J., Brown, D. M., Karn, J., Moerman, D. G., Bolten, S. L., & Waterston, R. H. (1985). Sequence analysis of mutations that affect the synthesis, assembly and enzymatic activity of the unc-54 myosin heavy chain of Caenorhabditis elegans. *J Mol Biol*, *183*(4), 543-551.

Dibb, N. J., Maruyama, I. N., Krause, M., & Karn, J. (1989). Sequence analysis of the complete Caenorhabditis elegans myosin heavy chain gene family. *J Mol Biol*, *205*(3), 603-613.

Dilucca, M., Forcelloni, S., Georgakilas, A. G., Giansanti, A., & Pavlopoulou, A. (2020). Codon Usage and Phenotypic Divergences of SARS-CoV-2 Genes. *Viruses*, *12*(5).

Dimitrova, L. N., Kuroha, K., Tatematsu, T., & Inada, T. (2009). Nascent peptide-dependent translation arrest leads to Not4p-mediated protein degradation by the proteasome. *J Biol Chem*, *284*(16), 10343-10352.

Dobin, A., Davis, C. A., Schlesinger, F., Drenkow, J., Zaleski, C., Jha, S., Batut, P., Chaisson, M., & Gingeras, T. R. (2013). STAR: ultrafast universal RNA-seq aligner. *Bioinformatics*, *29*(1), 15-21.

Doitsidou, M., Poole, R. J., Sarin, S., Bigelow, H., & Hobert, O. (2010). C. elegans mutant identification with a one-step whole-genome-sequencing and SNP mapping strategy. *PLoS One*, *5*(11), e15435.

Doma, M. K., & Parker, R. (2006). Endonucleolytic cleavage of eukaryotic mRNAs with stalls in translation elongation. *Nature*, *440*(7083), 561-564.

Epstein, H. F., Waterston, R. H., & Brenner, S. (1974). A mutant affecting the heavy chain of myosin in Caenorhabditis elegans. *J Mol Biol*, *90*(2), 291-300.

Eyler, D. E., & Green, R. (2011). Distinct response of yeast ribosomes to a miscoding event during translation. *RNA*, *17*(5), 925-932.

Fabre, A., Charroux, B., Martinez-Vinson, C., Roquelaure, B., Odul, E., Sayar, E., Smith, H., Colomb, V., Andre, N., Hugot, J. P., Goulet, O., Lacoste, C., Sarles, J., Royet, J., Levy, N., & Badens, C. (2012). SKIV2L mutations cause syndromic diarrhea, or trichohepatoenteric syndrome. *Am J Hum Genet*, *90*(4), 689-692.

Fehr, A. R., & Perlman, S. (2015). Coronaviruses: an overview of their replication and pathogenesis. *Methods Mol Biol*, *1282*, 1-23.

Finn, R. D., Coggill, P., Eberhardt, R. Y., Eddy, S. R., Mistry, J., Mitchell, A. L., Potter, S. C., Punta, M., Qureshi, M., Sangrador-Vegas, A., Salazar, G. A., Tate, J., & Bateman, A. (2016). The Pfam protein families database: towards a more sustainable future. *Nucleic Acids Res*, *44*(D1), D279-285.

Fire, A., Xu, S., Montgomery, M. K., Kostas, S. A., Driver, S. E., & Mello, C. C. (1998). Potent and specific genetic interference by double-stranded RNA in Caenorhabditis elegans. *Nature*, *391*(6669), 806-811.

Flis, J., Holm, M., Rundlet, E. J., Loerke, J., Hilal, T., Dabrowski, M., Burger, J., Mielke, T., Blanchard, S. C., Spahn, C. M. T., & Budkevich, T. V. (2018). tRNA Translocation by the Eukaryotic 80S Ribosome and the Impact of GTP Hydrolysis. *Cell Rep*, *25*(10), 2676-2688 e2677.

Friedland, A. E., Tzur, Y. B., Esvelt, K. M., Colaiacovo, M. P., Church, G. M., & Calarco, J. A. (2013). Heritable genome editing in C. elegans via a CRISPR-Cas9 system. *Nat Methods*, *10*(8), 741-743.

Frischmeyer, P. A., van Hoof, A., O'Donnell, K., Guerrerio, A. L., Parker, R., & Dietz, H. C. (2002). An mRNA surveillance mechanism that eliminates transcripts lacking termination codons. *Science*, *295*(5563), 2258-2261.

Frolova, L. Y., Tsivkovskii, R. Y., Sivolobova, G. F., Oparina, N. Y., Serpinsky, O. I., Blinov, V. M., Tatkov, S. I., & Kisselev, L. L. (1999). Mutations in the highly conserved GGQ motif of class 1 polypeptide release factors abolish ability of human eRF1 to trigger peptidyl-tRNA hydrolysis. *RNA*, *5*(8), 1014-1020.

Fukui, K., Nakagawa, N., Kitamura, Y., Nishida, Y., Masui, R., & Kuramitsu, S. (2008). Crystal structure of MutS2 endonuclease domain and the mechanism of homologous recombination suppression. *J Biol Chem*, *283*(48), 33417-33427.

Garcia, D., Garcia, S., & Voinnet, O. (2014). Nonsense-mediated decay serves as a general viral restriction mechanism in plants. *Cell Host Microbe*, *16*(3), 391-402.

Garzia, A., Jafarnejad, S. M., Meyer, C., Chapat, C., Gogakos, T., Morozov, P., Amiri, M., Shapiro, M., Molina, H., Tuschl, T., & Sonenberg, N. (2017). The E3 ubiquitin ligase and RNA-binding protein ZNF598 orchestrates ribosome quality control of premature polyadenylated mRNAs. *Nat Commun*, *8*, 16056.

Gingras, A. C., Raught, B., & Sonenberg, N. (1999). eIF4 initiation factors: effectors of mRNA recruitment to ribosomes and regulators of translation. *Annu Rev Biochem*, *68*, 913-963.

Gout, J. F., Li, W., Fritsch, C., Li, A., Haroon, S., Singh, L., Hua, D., Fazelinia, H., Smith, Z., Seeholzer, S., Thomas, K., Lynch, M., & Vermulst, M. (2017). The landscape of transcription errors in eukaryotic cells. *Sci Adv*, *3*(10), e1701484.

Graber, J. H., Cantor, C. R., Mohr, S. C., & Smith, T. F. (1999). In silico detection of control signals: mRNA 3'-end-processing sequences in diverse species. *Proc Natl Acad Sci U S A*, *96*(24), 14055-14060.

Graille, M., Chaillet, M., & van Tilbeurgh, H. (2008). Structure of yeast Dom34: a protein related to translation termination factor Erf1 and involved in No-Go decay. *J Biol Chem*, *283*(11), 7145-7154.

Grant, O. C., Montgomery, D., Ito, K., & Woods, R. J. (2020). Analysis of the SARS-CoV-2 spike protein glycan shield reveals implications for immune recognition. *Sci Rep*, *10*(1), 14991.

Gromadski, K. B., Schummer, T., Stromgaard, A., Knudsen, C. R., Kinzy, T. G., & Rodnina, M. V. (2007). Kinetics of the interactions between yeast elongation factors 1A and 1Balpha, guanine nucleotides, and aminoacyl-tRNA. *J Biol Chem*, *282*(49), 35629-35637.

Guo, J., Wang, J., Xi, L., Huang, W. D., Liang, J., & Chen, J. G. (2009). RACK1 is a negative regulator of ABA responses in Arabidopsis. *J Exp Bot*, *60*(13), 3819-3833.

Guo, L., Ding, J., Guo, R., Hou, Y., Wang, D. C., & Huang, L. (2014). Biochemical and structural insights into RNA binding by Ssh10b, a member of the highly conserved Sac10b protein family in Archaea. *J Biol Chem*, *289*(3), 1478-1490.

Guydosh, N. R., & Green, R. (2014). Dom34 rescues ribosomes in 3' untranslated regions. *Cell*, *156*(5), 950-962.

Guydosh, N. R., & Green, R. (2017). Translation of poly(A) tails leads to precise mRNA cleavage. *RNA*, *23*(5), 749-761.

Halbach, F., Reichelt, P., Rode, M., & Conti, E. (2013). The yeast ski complex: crystal structure and RNA channeling to the exosome complex. *Cell*, *154*(4), 814-826.

Haley, B., & Zamore, P. D. (2004). Kinetic analysis of the RNAi enzyme complex. *Nat Struct Mol Biol*, *11*(7), 599-606.

Hashimoto, S., Sugiyama, T., Yamazaki, R., Nobuta, R., & Inada, T. (2020). Identification of a novel trigger complex that facilitates ribosome-associated quality control in mammalian cells. *Sci Rep*, *10*(1), 3422.

Hashimoto, Y., Takahashi, M., Sakota, E., & Nakamura, Y. (2017). Nonstop-mRNA decay machinery is involved in the clearance of mRNA 5'-fragments produced by RNAi and NMD in Drosophila melanogaster cells. *Biochem Biophys Res Commun*, *484*(1), 1-7.

Hellen, C. U. T. (2018). Translation Termination and Ribosome Recycling in Eukaryotes. *Cold Spring Harb Perspect Biol*, *10*(10).

Hendriks, G. J., Gaidatzis, D., Aeschimann, F., & Grosshans, H. (2014). Extensive oscillatory gene expression during C. elegans larval development. *Mol Cell*, *53*(3), 380-392.

Heuer, A., Gerovac, M., Schmidt, C., Trowitzsch, S., Preis, A., Kotter, P., Berninghausen, O., Becker, T., Beckmann, R., & Tampe, R. (2017). Structure of the 40S-ABCE1 post-splitting complex in ribosome recycling and translation initiation. *Nat Struct Mol Biol*, *24*(5), 453-460.

Hickey, K. L., Dickson, K., Cogan, J. Z., Replogle, J. M., Schoof, M., D'Orazio, K. N., Sinha, N. K., Hussmann, J. A., Jost, M., Frost, A., Green, R., Weissman, J. S., & Kostova, K. K. (2020). GIGYF2 and 4EHP Inhibit Translation Initiation of Defective Messenger RNAs to Assist Ribosome-Associated Quality Control. *Mol Cell*, *79*(6), 950-962 e956.

Hilal, T., Yamamoto, H., Loerke, J., Burger, J., Mielke, T., & Spahn, C. M. (2016). Structural insights into ribosomal rescue by Dom34 and Hbs1 at near-atomic resolution. *Nat Commun*, *7*, 13521.

Hinnebusch, A. G., & Lorsch, J. R. (2012). The mechanism of eukaryotic translation initiation: new insights and challenges. *Cold Spring Harb Perspect Biol*, *4*(10).

Hodgkin, J., Papp, A., Pulak, R., Ambros, V., & Anderson, P. (1989). A new kind of informational suppression in the nematode Caenorhabditis elegans. *Genetics*, *123*(2), 301-313.

Holm, L., & Sander, C. (1995). Dali: a network tool for protein structure comparison. *Trends Biochem Sci*, *20*(11), 478-480.

Horikawa, W., Endo, K., Wada, M., & Ito, K. (2016). Mutations in the G-domain of Ski7 cause specific dysfunction in non-stop decay. *Sci Rep*, *6*, 29295.

Hou, W. (2020). Characterization of codon usage pattern in SARS-CoV-2. *Virol J*, *17*(1), 138.

Hussain, S., Shinu, P., Islam, M. M., Chohan, M. S., & Rasool, S. T. (2020). Analysis of Codon Usage and Nucleotide Bias in Middle East Respiratory Syndrome Coronavirus Genes. *Evol Bioinform Online*, *16*, 1176934320918861.

Ibrahim, F., Maragkakis, M., Alexiou, P., & Mourelatos, Z. (2018). Ribothrypsis, a novel process of canonical mRNA decay, mediates ribosome-phased mRNA endonucleolysis. *Nat Struct Mol Biol*, *25*(4), 302-310.

Ikeuchi, K., & Inada, T. (2016). Ribosome-associated Asc1/RACK1 is required for endonucleolytic cleavage induced by stalled ribosome at the 3' end of nonstop mRNA. *Sci Rep*, *6*, 28234.

Ikeuchi, K., Tesina, P., Matsuo, Y., Sugiyama, T., Cheng, J., Saeki, Y., Tanaka, K., Becker, T., Beckmann, R., & Inada, T. (2019). Collided ribosomes form a unique structural interface to induce Hel2-driven quality control pathways. *EMBO J*, *38*(5).

Inada, T., & Aiba, H. (2005). Translation of aberrant mRNAs lacking a termination codon or with a shortened 3'-UTR is repressed after initiation in yeast. *EMBO J*, *24*(8), 1584-1595.

Ingolia, N. T., Ghaemmaghami, S., Newman, J. R., & Weissman, J. S. (2009). Genome-wide analysis in vivo of translation with nucleotide resolution using ribosome profiling. *Science*, *324*(5924), 218-223.

Joazeiro, C. A. P. (2017). Ribosomal Stalling During Translation: Providing Substrates for Ribosome-Associated Protein Quality Control. *Annu Rev Cell Dev Biol*, *33*, 343-368.

Jorgensen, E. M., & Mango, S. E. (2002). The art and design of genetic screens: caenorhabditis elegans. *Nat Rev Genet*, *3*(5), 356-369.

Juszkiewicz, S., Chandrasekaran, V., Lin, Z., Kraatz, S., Ramakrishnan, V., & Hegde, R. S. (2018). ZNF598 Is a Quality Control Sensor of Collided Ribosomes. *Mol Cell*, *72*(3), 469-481 e467.

Juszkiewicz, S., & Hegde, R. S. (2017). Initiation of Quality Control during Poly(A) Translation Requires Site-Specific Ribosome Ubiquitination. *Mol Cell*, *65*(4), 743-750 e744.

Juszkiewicz, S., Slodkowicz, G., Lin, Z., Freire-Pritchett, P., Peak-Chew, S. Y., & Hegde, R. S. (2020). Ribosome collisions trigger cis-acting feedback inhibition of translation initiation. *Elife*, *9*.

Juszkiewicz, S., Speldewinde, S. H., Wan, L., Svejstrup, J. Q., & Hegde, R. S. (2020). The ASC-1 Complex Disassembles Collided Ribosomes. *Mol Cell*, *79*(4), 603-614 e608.

Kadrmas, J. L., Smith, M. A., Pronovost, S. M., & Beckerle, M. C. (2007). Characterization of RACK1 function in Drosophila development. *Dev Dyn*, *236*(8), 2207-2215.

Kaletta, T., & Hengartner, M. O. (2006). Finding function in novel targets: C. elegans as a model organism. *Nat Rev Drug Discov*, *5*(5), 387-398.

Kalisiak, K., Kulinski, T. M., Tomecki, R., Cysewski, D., Pietras, Z., Chlebowski, A., Kowalska, K., & Dziembowski, A. (2017). A short splicing isoform of HBS1L links the cytoplasmic exosome and SKI complexes in humans. *Nucleic Acids Res*, *45*(4), 2068-2080.

Kang, R. S., Daniels, C. M., Francis, S. A., Shih, S. C., Salerno, W. J., Hicke, L., & Radhakrishnan, I. (2003). Solution structure of a CUE-ubiquitin complex reveals a conserved mode of ubiquitin binding. *Cell*, *113*(5), 621-630.

Kapp, L. D., & Lorsch, J. R. (2004). GTP-dependent recognition of the methionine moiety on initiator tRNA by translation factor eIF2. *J Mol Biol*, *335*(4), 923-936.

Kolupaeva, V. G., Unbehaun, A., Lomakin, I. B., Hellen, C. U., & Pestova, T. V. (2005). Binding of eukaryotic initiation factor 3 to ribosomal 40S subunits and its role in ribosomal dissociation and anti-association. *RNA*, *11*(4), 470-486.

Kostova, K. K., Hickey, K. L., Osuna, B. A., Hussmann, J. A., Frost, A., Weinberg, D. E., & Weissman, J. S. (2017). CAT-tailing as a fail-safe mechanism for efficient degradation of stalled nascent polypeptides. *Science*, *357*(6349), 414-417.

Kowalinski, E., Kogel, A., Ebert, J., Reichelt, P., Stegmann, E., Habermann, B., & Conti, E. (2016). Structure of a Cytoplasmic 11-Subunit RNA Exosome Complex. *Mol Cell*, *63*(1), 125-134.

Kozak, M. (1978). How do eucaryotic ribosomes select initiation regions in messenger RNA? *Cell*, *15*(4), 1109-1123.

Krishnan, A., Iyer, L. M., Holland, S. J., Boehm, T., & Aravind, L. (2018). Diversification of AID/APOBEC-like deaminases in metazoa: multiplicity of clades and widespread roles in immunity. *Proc Natl Acad Sci U S A*, *115*(14), E3201-E3210.

Kuroha, K., Akamatsu, M., Dimitrova, L., Ito, T., Kato, Y., Shirahige, K., & Inada, T. (2010). Receptor for activated C kinase 1 stimulates nascent polypeptide-dependent translation arrest. *EMBO Rep*, *11*(12), 956-961.

Langmead, B., & Salzberg, S. L. (2012). Fast gapped-read alignment with Bowtie 2. *Nat Methods*, *9*(4), 357-359.

LaRiviere, F. J., Cole, S. E., Ferullo, D. J., & Moore, M. J. (2006). A late-acting quality control process for mature eukaryotic rRNAs. *Mol Cell*, *24*(4), 619-626.

Lassmann, T., Frings, O., & Sonnhammer, E. L. (2009). Kalign2: high-performance multiple alignment of protein and nucleotide sequences allowing external features. *Nucleic Acids Res*, *37*(3), 858-865.

Lee, H. H., Kim, Y. S., Kim, K. H., Heo, I., Kim, S. K., Kim, O., Kim, H. K., Yoon, J. Y., Kim, H. S., Kim, D. J., Lee, S. J., Yoon, H. J., Kim, S. J., Lee, B. G., Song, H. K., Kim, V. N., Park, C. M., & Suh, S. W. (2007). Structural and

functional insights into Dom34, a key component of no-go mRNA decay. *Mol Cell*, *27*(6), 938-950.

Lee, R. Y. N., Howe, K. L., Harris, T. W., Arnaboldi, V., Cain, S., Chan, J., Chen, W. J., Davis, P., Gao, S., Grove, C., Kishore, R., Muller, H. M., Nakamura, C., Nuin, P., Paulini, M., Raciti, D., Rodgers, F., Russell, M., Schindelman, G., Tuli, M. A., Van Auken, K., Wang, Q., Williams, G., Wright, A., Yook, K., Berriman, M., Kersey, P., Schedl, T., Stein, L., & Sternberg, P. W. (2018). WormBase 2017: molting into a new stage. *Nucleic Acids Res*, *46*(D1), D869-D874.

Leipe, D. D., Koonin, E. V., & Aravind, L. (2003). Evolution and classification of P-loop kinases and related proteins. *J Mol Biol*, *333*(4), 781-815.

Lespinet, O., Wolf, Y. I., Koonin, E. V., & Aravind, L. (2002). The role of lineage-specific gene family expansion in the evolution of eukaryotes. *Genome Res*, *12*(7), 1048-1059.

Letzring, D. P., Wolf, A. S., Brule, C. E., & Grayhack, E. J. (2013). Translation of CGA codon repeats in yeast involves quality control components and ribosomal protein L1. *RNA*, *19*(9), 1208-1217.

Li, M., Kao, E., Gao, X., Sandig, H., Limmer, K., Pavon-Eternod, M., Jones, T. E., Landry, S., Pan, T., Weitzman, M. D., & David, M. (2012). Codon-usage-based inhibition of HIV protein synthesis by human schlafen 11. *Nature*, *491*(7422), 125-128.

Li, M., Kao, E., Malone, D., Gao, X., Wang, J. Y. J., & David, M. (2018). DNA damage-induced cell death relies on SLFN11-dependent cleavage of distinct type II tRNAs. *Nat Struct Mol Biol*, *25*(11), 1047-1058.

Lima, S. A., Chipman, L. B., Nicholson, A. L., Chen, Y. H., Yee, B. A., Yeo, G. W., Coller, J., & Pasquinelli, A. E. (2017). Short poly(A) tails are a conserved feature of highly expressed genes. *Nat Struct Mol Biol*, *24*(12), 1057-1063.

Liu, J., Carmell, M. A., Rivas, F. V., Marsden, C. G., Thomson, J. M., Song, J. J., Hammond, S. M., Joshua-Tor, L., & Hannon, G. J. (2004). Argonaute2 is the catalytic engine of mammalian RNAi. *Science*, *305*(5689), 1437-1441.

Liu, Q., Rand, T. A., Kalidas, S., Du, F., Kim, H. E., Smith, D. P., & Wang, X. (2003). R2D2, a bridge between the initiation and effector steps of the Drosophila RNAi pathway. *Science*, *301*(5641), 1921-1925.

Liu, S., Melonek, J., Boykin, L. M., Small, I., & Howell, K. A. (2013). PPR-SMRs: ancient proteins with enigmatic functions. *RNA Biol*, *10*(9), 1501-1510.

Lodish H, Berk A, Zipursky SL, et al. Molecular Cell Biology. 4th edition. New York: W. H. Freeman; 2000. https://www.ncbi.nlm.nih.gov/books/NBK21475/

Loh, P. G., & Song, H. (2010). Structural and mechanistic insights into translation termination. *Curr Opin Struct Biol*, *20*(1), 98-103.

Losson, R., & Lacroute, F. (1979). Interference of nonsense mutations with eukaryotic messenger RNA stability. *Proc Natl Acad Sci U S A*, *76*(10), 5134-5137.

Loveland, A. B., Demo, G., Grigorieff, N., & Korostelev, A. A. (2017). Ensemble cryo-EM elucidates the mechanism of translation fidelity. *Nature*, *546*(7656), 113-117.

Lykke-Andersen, S., & Jensen, T. H. (2015). Nonsense-mediated mRNA decay: an intricate machinery that shapes transcriptomes. *Nat Rev Mol Cell Biol*, *16*(11), 665-677.

Lyumkis, D., Oliveira dos Passos, D., Tahara, E. B., Webb, K., Bennett, E. J., Vinterbo, S., Potter, C. S., Carragher, B., & Joazeiro, C. A. (2014). Structural basis for translational surveillance by the large ribosomal subunit-associated protein quality control complex. *Proc Natl Acad Sci U S A*, *111*(45), 15981-15986.

Makarova, K. S., Aravind, L., Wolf, Y. I., Tatusov, R. L., Minton, K. W., Koonin, E. V., & Daly, M. J. (2001). Genome of the extremely radiation-resistant bacterium Deinococcus radiodurans viewed from the perspective of comparative genomics. *Microbiol Mol Biol Rev*, *65*(1), 44-79.

Marchler-Bauer, A., & Bryant, S. H. (2004). CD-Search: protein domain annotations on the fly. *Nucleic Acids Res*, *32*(Web Server issue), W327-331.

Marshall, A. N., Han, J., Kim, M., & van Hoof, A. (2018). Conservation of mRNA quality control factor Ski7 and its diversification through changes in alternative splicing and gene duplication. *Proc Natl Acad Sci U S A*, *115*(29), E6808-E6816.

Marshall, A. N., Montealegre, M. C., Jimenez-Lopez, C., Lorenz, M. C., & van Hoof, A. (2013). Alternative splicing and subfunctionalization generates functional diversity in fungal proteomes. *PLoS Genet*, *9*(3), e1003376.

Martin, M. (2011). Cutadapt removes adapter sequences from high-throughput sequencing reads. EMBnet.journal *17*, 10-12.

Matranga, C., Tomari, Y., Shin, C., Bartel, D. P., & Zamore, P. D. (2005). Passenger-strand cleavage facilitates assembly of siRNA into Ago2-containing RNAi enzyme complexes. *Cell*, *123*(4), 607-620.

Matsuo, Y., Ikeuchi, K., Saeki, Y., Iwasaki, S., Schmidt, C., Udagawa, T., Sato, F., Tsuchiya, H., Becker, T., Tanaka, K., Ingolia, N. T., Beckmann, R., & Inada, T. (2017). Ubiquitination of stalled ribosome triggers ribosome-associated quality control. *Nat Commun*, *8*(1), 159.

Matsuo, Y., Tesina, P., Nakajima, S., Mizuno, M., Endo, A., Buschauer, R., Cheng, J., Shounai, O., Ikeuchi, K., Saeki, Y., Becker, T., Beckmann, R., & Inada, T. (2020). RQT complex dissociates ribosomes collided on endogenous RQC substrate SDD1. *Nat Struct Mol Biol*, *27*(4), 323-332.

McKenna, A., Hanna, M., Banks, E., Sivachenko, A., Cibulskis, K., Kernytsky, A., Garimella, K., Altshuler, D., Gabriel, S., Daly, M., & DePristo, M. A. (2010). The Genome Analysis Toolkit: a MapReduce framework for analyzing next-generation DNA sequencing data. *Genome Res*, *20*(9), 1297-1303.

McLeod, M., Shor, B., Caporaso, A., Wang, W., Chen, H., & Hu, L. (2000). Cpc2, a fission yeast homologue of mammalian RACK1 protein, interacts with Ran1 (Pat1) kinase To regulate cell cycle progression and meiotic development. *Mol Cell Biol*, *20*(11), 4016-4027.

Meaux, S., & Van Hoof, A. (2006). Yeast transcripts cleaved by an internal ribozyme provide new insight into the role of the cap and poly(A) tail in translation and mRNA decay. *RNA*, *12*(7), 1323-1337.

Merrick, W. C., & Pavitt, G. D. (2018). Protein Synthesis Initiation in Eukaryotic Cells. *Cold Spring Harb Perspect Biol*, *10*(12).

Moerman, D. G., Plurad, S., Waterston, R. H., & Baillie, D. L. (1982). Mutations in the unc-54 myosin heavy chain gene of Caenorhabditis elegans that alter contractility but not muscle structure. *Cell*, *29*(3), 773-781.

Morita, M., Ler, L. W., Fabian, M. R., Siddiqui, N., Mullin, M., Henderson, V. C., Alain, T., Fonseca, B. D., Karashchuk, G., Bennett, C. F., Kabuta, T., Higashi, S., Larsson, O., Topisirovic, I., Smith, R. J., Gingras, A. C., & Sonenberg, N. (2012). A novel 4EHP-GIGYF2 translational repressor complex is essential for mammalian development. *Mol Cell Biol*, *32*(17), 3585-3593.

Navickas, A., Chamois, S., Saint-Fort, R., Henri, J., Torchet, C., & Benard, L. (2020). No-Go Decay mRNA cleavage in the ribosome exit tunnel produces 5'-OH ends phosphorylated by Trl1. *Nat Commun*, *11*(1), 122.

Ortiz, M. A., Noble, D., Sorokin, E. P., & Kimble, J. (2014). A new dataset of spermatogenic vs. oogenic transcriptomes in the nematode Caenorhabditis elegans. *G3 (Bethesda)*, *4*(9), 1765-1772.

Palm, G. J., Billy, E., Filipowicz, W., & Wlodawer, A. (2000). Crystal structure of RNA 3'-terminal phosphate cyclase, a ubiquitous enzyme with unusual topology. *Structure*, *8*(1), 13-23.

Passos, D. O., Doma, M. K., Shoemaker, C. J., Muhlrad, D., Green, R., Weissman, J., Hollien, J., & Parker, R. (2009). Analysis of Dom34 and its function in no-go decay. *Mol Biol Cell*, *20*(13), 3025-3032.

Pestova, T. V., Borukhov, S. I., & Hellen, C. U. (1998). Eukaryotic ribosomes require initiation factors 1 and 1A to locate initiation codons. *Nature*, *394*(6696), 854-859.

Pestova, T. V., Lomakin, I. B., Lee, J. H., Choi, S. K., Dever, T. E., & Hellen, C. U. (2000). The joining of ribosomal subunits in eukaryotes requires eIF5B. *Nature*, *403*(6767), 332-335.

Pisarev, A. V., Kolupaeva, V. G., Pisareva, V. P., Merrick, W. C., Hellen, C. U., & Pestova, T. V. (2006). Specific functional interactions of nucleotides at key -3 and +4 positions flanking the initiation codon with components of the mammalian 48S translation initiation complex. *Genes Dev*, *20*(5), 624-636.

Pisarev, A. V., Skabkin, M. A., Pisareva, V. P., Skabkina, O. V., Rakotondrafara, A. M., Hentze, M. W., Hellen, C. U., & Pestova, T. V. (2010). The role of ABCE1 in eukaryotic posttermination ribosomal recycling. *Mol Cell*, *37*(2), 196-210.

Pisareva, V. P., Skabkin, M. A., Hellen, C. U., Pestova, T. V., & Pisarev, A. V. (2011). Dissociation by Pelota, Hbs1 and ABCE1 of mammalian vacant 80S ribosomes and stalled elongation complexes. *EMBO J*, *30*(9), 1804-1817.

Pratt, A. J., & MacRae, I. J. (2009). The RNA-induced silencing complex: a versatile gene-silencing machine. *J Biol Chem*, *284*(27), 17897-17901.

Preis, A., Heuer, A., Barrio-Garcia, C., Hauser, A., Eyler, D. E., Berninghausen, O., Green, R., Becker, T., & Beckmann, R. (2014). Cryoelectron microscopic

structures of eukaryotic translation termination complexes containing eRF1-eRF3 or eRF1-ABCE1. *Cell Rep*, *8*(1), 59-65.

Price, M. N., Dehal, P. S., & Arkin, A. P. (2010). FastTree 2--approximately maximum-likelihood trees for large alignments. *PLoS One*, *5*(3), e9490.

Pule, M. N., Glover, M. L., Fire, A. Z., & Arribere, J. A. (2019). Ribosome clearance during RNA interference. *RNA*, *25*(8), 963-974.

Roach, N. P., Sadowski, N., Alessi, A. F., Timp, W., Taylor, J., & Kim, J. K. (2020). The full-length transcriptome of C. elegans using direct RNA sequencing. *Genome Res*, *30*(2), 299-312.

Rodnina, M. V., Beringer, M., & Wintermeyer, W. (2007). How ribosomes make peptide bonds. *Trends Biochem Sci*, *32*(1), 20-26.

Rodnina, M. V., Gromadski, K. B., Kothe, U., & Wieden, H. J. (2005). Recognition and selection of tRNA in translation. *FEBS Lett*, *579*(4), 938-942.

Saito, K., Horikawa, W., & Ito, K. (2015). Inhibiting K63 polyubiquitination abolishes no-go type stalled translation surveillance in Saccharomyces cerevisiae. *PLoS Genet*, *11*(4), e1005197.

Saito, S., Hosoda, N., & Hoshino, S. (2013). The Hbs1-Dom34 protein complex functions in non-stop mRNA decay in mammalian cells. *J Biol Chem*, *288*(24), 17832-17843.

Schaeffer, D., & van Hoof, A. (2011). Different nuclease requirements for exosome-mediated degradation of normal and nonstop mRNAs. *Proc Natl Acad Sci U S A*, *108*(6), 2366-2371.

Schindelin, J., Arganda-Carreras, I., Frise, E., Kaynig, V., Longair, M., Pietzsch, T., Preibisch, S., Rueden, C., Saalfeld, S., Schmid, B., Tinevez, J. Y., White, D. J., Hartenstein, V., Eliceiri, K., Tomancak, P., & Cardona, A. (2012). Fiji: an open-source platform for biological-image analysis. *Nat Methods*, *9*(7), 676-682.

Schmeing, T. M., Huang, K. S., Strobel, S. A., & Steitz, T. A. (2005). An induced-fit mechanism to promote peptide bond formation and exclude hydrolysis of peptidyl-tRNA. *Nature*, *438*(7067), 520-524.

Schmidt, C., Kowalinski, E., Shanmuganathan, V., Defenouillere, Q., Braunger, K., Heuer, A., Pech, M., Namane, A., Berninghausen, O., Fromont-Racine, M., Jacquier, A., Conti, E., Becker, T., & Beckmann, R. (2016). The cryo-EM

structure of a ribosome-Ski2-Ski3-Ski8 helicase complex. *Science*, *354*(6318), 1431-1433.

Searfoss, A., Dever, T. E., & Wickner, R. (2001). Linking the 3' poly(A) tail to the subunit joining step of translation initiation: relations of Pab1p, eukaryotic translation initiation factor 5b (Fun12p), and Ski2p-Slh1p. *Mol Cell Biol*, *21*(15), 4900-4908.

Searfoss, A. M., & Wickner, R. B. (2000). 3' poly(A) is dispensable for translation. *Proc Natl Acad Sci U S A*, *97*(16), 9133-9137.

Shakes, D. C., Miller, D. M., 3rd, & Nonet, M. L. (2012). Immunofluorescence microscopy. *Methods Cell Biol*, *107*, 35-66.

Shao, S., Brown, A., Santhanam, B., & Hegde, R. S. (2015). Structure and assembly pathway of the ribosome quality control complex. *Mol Cell*, *57*(3), 433-444.

Shao, S., & Hegde, R. S. (2014). Reconstitution of a minimal ribosome-associated ubiquitination pathway with purified factors. *Mol Cell*, *55*(6), 880-890.

Shao, S., Murray, J., Brown, A., Taunton, J., Ramakrishnan, V., & Hegde, R. S. (2016). Decoding Mammalian Ribosome-mRNA States by Translational GTPase Complexes. *Cell*, *167*(5), 1229-1240 e1215.

Shao, S., von der Malsburg, K., & Hegde, R. S. (2013). Listerin-dependent nascent protein ubiquitination relies on ribosome subunit dissociation. *Mol Cell*, *50*(5), 637-648.

Shen, P. S., Park, J., Qin, Y., Li, X., Parsawar, K., Larson, M. H., Cox, J., Cheng, Y., Lambowitz, A. M., Weissman, J. S., Brandman, O., & Frost, A. (2015). Protein synthesis. Rqc2p and 60S ribosomal subunits mediate mRNA-independent elongation of nascent chains. *Science*, *347*(6217), 75-78.

Shoemaker, C. J., & Green, R. (2011). Kinetic analysis reveals the ordered coupling of translation termination and ribosome recycling in yeast. *Proc Natl Acad Sci U S A*, *108*(51), E1392-1398.

Simms, C. L., Hudson, B. H., Mosior, J. W., Rangwala, A. S., & Zaher, H. S. (2014). An active role for the ribosome in determining the fate of oxidized mRNA. *Cell Rep*, *9*(4), 1256-1264.

Simms, C. L., Thomas, E. N., & Zaher, H. S. (2017). Ribosome-based quality control of mRNA and nascent peptides. *Wiley Interdiscip Rev RNA*, *8*(1).

Simms, C. L., Yan, L. L., & Zaher, H. S. (2017). Ribosome Collision Is Critical for Quality Control during No-Go Decay. *Mol Cell*, *68*(2), 361-373 e365.

Sitron, C. S., & Brandman, O. (2019). CAT tails drive degradation of stalled polypeptides on and off the ribosome. *Nat Struct Mol Biol*, *26*(6), 450-459.

Sitron, C. S., Park, J. H., & Brandman, O. (2017). Asc1, Hel2, and Slh1 couple translation arrest to nascent chain degradation. *RNA*, *23*(5), 798-810.

Skandalis, A. (2016). Estimation of the minimum mRNA splicing error rate in vertebrates. *Mutat Res*, *784-785*, 34-38.

Sparks, K. A., & Dieckmann, C. L. (1998). Regulation of poly(A) site choice of several yeast mRNAs. *Nucleic Acids Res*, *26*(20), 4676-4687.

Spencer, P. S., & Barral, J. M. (2012). Genetic code redundancy and its influence on the encoded polypeptides. *Comput Struct Biotechnol J*, *1*, e201204006.

Stansfield, I., Jones, K. M., Kushnirov, V. V., Dagkesamanskaya, A. R., Poznyakovski, A. I., Paushkin, S. V., Nierras, C. R., Cox, B. S., Ter-Avanesyan, M. D., & Tuite, M. F. (1995). The products of the SUP45 (eRF1) and SUP35 genes interact to mediate translation termination in Saccharomyces cerevisiae. *EMBO J*, *14*(17), 4365-4373.

Sundaramoorthy, E., Leonard, M., Mak, R., Liao, J., Fulzele, A., & Bennett, E. J. (2017). ZNF598 and RACK1 Regulate Mammalian Ribosome-Associated Quality Control Function by Mediating Regulatory 40S Ribosomal Ubiquitylation. *Mol Cell*, *65*(4), 751-760 e754.

Szadeczky-Kardoss, I., Csorba, T., Auber, A., Schamberger, A., Nyiko, T., Taller, J., Orban, T. I., Burgyan, J., & Silhavy, D. (2018). The nonstop decay and the RNA silencing systems operate cooperatively in plants. *Nucleic Acids Res*, *46*(9), 4632-4648.

Takata, M. A., Goncalves-Carneiro, D., Zang, T. M., Soll, S. J., York, A., Blanco-Melo, D., & Bieniasz, P. D. (2017). CG dinucleotide suppression enables antiviral defence targeting non-self RNA. *Nature*, *550*(7674), 124-127.

Taylor, D. J., Nilsson, J., Merrill, A. R., Andersen, G. R., Nissen, P., & Frank, J. (2007). Structures of modified eEF2 80S ribosome complexes reveal the role of GTP hydrolysis in translocation. *EMBO J*, *26*(9), 2421-2431.

Thompson, O., Edgley, M., Strasbourger, P., Flibotte, S., Ewing, B., Adair, R., Au, V., Chaudhry, I., Fernando, L., Hutter, H., Kieffer, A., Lau, J., Lee, N., Miller,

A., Raymant, G., Shen, B., Shendure, J., Taylor, J., Turner, E. H., Hillier, L. W., Moerman, D. G., & Waterston, R. H. (2013). The million mutation project: a new approach to genetics in Caenorhabditis elegans. *Genome Res*, *23*(10), 1749-1762.

Toh, E. A., Guerry, P., & Wickner, R. B. (1978). Chromosomal superkiller mutants of Saccharomyces cerevisiae. *J Bacteriol*, *136*(3), 1002-1007.

Tsai, H. Y., Chen, C. C., Conte, D., Jr., Moresco, J. J., Chaves, D. A., Mitani, S., Yates, J. R., 3rd, Tsai, M. D., & Mello, C. C. (2015). A ribonuclease coordinates siRNA amplification and mRNA cleavage during RNAi. *Cell*, *160*(3), 407-419.

Tsuboi, T., Kuroha, K., Kudo, K., Makino, S., Inoue, E., Kashima, I., & Inada, T. (2012). Dom34:hbs1 plays a general role in quality-control systems by dissociation of a stalled ribosome at the 3' end of aberrant mRNA. *Mol Cell*, *46*(4), 518-529.

van Hoof, A., Frischmeyer, P. A., Dietz, H. C., & Parker, R. (2002). Exosome-mediated recognition and degradation of mRNAs lacking a termination codon. *Science*, *295*(5563), 2262-2264.

Verma, R., Oania, R. S., Kolawa, N. J., & Deshaies, R. J. (2013). Cdc48/p97 promotes degradation of aberrant nascent polypeptides bound to the ribosome. *Elife*, *2*, e00308.

Verma, R., Reichermeier, K. M., Burroughs, A. M., Oania, R. S., Reitsma, J. M., Aravind, L., & Deshaies, R. J. (2018). Vms1 and ANKZF1 peptidyl-tRNA hydrolases release nascent chains from stalled ribosomes. *Nature*, *557*(7705), 446-451.

Voorhees, R. M., & Ramakrishnan, V. (2013). Structural basis of the translational elongation cycle. *Annu Rev Biochem*, *82*, 203-236.

Wang, L., Lewis, M. S., & Johnson, A. W. (2005). Domain interactions within the Ski2/3/8 complex and between the Ski complex and Ski7p. *RNA*, *11*(8), 1291-1302.

Wang, L. K., Das, U., Smith, P., & Shuman, S. (2012). Structure and mechanism of the polynucleotide kinase component of the bacterial Pnkp-Hen1 RNA repair system. *RNA*, *18*(12), 2277-2286.

Wang, L. K., Lima, C. D., & Shuman, S. (2002). Structure and mechanism of T4 polynucleotide kinase: an RNA repair enzyme. *EMBO J*, *21*(14), 3873-3880.

Wang, X., Zhao, Y., Wong, K., Ehlers, P., Kohara, Y., Jones, S. J., Marra, M. A., Holt, R. A., Moerman, D. G., & Hansen, D. (2009). Identification of genes expressed in the hermaphrodite germ line of C. elegans using SAGE. *BMC Genomics*, *10*, 213.

Widner, W. R., & Wickner, R. B. (1993). Evidence that the SKI antiviral system of Saccharomyces cerevisiae acts by blocking expression of viral mRNA. *Mol Cell Biol*, *13*(7), 4331-4341.

Wilson, M. A., Meaux, S., & van Hoof, A. (2007). A genomic screen in yeast reveals novel aspects of nonstop mRNA metabolism. *Genetics*, *177*(2), 773-784.

Wolf, A. S., & Grayhack, E. J. (2015). Asc1, homolog of human RACK1, prevents frameshifting in yeast by ribosomes stalled at CGA codon repeats. *RNA*, *21*(5), 935-945.

Woo, P. C., Lau, S. K., Huang, Y., & Yuen, K. Y. (2009). Coronavirus diversity, phylogeny and interspecies jumping. *Exp Biol Med (Maywood)*, *234*(10), 1117-1127.

Wu, W., Liu, S., Ruwe, H., Zhang, D., Melonek, J., Zhu, Y., Hu, X., Gusewski, S., Yin, P., Small, I. D., Howell, K. A., & Huang, J. (2016). SOT1, a pentatricopeptide repeat protein with a small MutS-related domain, is required for correct processing of plastid 23S-4.5S rRNA precursors in Arabidopsis thaliana. *Plant J*, *85*(5), 607-621.

Yang, J. Y., Deng, X. Y., Li, Y. S., Ma, X. C., Feng, J. X., Yu, B., Chen, Y., Luo, Y. L., Wang, X., Chen, M. L., Fang, Z. X., Zheng, F. X., Li, Y. P., Zhong, Q., Kang, T. B., Song, L. B., Xu, R. H., Zeng, M. S., Chen, W., Zhang, H., Xie, W., & Gao, S. (2018). Structure of Schlafen13 reveals a new class of tRNA/rRNA- targeting RNase engaged in translational control. *Nat Commun*, *9*(1), 1165.

Yonashiro, R., Tahara, E. B., Bengtson, M. H., Khokhrina, M., Lorenz, H., Chen, K. C., Kigoshi-Tansho, Y., Savas, J. N., Yates, J. R., Kay, S. A., Craig, E. A., Mogk, A., Bukau, B., & Joazeiro, C. A. (2016). The Rqc2/Tae2 subunit of the ribosome-associated quality control (RQC) complex marks ribosome-stalled nascent polypeptide chains for aggregation. *Elife*, *5*, e11794.

Zaher, H. S., & Green, R. (2009). Fidelity at the molecular level: lessons from protein synthesis. *Cell*, *136*(4), 746-762.

Zamore, P. D., Tuschl, T., Sharp, P. A., & Bartel, D. P. (2000). RNAi: double-stranded RNA directs the ATP-dependent cleavage of mRNA at 21 to 23 nucleotide intervals. *Cell*, *101*(1), 25-33.

Zhang, D., Burroughs, A. M., Vidal, N. D., Iyer, L. M., & Aravind, L. (2016). Transposons to toxins: the provenance, architecture and diversification of a widespread class of eukaryotic effectors. *Nucleic Acids Res*, *44*(8), 3513-3533.

Zhou, W., Lu, Q., Li, Q., Wang, L., Ding, S., Zhang, A., Wen, X., Zhang, L., & Lu, C. (2017). PPR-SMR protein SOT1 has RNA endonuclease activity. *Proc Natl Acad Sci U S A*, *114*(8), E1554-E1563.

Zhouravleva, G., Frolova, L., Le Goff, X., Le Guellec, R., Inge-Vechtomov, S., Kisselev, L., & Philippe, M. (1995). Termination of translation in eukaryotes is governed by two interacting polypeptide chain release factors, eRF1 and eRF3. *EMBO J*, *14*(16), 4065-4072.

Zimmermann, L., Stephens, A., Nam, S. Z., Rau, D., Kubler, J., Lozajic, M., Gabler, F., Soding, J., Lupas, A. N., & Alva, V. (2018). A Completely Reimplemented MPI Bioinformatics Toolkit with a New HHpred Server at its Core. *J Mol Biol*, *430*(15), 2237-2243.

Zinoviev, A., Ayupov, R. K., Abaeva, I. S., Hellen, C. U. T., & Pestova, T. V. (2020). Extraction of mRNA from Stalled Ribosomes by the Ski Complex. *Mol Cell*, *77*(6), 1340-1349 e1346.